Alma Mater Studiorum - Università di Bologna

DOTTORATO DI RICERCA IN

INGEGNERIA CIVILE, CHIMICA, AMBIENTALE E DEI MATERIALI

Ciclo 35

Settore Concorsuale: 09/D2 - SISTEMI, METODI E TECNOLOGIE DELL'INGEGNERIA CHIMICA E DI PROCESSO

Settore Scientifico Disciplinare: ING-IND/24 - PRINCIPI DI INGEGNERIA CHIMICA

ELECTROSPINNING OF POLYMERIC COMPOSITES WITH GRMS FOR DIFFERENT INDUSTRIAL APPLICATIONS

Presentata da: Claudio Gasparini

Coordinatore Dottorato

Alessandro Tugnoli

Supervisore

Matteo Minelli

Co-supervisore

Andrea Liscio

Esame finale anno 2023

ACKNOWLEDGEMENTS AND DEDICATIONS

The entirety of this work would have not been possible without the collective participation of many competent researchers and wonderful people.

First of all my supervisors, Matteo Minelli and Andrea Liscio, who guided my path but encouraged my intuitions. Thanks for not letting me down when I was losing my focus.

Thanks to Vincenzo Palermo and Emanuele Treossi who followed my practical work closer and gave me the opportunity to complete this path in CNR. And thanks to all the people in ISOF that make the institute work and help in everyday problems.

Thanks to my parents and my family for all the support and encouragement throughout my entire academic career. Thanks for giving me the opportunity to be proud of myself, I hope you are too.

Thanks to all my colleagues at ISOF, for the help, the laughs, the adventures, the precious talks and moments. You made these years pass too fast.

And thanks to all the people that help me stay young while growing up.

ABSTRACT

Electrospinning is the most common and industrially scalable technique for the production of polymeric nanofibers. Nanostructured textiles with nanofiber morphology have been widely studied for different applications such as energy harvesting devices, conductive textiles and adsorption membranes.

Currently, nanocomposites are drawing much interest for their excellent properties in terms of flexibility, electrical conductivity and high surface area, which enhances the interaction with the surrounding environment.

The objective of this thesis was the optimization of different electrospinning setups for the production of nanostructured polymeric composites using graphene-related materials as nanofillers. Such composites were obtained using different polymers as matrix (polyamide 6, polyinylidene fluoride and polylactic acid) that were selected and combined with the appropriate reinforcements based on their properties and their interest for specific applications.

Moreover, this study highlighted the possibility to tune the morphology and size of the produced nanofibers by the addition of appropriate nanofillers even in low amounts. The addition of only 0.5% of GO allowed the production of smooth nanofibers with diameters up to 75% thinner (in the case of PLA) than the ones obtained from the pristine polymer.

PVdF was charged with GO to produce triboelectric materials that can be exploited in a wearable nanogenerator for the conversion of human motion energy in electrical energy. The addition of GO improved the open circuit voltage and power output of a generator prototype by 3.5 times, reaching values of ≈ 60 V and ≈ 5 $\mu W/cm^2$ respectively.

Electrospun PA6 membranes were coated with rGO using a simple two-step technique to produce conductive textiles for wearable electronic applications. The sheet resistance of the produced materials was measured in approximately 500 Ω/sq and their resistance to washing and bending was successfully tested. These materials could be exploited as strain sensors or heating elements in smart textiles.

PLA was co-electrospun with GO and cellulose nanofibers to produce high-surface area (≈ 3.5 m^2/g) and porosity ($\approx$ 95%) mats that could be exploited for the production of high-capacity adsorption membranes with low pressure drops. The presence of nanocellulose in the composite could also open the possibility of functionalizing the membrane to increase its selectivity towards different analytes and contaminants.

INTRODUCTION

Nanomaterials are one of the scientific topics that are attracting more interest in the latest years thanks to the unique properties that materials possess in the nanoscale. In particular, in the field of polymers, nanometric fillers are very promising for the production of composites since their nanoscale dimensions allow to enhance the properties of the final material even at lower loadings when compared to the relative micrometric fillers.

To exploit extensively the superior properties of nanomaterials in terms of mechanical resistance, electric properties and interactions with the environment, this research work aims to the production of nanostructured polymer composites that use as reinforcements materials deriving from graphene and cellulose. Such nanomaterials were selected for their strong mechanical properties and, in case of graphene, high electrical conductivity.

The electrospinning technique was used for the production of nanostructured composites with 1D fibre morphology. Electrospinning is the most common and more industrially ready technique for the production of polymeric fabrics composed by nanofibers.

The possibility to tune the morphology of the nanofibers through the addition of such materials to the electrospinning solution was deeply analysed. An appropriate production setup was optimized for each selected composite.

Different methods were explored for the addition of nanofillers, and the final properties of the composites were characterized using different techniques to inspect their possible use in different industrial applications.

The obtained materials are highly promising for early-stage applications in the field of energy harvesting, e-textiles and filtration membranes.

Sommario

1. NANOFIBERS AND ELECTROSPINNING

Nanomaterials have attracted increasing interest in the latest years thanks to their unique properties, which are often drastically different when compared to the same material in its micro- or macroscopic form [1]. At the nanoscale, some materials exhibit different properties than those of traditional bulk materials. Furthermore, in composites or other materials containing fillers, the property enhancement effect deriving from the addition of nanomaterials can be seen at lower loadings than its relative bulk material. This reflects in lower production and processing costs for the manufacturer and, in fields such electronics, in the production of smaller devices without compromising their performances.

In general, a material is defined “nanomaterial” when at least one of its dimensions is between 1 and 100 nanometres. From this perspective, nanomaterials are defined based on the number of their dimensions that are confined in the nanoscale [2]:

- 0D materials (three nanoscale dimensions)
- 1D materials (two nanoscale dimensions)
- 2D materials (one nanoscale dimensions)
- 3D materials (no dimension in the nanoscale, they are usually bundles or stacks of 1D or 2D materials

An example of these different class of nanomaterials can be seen in Figure 1.

For the purpose of this thesis, the focus will be set on 1D and 2D materials. In particular, one of the most interesting class of 1D materials are nanofibers, which will be discussed in the following chapter.

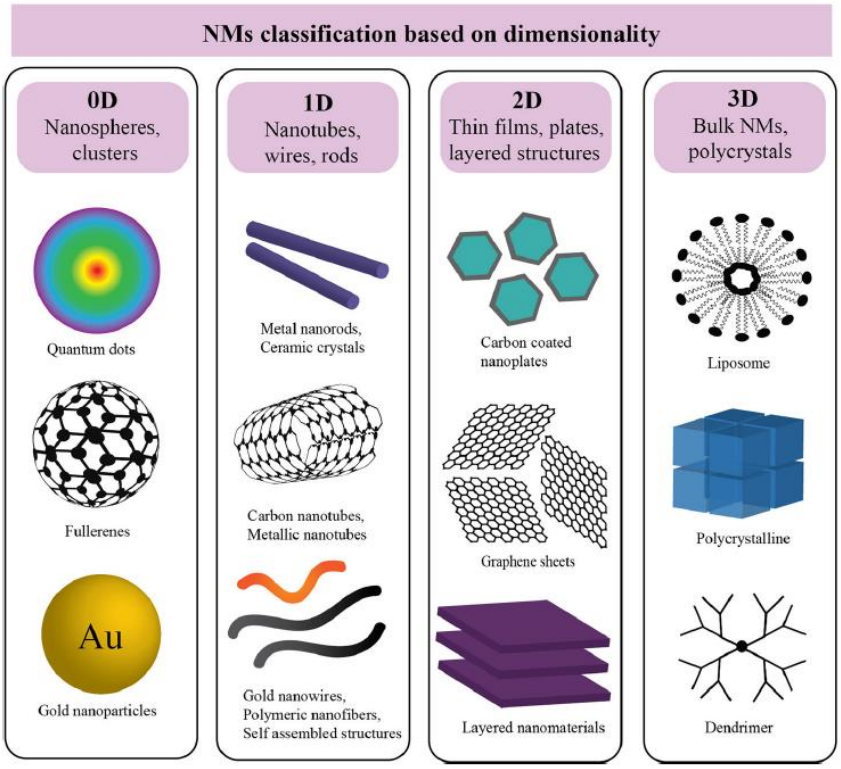

Figure 1: Schematic illustration of examples of 0D, 1D, 2D and 3D nanomaterials

1.1 POLYMERIC NANOFIBERS

In polymer science, nanofibers are the most widespread and studied form of nanomaterials. By definition, nanofibers are 1D materials, meaning that their diameter is negligible in comparison to their length.

Polymeric nanofibers allow the production of fabrics with tunable morphology and outstanding properties when compared to other non-woven textiles, such as high surface area, high porosity, low apparent density and fast response to external stimuli. Moreover they can be produced as very low-thickness mats characterized by superior directional strength [3].

The ability to fabricate such fabrics with pre-programmed morphological properties makes these materials promising towards a wide range of applications, from low-cost products to high tech applications. Some examples of possible application fields are energy storage and conversion (supercapacitors, nanogenerators, fuel cells), medical and bioengineering, filtration systems, aerospace and smart textiles [4], [5].

1.2 NANOFIBERS CLASSIFICATION

Polymeric fibres are typically distinguished in two classes according to their diameter (d). When d < 100 nm we usually refer to them as nanofibers, while when 100 nm < d < 1 μm they are called sub-micrometric fibres. Such classification is crucial in order to understand and predict their properties, but nanofiber morphology can be classified not only based on their dimension but also on their surface aspect and composition.

A further qualitative classification is related to the description of surface morphology being often called "secondary surface morphology". We can distinguish six cases, that can be seen in figure 2. Strongly depending on different production methods and setups, such small difference can affect significantly the properties of the final material, making it more suitable for certain kind of applications [6]. Moreover, hollow nanofibers can be obtained in different ways by post-treatments of the as-spun nanofibers.

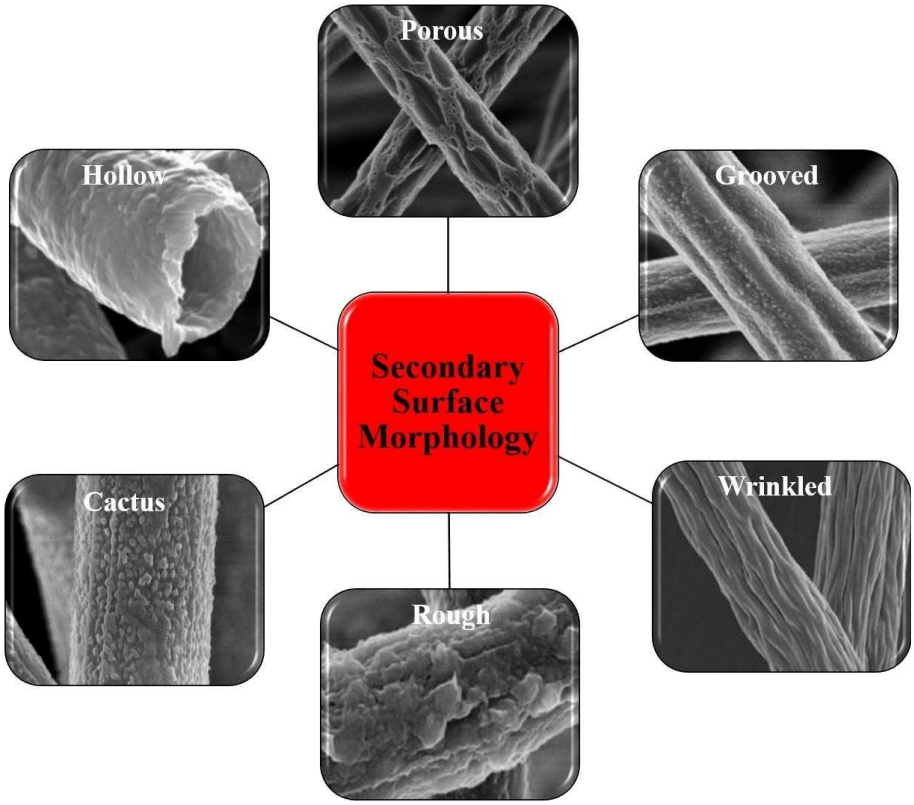

Figure 2:Different surface morphologies of nanofibers [6]

It is also possible to produce nanofibers composed by two different polymers to combine the properties of the two materials in the final composite and produce materials with unique properties. In this case, they can be randomly distributed (complex nanofibers) or, with the appropriate setup, they can be formed in a core-sheath morphology. This morphology (figure 3) indicates a material

whose outer layer is composed by a different polymer than its inner core, allowing to further increase the range of properties that can be exploited [7].

Figure 3:Schematic of core-sheat nanofiber formation [7]

1.3 POLYMER NANOFIBER PRODUCTION

Thanks to the rapid growth of nanoscience and to the properties of such nanosized 1D polymeric systems, polymeric nanofibers have attracted high interest in the latest years, and different processes have been exploited and optimized to produce nanofibers from a broad range of polymers. Such techniques include drawing, phase separation, template synthesis, meltblown spinning, centrifugal spinning and electrospinning.

Among these techniques, the electrospinning is the most studied and implemented in industries, thanks to its simplicity, scalability and reproducibility [8].

A short overview of the aforementioned techniques will be now discussed with particular attention on their scalability. General advantages and disadvantages of these techniques and a comparison between them in terms of scalability, repeatability and possibility of controlling the morphology of the obtained nanofibers are summarized in table 1 and table 2.

Process	Technological advances	Can the process be scaled?	Repeatability	Convenient to process?	Control on fiber dimensions
Drawing	Laboratory	×	√	√	×
Template Synthesis	Laboratory	×	√	√	√
Phase Separation	Laboratory	×	√	√	×
Self-Assembly	Laboratory	×	√	×	×
Electrospinning	Laboratory (with potential for industrial processing)	√	√	√	√

Table 1: comparison between electrospinning and other techniques for the production of nanofibers [9]

Process	Advantages	Disadvantages
Drawing	Minimum equipment requirement.	Discontinuous process
Template Synthesis	Fibers of different diameters can be easily achieved by using different templates.	Cannot produce long, continuous nanofibers
Phase Separation	Minimum equipment requirement. The process can directly fabricate a nanofiber matrix. Batch-to-batch consistency is achieved easily. The mechanical properties of the matrix can be tailored by adjusting polymer concentration.	Limited to specific polymers
Self-Assembly	Suitable for obtaining smaller nanofibers.	Complex process
Electrospinning	Cost-effective. Long, continuous nanofibers can be produced.	Jet instability

Table 2: Main advantages and disadvantages of the most common techniques for the production of nanofibers [9]

- DRAWING

Drawing process can be performed only with viscoelastic polymers that can also undergo high deformations while remaining sufficiently strong to resist the stress they experience during deformation.

A typical drawing setup is usually composed by a micropipette and a solid, flat surface (e.g. SiO2). The tip of the micropipette must have a diameter of just a few micrometres. After dipping the tip of the micropipette in a droplet of polymeric solution or melt polymer, it is slowly moved away with the help of a manipulator at a constant speed. This produces a thin nanofiber that can be simply collected.

The main constraint of this method, however, is the low production rate that prevents it from being scaled-up at industrial scale [10].

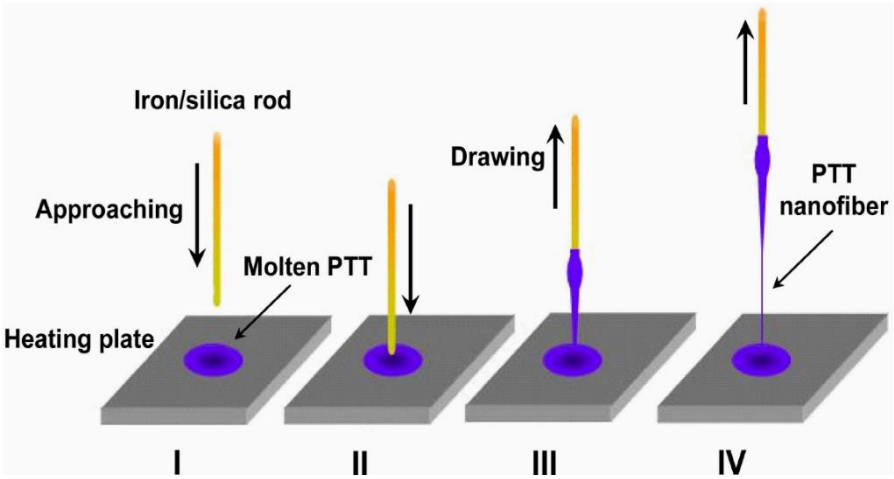

Figure 4:Schematic illustration of direct drawing of PTT nanofiber [11]

- PHASE SEPARATION

Phase separation method in conducted starting from a concentrated solution of the polymer in an appropriate solvent. This solution, which is thermodynamically unstable, tends to separate into a polymer-rich phase and a polymer-lean phase when exposed to appropriate temperatures [12].
After solvent extraction, the polymer-rich phase will solidify to form the polymeric scaffold, while the polymer-lean phase will form the pores inside this structure. This technique is widely used for 3-D scaffold for tissue engineering applications.

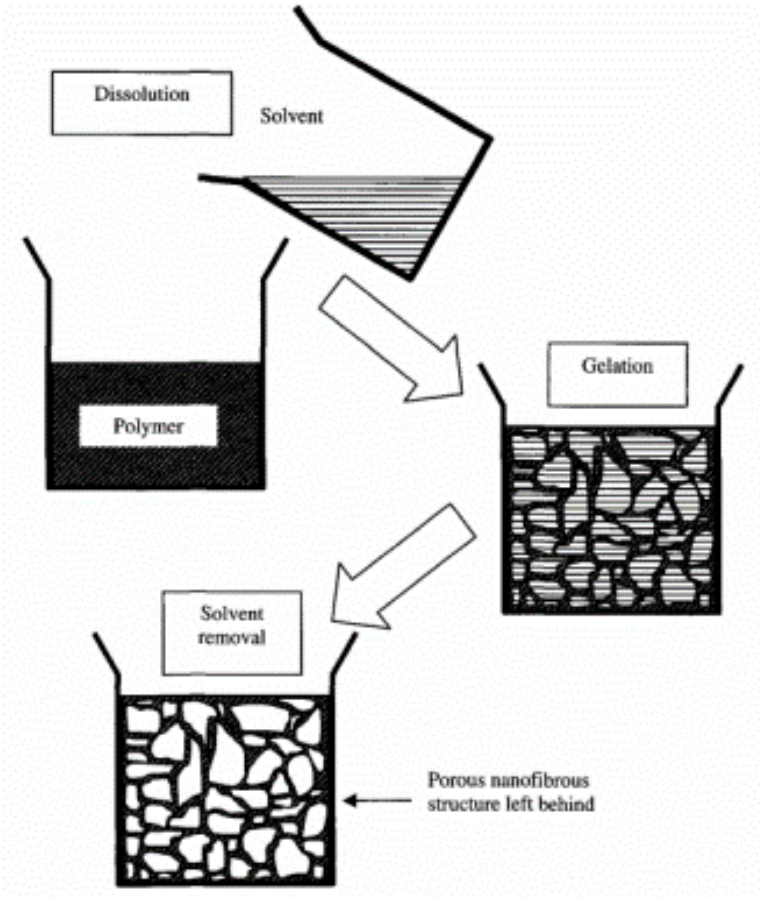

Figure 5:Schematic illustration of a typical phase separation lab-scale process [13]

- TEMPLATE SYNTHESIS

Template synthesis is mostly used to produce conductive polymer nanofibers or inorganic nanofibers, such as carbon nanotubes.

This method involves the use of a mold, such as a thin metal oxide membrane with controlled diameter pores. The polymer is then extruded through these pores by applying a constant pressure and the nanofibers are then produced once they come in contact with a solidifying solution [14].

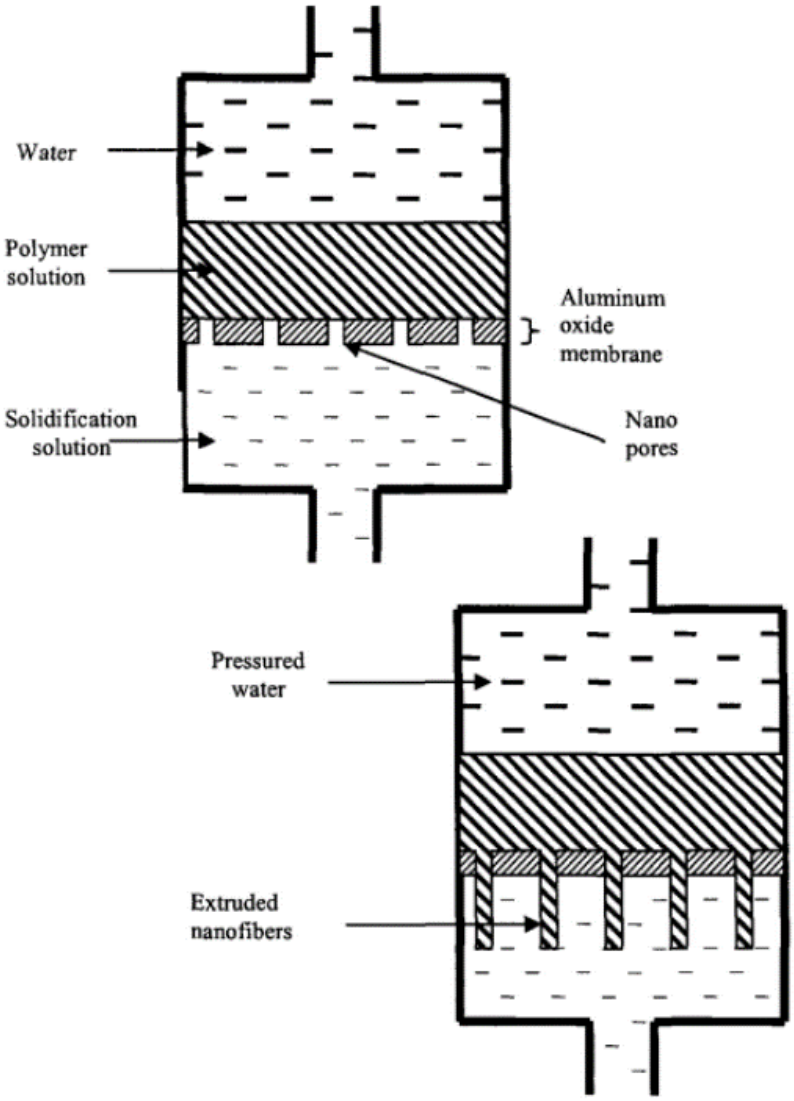

Figure 6: Schematic illustration on the obtainment of nanofibres through template synthesys [15]

- MELTBLOWN SPINNING

Meltblown spinning is a production technique that involves the stretching of the melt polymer into nanofibers by using hot air. Such manufacturing approach has been widely exploited in the pandemic years for the production of face masks.
The melt polymer is first extruded through a small diameter orifice, then compressed hot air, usually at a temperature near to the melting point of the polymer, is used to draw polymeric nanofibers into a rotating drum that acts as a collector [16].
Simple, cheap and easily up-scalable using thermoplastic polymers, such approach has the main disadvantage of a poor control of the diameter and morphology of the produced nanofibers.

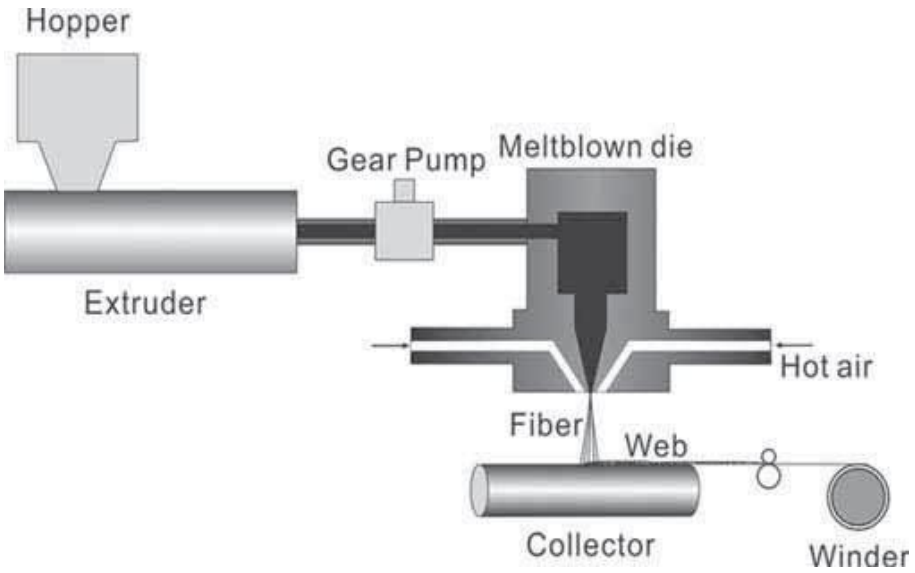

Figure 7: Detailed shematic of meltblown spinning process [16]

- CENTRIFUGAL SPINNING

Centrifugal spinning is one of the most recently developed production methods for polymeric nanofibers. It works by using centrifugal force as drawing force for the stretching of nanofibers out of polymer melts or solutions.
The entire process can be summarized in three main steps [17].

- During the jet-initiation step, a fast-spinning motor applies a high centrifugal force to the polymeric fluid, forcing it to stretch and extrude through a small orifice.
- After that, the external centrifugal force and rotation inertia cause a further stretching of the polymeric jet while it reaches the collector placed all around the motor. This causes the jet diameter to decrease and it is a crucial step to obtain small-diameter nanofibers, highly

dependent on the distance between orifice and collector. At the same time, the solvent in the polymer solution evaporates (or the melt polymer starts solidifying).

- This causes the nanofibers to solidify and further reduces their diameter and a complete solidification has to happen before the nanofibers reach the collector. Hence, to achieve good results it is crucial to choose an appropriate solvent.

The advantages of such production method is drawing high interest because of its high production rate and safety [18]. However the complexity of the factors that influence the final nanofibers diameter and morphologies reflects in a poor reproducibility and hinders its large scale application [19].

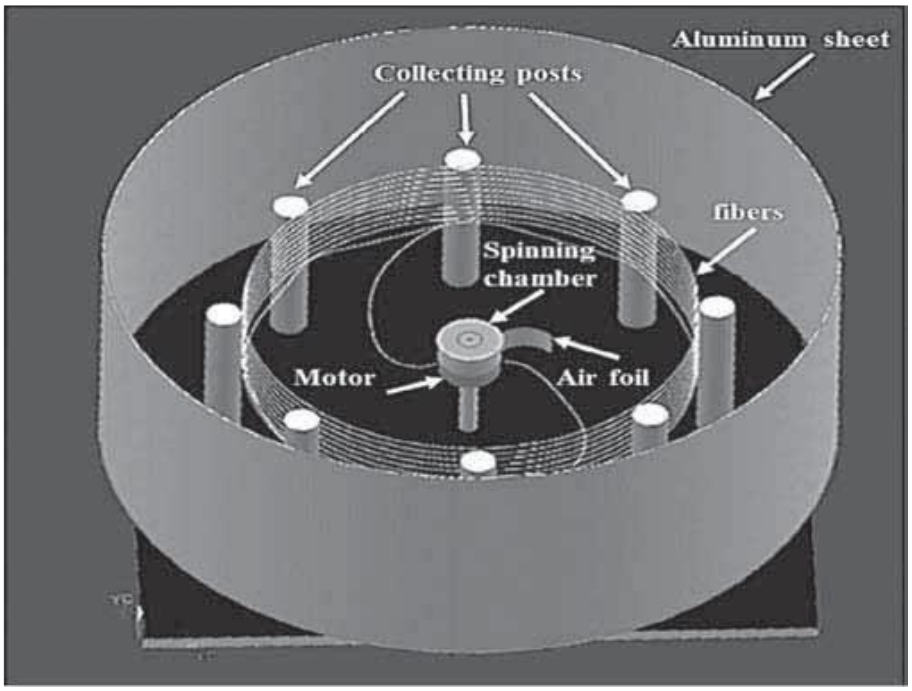

Figure 8: Schematic illustration of a centrifugal spinning apparatus [20]

1.4 ELECTROSPINNING

Electrospinning is the most exploited and studied technique for the production of polymeric nanofibers because of good compromise between an easy scalability to industrial scale and a good control over the characteristics of the obtained nanofibers [21] [22]. Moreover, this technique is capable to yield continuous and fine nanofibers (from 10 μm to 5 nm) and can be used for a large variety of different polymers and composites.

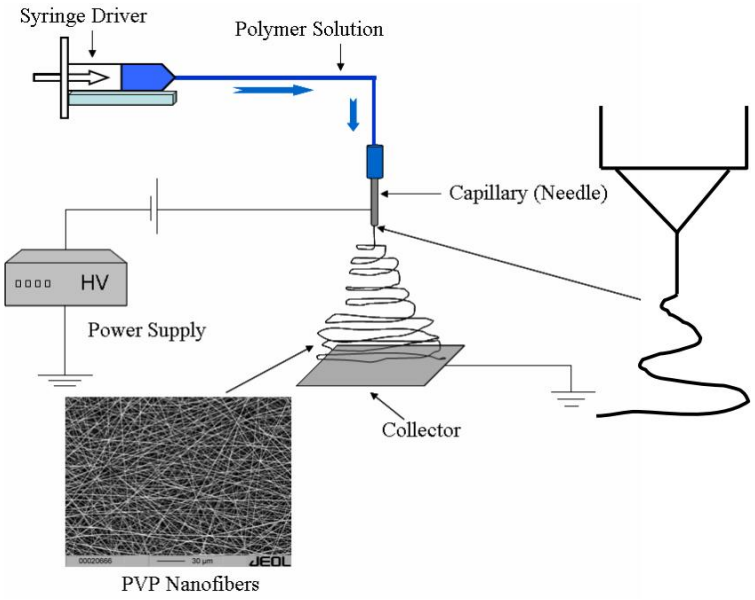

Figure 9: Schematic illustration of electrospinning process

First studies on electro-spraying date back to the beginning of XX century and the first patent on production of polymeric textile yarns using such technique was patented by Anton Formhals in 1934 [23].

In late of ’60s, Geoffrey Ingram Taylor deepened the understanding of the mechanism by mathematically modelling the shape of the cone formed by a polymer stretched by an electric field, which will be named Taylor cone [24].

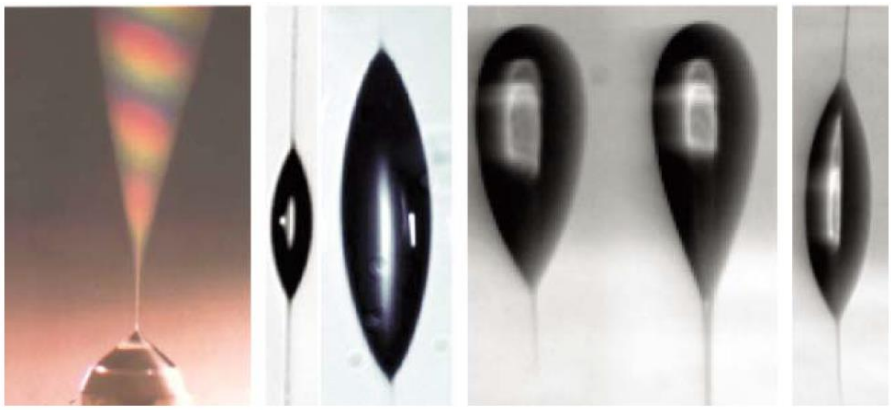

Figure 10: Examples of stationary and transient Taylor cones from different electrospinning solutions and setups [25]

Only in mid-’90s the increasing interest on nanomaterials caused electrospinning to receive new attention by the scientific community.

Electrospinning works thanks to the stretching that a high-voltage electric field can confer to a polymer solution or melt. The polymer is first extruded through a thin needle (spinneret) and a high-voltage is applied, forming a pendant droplet at the end of the needle. When the electrostatic repulsion starts to overcome the fluid's surface tension, this droplet will deform into a cone shape, known as the Taylor cone. Then, as the electrostatic force starts to overcome the surface tension of

the cone-shaped droplet, a charged jet stream of the polymer melt is ejected from the needle tip [26] [27]. This bending instability causes the jet stream to continue lengthen as a long, thin filament. As the stretched jet travels to the collector, the solvent evaporates, solidifying the solution into nanofibers [28].

1.5 COMPARISON BETWEEN ELECTROSPINNING AND OTHER TECHNIQUES

Scalability, repeatability, control over nanofibers and costs are the main characteristics used to evaluate nanofiber production techniques, as resumed in Table 1. Table 2 instead gives an outlook on the main advantages and disadvantages of each technique.
It can easily be seen that electrospinning is the most promising and has several advantages over the other techniques. Moreover, using electrospinning it is also possible to have a better control over morphology, dimensions and porosity of the nanofibers, in comparison to other techniques.
Its main disadvantage, apart from the intrinsic risks of working near high-voltages and evaporating solvents, is the jet instability that can easily occur if the operative parameters are not appropriately set. The bending instability caused by the strong electric field is actually needed to stretch the Taylor cone into the polymeric jet that forms the nanofibers [25] [29].
However two other types of instability can occur and cause defects on the final product [30].
Rayleigh instability causes the jet to break into smaller droplets, impeding the formation of continuous nanofibers. Axisymmetric conduction instability, instead, causes the formation of larger polymeric aggregates called beads along the length of the nanofiber.

1.6 ELECTROSPINNING APPARATUS AND SETUP

The experimental apparatus needed for electrospinning is usually composed by three main components: a high-voltage power supply, a grounded collector and an extrusion system, which usually consists in a syringe with a metal needle (figure 11). Moreover, the entirety of the process is usually performed in a Faraday cage, to prevent electrical interferences and for safety reasons, due to the risks associated with high-voltages.

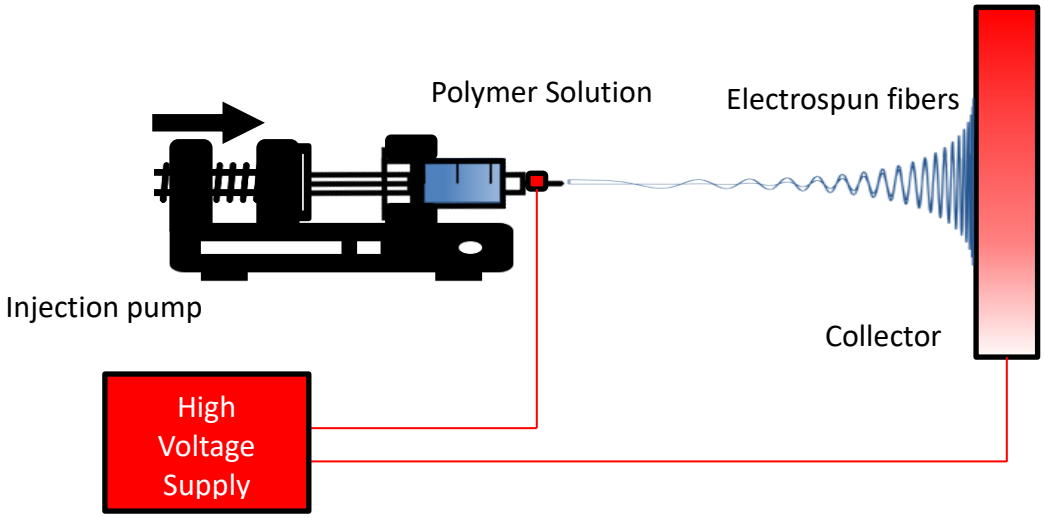

Figure 11: Schematic representation of the electrospinning apparatus and its main components

One of the main advantages of electrospinning is the possibility to customize the setup, adapting it to the user's needs. This makes the process suitable for processing a wide number of different polymers and composite and, moreover, allows to obtain different morphologies and characteristics in the final product. As an example, the setup can be placed in horizontal configuration, extruding the polymer through the needle using a pump, or in vertical mode letting the polymer flow through the needle by gravity. Moreover, the vertical configuration allows to add a coagulation bath on top of the collector if needed to solidify the polymeric nanofibers. Another customizable component is the collector. Different collectors can be used to obtain specific morphologies and orientations in the produced nanofibers. Flat metal plates are used to obtain randomly aligned nanofibers, while grids, parallel plates and rotating drums can confer a specific orientation to them [31]. The outcome of the polymeric nanofibers will strongly depend on the chosen setup, but can be controlled and optimized by carefully choosing the electrospinning conditions.

Since the technique involve different mechanisms, the chemico/physical properties of the produced nanofibers depend on several experimental parameters, which can be summarized in three main classes: i) solution, ii) processing and iii) environmental parameters.

Solution parameters are crucial to form the Taylor cone and therefore they must be accurately optimized in order to be able to perform the whole process. The final result is affected by polymer molecular weight distribution, crystallization and glass transition temperatures. In particular, solution concentration has to be over the entanglement concentration (C_e) to produce defect-free nanofibers [32]. Furthermore, the solubility of the polymer in the chosen solvent is crucial since if the saturation limit of the polymer in the chosen solvent is too low, the range of possible concentration and, thus, viscosities of the solution will be limited. Consequently, it will be more

difficult to tune effectively nanofiber morphology. Solvent must also be sufficiently volatile to completely evaporate before getting to the collector [21].

Once an appropriate solution is prepared, processing parameters must be set. Electrospinning process is influenced by needle internal diameter [33], electric field strength (usually controlled by the high-voltage source) [27], tip-to-collector distance [34] and extrusion flow [35]. These parameters highly influence nanofibers diameter and the presence of defects on the final product. For example, low applied voltage lead to thicker nanofibers, while increasing the applied voltage, the polymeric jet will be more stretched and smaller diameter nanofibers will be formed. However, this will also increase jet instability, thus increasing the number of defects in the final product.

Finally, also the environmental condition plays a crucial role. In particular, temperature and relative humidity [36] both influence nanofiber diameter and solvent evaporation. Moreover, high relative humidity may also confer a porous morphology to nanofibers produced starting from a non-aqueous solution.

1.7 NANOFIBERS MORPHOLOGY

A core aspect and one of the greatest advantages of electrospinning is the superior control over the morphology of the produced nanofibers in comparison to the other common nanofiber production techniques [37]. It is possible to produce nanofibers with different morphologies by tuning the electrospinning conditions or by using different electrospinning apparatus setups:

- Porous nanofibers

  Porous nanofibers are heavily studied for a wide range of applications since their unique morphology further increases the surface area of the final product. Different techniques are currently used to obtain this morphology. Ramakrishna et al. [38] were able to produce porous nanofibers by rapid phase separation during the electrospinning process. To achieve this result it is crucial to use a solvent with a high evaporation rate, which leads to the formation of small holes on the surface of the nanofibers.

  For certain polymers, it is also possible to obtain pores on the surface simply by using appropriate environmental conditions, such as temperature and humidity. A different approach for the production of porous nanofibers is to spin a blend of two different polymers, appropriately chosen so that one of them can be easily removed by selective dissolution in a solvent after the nanofiber formation.

- Ribbon-like nanofibers

  Ribbon-like nanofibers (or flattened nanofibers) are obtained from certain polymers by accurately setting the electrospinning conditions.

  This particular morphology is caused by an especially fast solvent evaporation at the jet surface, that leads to the formation of a thin solid polymer "skin" surrounding a liquid core.

  Then, during jet stretching, the critical pressure difference causes the nanofiber structure to collapse and flatten, creating a ribbon-like morphology [26].

- Core-shell nanofibers

  Core-shell nanofibers are extensively studied because they allow to enhance the properties of the final product by combining the properties of two different materials that are found in them as two separate phases, one in the core of the nanofibers and the other on the surface.

  Moreover, they open the way to the production of hollow nanofibers by using mineral oil as core material, which can be easily removed afterwards, leaving only a hollow shell of polymer.

  This morphology can be obtained by co-axial electrospinning, using a particular spinneret that allows the simultaneous extrusion of the two phases from two circular concentric nozzles. The electrospinning is performed as usual, with the formation of a core-sheath Taylor cone, its stretching and the evaporation of the solvent before the deposition of the nanofibers on the collector [39].

- Helical nanofibers

  Many researchers debated on the mechanism for the formation of helical nanofibers. Kessick et al. [40] reported a mechanism based on the coulombic repulsion force between two nanofibers with the same surface charge.

  When a nanofiber is deposited on the conductive collector, two forces are simultaneously applied to the polymer jet: the coulombic repulsion force and a contracting viscoelastic force typical of the polymeric chains. When these two forces are not in equilibrium, the jet spontaneously rearranges in a helical structure to restore it. This rare morphology is attracting interest for applications in electromechanical devices, optical components and drug delivery.

- Branched nanofibers

  Branched nanofibers are considered a defect due to the jet-splitting phenomenon. It occurs when the charge density on the stretching jet becomes too high from the effect of solvent evaporation and jet elongation. This causes an instability that causes the ejection of a smaller jet from the

surface of the primary jet in order to reduce the charge density, and thus the instability, on both [26].

Branched nanofibers still possess a high surface area, but are characterized by an uneven distribution of the nanofiber diameters.

- Beaded nanofibers

  Another type of defective nanofibers are the beaded ones. Beaded nanofibers are formed when the surface tension of the polymer is stronger than the electric force that tries to stretch the polymer jet and increase its surface area. In this particular case, polymer agglomerates (beads) can be seen along the length of the nanofibers. This defects cause a reduction in the overall surface area of the final product.

  In practice, these imperfections can be avoided by accurately tuning some electrospinning conditions, such as applied voltage, solution viscosity and concentration [41]. Moreover, different studies report that the addition of small amounts of salts or polyelectrolytes to the electrospinning solution may increase the charge carried by the jet and its conductivity, increasing the jet stretching and leading to beads-free nanofibers.

1.8 FIELD OF APPLICATIONS

The nanometric dimension confer nanofibers unique properties that can be exploited in several industrial and research fields. The ones that are mainly studied and sought-after are their enhanced surface-to-volume ratio and their nanometric porous structure. Moreover, the higher molecular orientation of the polymeric chains can confer them mechanical properties that are superior to the ones measured in micro- and macro-fibres. In addition to this, nanofibrous mats are lightweight thanks to their low apparent density and possess great flexibility. These outstanding properties make nanofibers interesting for environmental applications, biomedical applications, electronics and energy harvesting and storage, as briefly listed in figure 13.

Here, we focus on two fields that have had extensive development in recent years, related to environmental and biomedical applications.

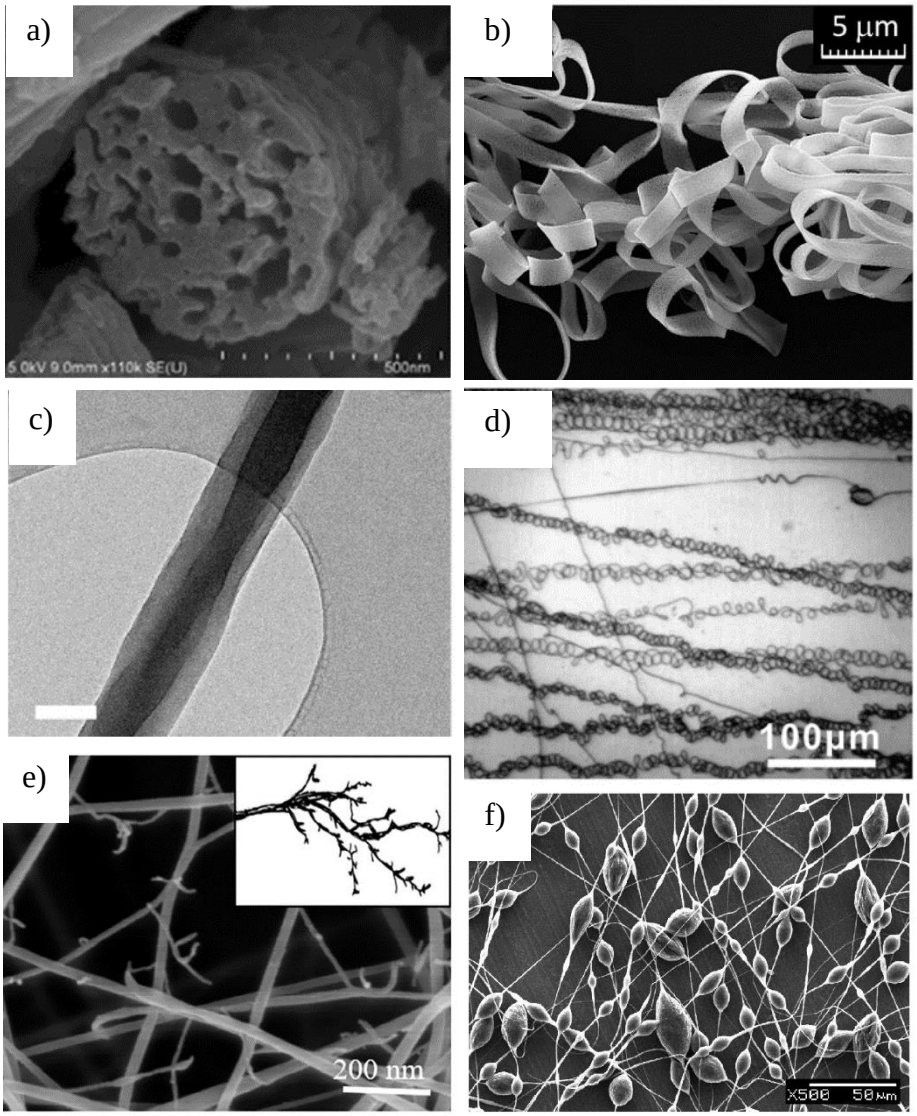

Figure 12: SEM and TEM images of nanofibers with different morphologies: a) porous, b) ribbon-like, c) core-shell, d) helical, e) branched and f) beaded.

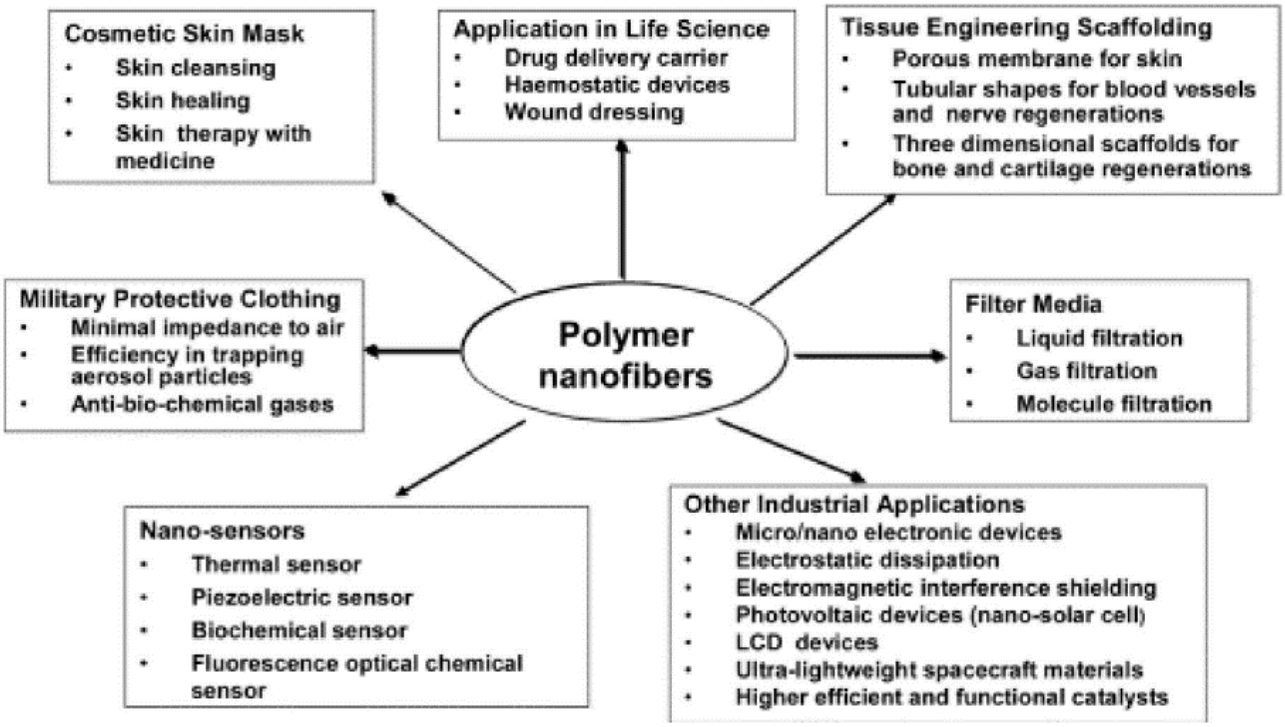

Figure 13: Main target applications for polymer nanofibers [42]

1.8.1 ENVIRONMENTAL APPLICATIONS

The mass transport of both gaseous and liquid samples is considerably assisted by the extremely porous structure created by the random entanglement of nanofibers. In fact, there is little resistance when a gas stream or solution flows through a nonwoven mat made of electrospun nanofibers [43]. For this reason, innovative filters for eliminating pollutants like particulate matters (PMs), harmful ions, and organic compounds from contaminated air and wastewater have been extensively researched using nanofiber-based mats, particularly those with alignment control and surface functionalization. According to the results, electrospun nanofiber-based membranes are superior at efficiently and rapidly eliminating contaminants and recovering precious metals with excellent selectivity, great recyclability, and visible stability [3].

In particular, several groups are actively researching over water treatment, exploring nanofiber-composed mats as active filtration membranes capable of a simultaneous separation and degradation of pollutants in wastewater. Air purification is another market sector in which nanofibrous membranes are highly studied for adsorption of common pollutants and PMs down to 300 nm in size. Their unique porous morphology can be exploited for the production of superior membranes with high filtration efficiencies and low pressure drops [44].

1.8.2 BIOMEDICAL APPLICATIONS

The biomedical field has shown growing interest in nanofibrous mats and scaffolds for various applications [45] [46] [47].

Biodegradable and biocompatible nanofiber-based scaffold are used in tissue engineering to promote the regeneration of damaged organs inside the human body. Using scaffolds made of nanofibers can improve the cell growth factor thanks to the similarity between these nanofibers and the natural extracellular matrix. Different biocompatible polymers are used for different organs, from bio-natural polymers (such as hyaluronic acid, alginate, chitosan...) for cartilage and skin regeneration to polylactic acid (PLA) and polycaprolactone (PCL) for bones.

Nanofibers properties can also be exploited in drug-delivery applications for different drugs, such as anticancer drugs, antibiotics and proteins. For this application, the main advantage of nanofibers is the high surface area, which allows a faster release of the drug in the target site.

For wound dressing application, antibacterial-modified polymer nanofibers can be used. In this case, several studies acknowledged their superior antibacterial effect, and the enhanced porosity of nanofibrous mats and scaffolds can keep a suitable environment for the correct healing of the abrasion.

2. GRAPHENE AND CARBON MATERIALS

To further exploit properties of nanomaterials, the work conducted in this thesis focused on the additivation of 1D nanostructures (such as the nanofibers obtained by electrospinning) with different 1D and 2D charges with dimensions similar to the nanofiber diameter. This could improve their affinity and will allow to produce polymeric composites in which both the matrix and the filler can benefit from their nanoscale morphology.
In particular, the 2D materials used as fillers are graphene and its derivatives, which will be discussed in the following chapter.

2.1 GRAPHENE

Graphene is a two-dimensional carbon allotrope only formed by sp2-hybridized carbon atoms. All the carbon atoms arrange in a honeycomb structure formed by covalent C-C σ bonds with delocalized π bonding that confers a strong and rigid structure and creates 120° bond angles on the horizontal plane. In this configuration, interatomic distances are d=1.42 Å and centre to centre distances are 2.46 Å [48].

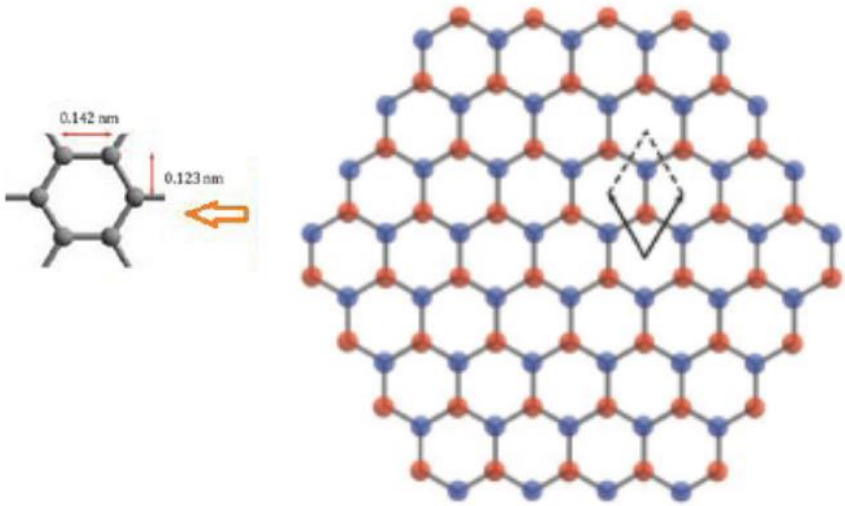

Figure 14: Schematic representation of the unit cell of graphene and of the crystalline honeycomb structure [49]

Due to the outstanding thermal, mechanical and electrical properties [48], graphene is being studied for numerous applications and some derivative materials are already on the market [50]
As an example, tests showed that electron mobility in graphene is especially high [51], and charge carriers can travel sub-micrometric distances without scattering. This can allow the production of

high-performance electronics, especially transistors. Its high conductivity, elasticity and transparency, instead, make it interesting for flexible electronics and conductive textiles.

After its discovery and isolation, the superior properties of graphene were analysed by several studies. The most interesting properties for industrial applications are its mechanical strength, electrical conductivity and thermal conductivity.

Graphene in its monoatomic layer form possesses superior mechanical properties. Various experiments report its tensile strength is higher than 100 GPa and its Young modulus is close to 1 TPa [48]. These values exceed the typical metal mechanical properties, for example steel has tensile strength of 400 MPa and Young modulus of 0.5 TPa. Moreover, graphene combines this mechanical strength with low density and weight.

Various tests reported that electron mobility in graphene is very high (10^5-10^6 $cm^2V^{-1}s^{-1}$) [51], although it is strongly influenced by the quality of graphene and of its substrate, and its electrical conductivity is estimated around 10^4-10^5 S/m [52].

Graphene has also shown exceptionally high thermal conductivity (approximately 3000 W/mK, almost an order of magnitude higher than copper) [48].

2.2 PRODUCTION OF GRAPHENE

Graphene was first isolated in 2004 by Geim and Novoselov. Only using adhesive tape, they exfoliated graphite leaving only a single layer micron-size irregular shaped on silicon substrate. Being such approach impossible to be upscaled, several other techniques have been developed [49]. All of them can summarised in two different approaches [53]:

Top-down approach [53]

Graphene can be synthesized starting from raw graphite, though this produces a large amount of refuse waste. Together with graphene, several other low-dimensional carbon-based materials (called graphene-based materials, GRMs) are industrially obtained this way, namely graphene oxide (GO), graphene nanoplatelets (GNPs), highly exfoliated oriented pyrolytic graphite (HOPG) and others.

Bottom-up approach [53]

Pure quality graphene can be grown on a suitable substrate using different techniques. Among those the most famous and employed is chemical vapour deposition (CVD). This approach may produce graphene sheets of high quality and with few defects, but it is challenging to scale this up to industrial production. For this reason, these techniques are mainly used for lab-scale applications

and research.

The morphology and characteristics of graphene is strongly affected by the production method. For this reason, we define the materials produced in a more general class called graphene-based materials (GRMs) while graphene indicates materials produced by means CVD (and scotch-tape).
The most developed and used techniques to produce graphene and GRMs production are briefly explained below.

2.2.1 LIQUID PHASE EXFOLIATION

Graphite is exfoliated into few-layer graphene sheets by treatment with a solvent having proper surface tension. For this application, non-aqueous solvents are the best suited, but aqueous solutions with surfactants can also be used. The solvent is able to promote the splitting of graphite crystalline planes, which are then effectively exfoliated by using a disruptive technique (e.g. sonication). A further approach exploits the chemical oxidation of graphite pellets followed by ultrasonication in aqueous solution. Thus, the obtained material is called graphene oxide.

2.2.2 THERMAL AND MECHANICAL EXFOLIATION

A molecular intercalant layer can be inserted through the graphite layers, obtaining what are called Graphite intercalated compounds (GICs).
GICs can then be used to obtain graphene nanoplatelets (GNPs) with a quick and scalable method. First, they are subjected to a thermal/microwave shock to separate the graphite layers, then by simple ball milling or sonication GNPs are obtained.

2.2.3 CHEMICAL VAPOR DEPOSITION

Chemical vapour deposition is the most studied bottom-up technique because it can lead to the production of large-area, uniform polycrystalline graphene films, which are virtually ready for transparent conductive coating applications.
This technique is based on the deposition of gaseous reactants on a solid substrate, which allows the growth of graphene on top of it. Despite the high-quality of the graphene that can be obtained this way, this technique has several limitations in its industrial application.

First of all, gaseous by-products formed during the process are usually highly toxic and difficult to remove from the highly-controlled environment of the deposition chamber.
Moreover, the overall graphene deposition is a very slow and expensive process, since it requires high quantities of energy during production and removal of the substrate. This makes the transfer of this process to industrial level trivial and, at the moment, not economically sustainable.

2.3 GRMs CLASSIFICATION AND GRAPHENE NOMENCLATURE

Since the large number of production techniques and material properties (oxygen content, defects, lateral dimensions, thicknesses, chemical functionalizations, etc.) the GRMs class collects an enormous number of different materials. Herr we report a short list of the most common GRMs following the classification proposed by Wick [54]:

- Graphene - a freestanding or supported single-atom-thick sheet of sp2-bonded carbon atoms arranged in an hexagonal geometry
- Graphene nanosheets - A monolayer graphene sheet with lateral dimensions below 100 nm
- Graphene microsheet - A monolayer graphene sheet with lateral dimensions between 100 nm and 10 μm
- Multilayer graphene (MLG) - 2D (sheet like) material consisting in stack of well-defined and countable number of single graphene layers of extensive lateral dimension. When the number of layers is below 5, it can also be indicated by few-layer graphene (FLG) or by the exact number of layers that are present in the structure (bilayer graphene, trilayer graphene)
- Graphite nanoplatelets - graphite nano-sheets or nano-flakes having dimensions below 100 nm.
- Exfoliated graphite - MLG obtained by exfoliation of graphite into thin stacks that retain the 3D crystal structure of graphite
- Graphene oxide (GO) - a highly oxidized mono- or multi-layer graphene, where the pure sp2 carbon structure is partially substituted by oxygen based groups such as -OH, =O and -O-
- Reduced graphene oxide (rGO) - a partially oxidized mono- or multi-layer graphene obtained by reduction of graphene oxide to recover the starting characteristics of graphene. This oxidation-reduction cycle can be useful since GO is much more soluble in water than graphene, so it it easier to process and transport.

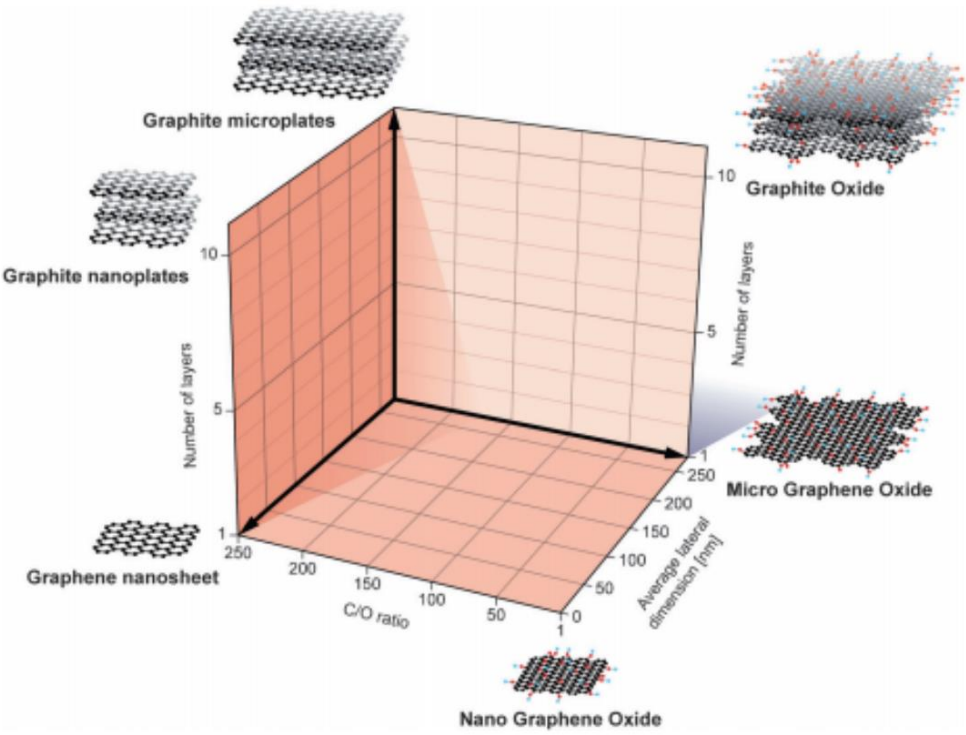

Figure 15: categorization of different graphene-related materials based on number of layers, lateral size and c/O ratio [54]

Kauling et al. [55] suggest a direct analogy between LPE and the production of oil derivatives from crude oil. Figure 16 can visually help understanding how it is possible to separate graphene materials with different number of stacked layers discerning between them through their difference in weight.

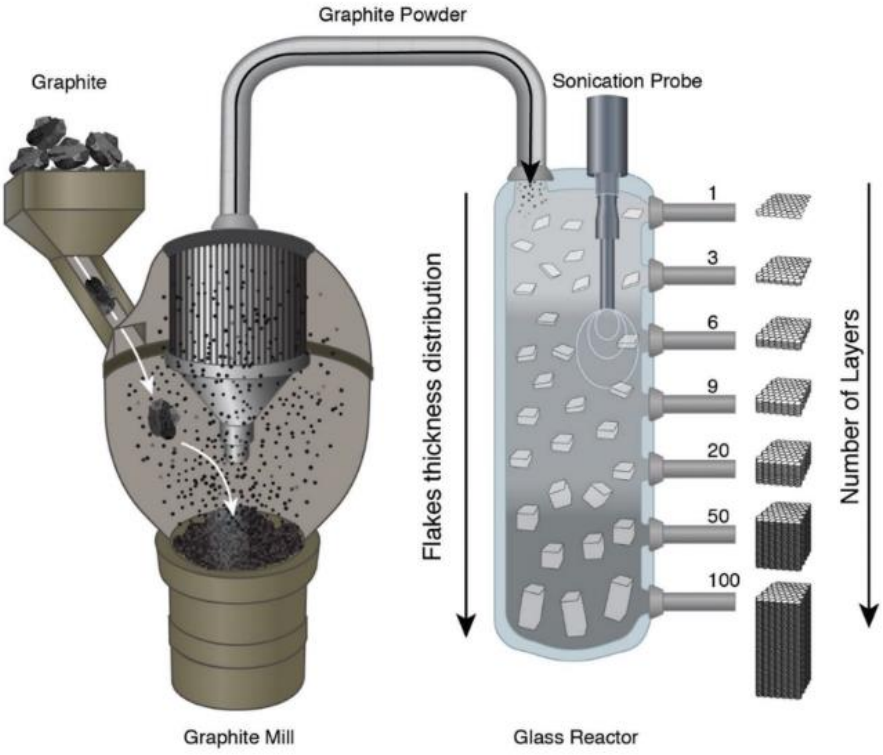

Figure 16: analogy between crude oil distillation and graphenic materials separation [55]

2.4 GRAPHENE COMPOSITE MATERIALS

Graphene and its related materials are drawing increasing attention in the field of polymeric composites.

Polymeric composites are materials in which the polymer matrix is bonded with a reinforcement material, typically in the form of short or long fibres. This can enhance the properties of the polymer or confer it new functionalities, making it suitable for different applications.

For this purpose, graphene and related materials are intensively studied as nano-fillers [56]. The unique properties of graphene could be the key for the production of multi-functional materials and can improve the mechanical properties [57] of the polymer matrix or confer it electrical conductivity [58], thermal conductivity [57] or gas barrier properties [58].

In graphene-based composites (and nano-composites in general) the interface between polymer matrix and reinforcement is maximized thanks to the 2-D dimensions and high aspect ratio of the fillers. This is a key aspect in the fabrication of composites because it can improve the dispersion of the reinforcement in the matrix and the matrix-filler interactions. For this reasons nano-composites often show superior properties when compared to microscale materials.

The industrial production of nano-composites, however, is strongly hindered by the high cost of nanodimensional reinforcements and by the complexity of the processes used to obtain high-performance composites [56].

Graphene and its related materials can offer a solution to this problem and a breakthrough technology to confer composites outstanding properties.

2.4.1 MECHANICAL REINFORCEMENT

The strong mechanical resistance of graphene can be exploited in composites, improving the overall mechanical properties of the material. As an example of the effect of graphene addition in a composite, Rafiee et al [59] produced an epoxy composite with only 0.1% weight fraction of graphene platelets. This composite outperformed pure epoxy resin in Young's modulus (+31%), tensile strength (+40%), fracture toughness (+53%) and fatigue resistance.

Graphene composites are currently being produces using a wide range of polymer matrix, including silicone, epoxy resin, polymethylmetacrylate (PMMA), polyvinylidene fluoride (PVdF), polyvinyl alcohol (PVA) and polyurethanes. These composites can be produced using different processes, both involving solution-based methods and in-situ polymerizations.

To maximize the effect of graphene reinforcement in composites it is mandatory to fine control three main parameters such as filler loading, lateral dimensions and dispersion [52] [60].
Different studies showed how loading of graphene, reduced graphene oxide or other graphene-related materials influence the mechanical properties of the composite. In particular, these studies highlighted how small differences in the amount of loaded reinforcement material reflect in strong variation of mechanical properties at low loading mass percentages. The effect of increasing the quantity of filler then starts to be less important the more the loaded mass percentage gets higher. Moreover, high reinforcement loading will also increase the brittleness of the composite, for this reason a the optimal loading amount is usually a compromise between mechanical strength, brittleness and cost of the composite.
Lateral dimension of graphene flakes and its dispersion strongly influence the way stresses are transmitted from the polymer matrix to the filler, thus also affecting the capability of the reinforcement to effectively improve the mechanical properties of the composite itself. In particular, dispersion plays a key role, and poor dispersions may completely compromise the properties of the nano-composite since it can generate weak spots or weaken the matrix-filler interactions.

2.4.2 ELECTRICAL CONDUCTIVITY

The high electron mobility and electrical conductivity found in graphene and conductive graphene-related materials can strongly improve the electrical conductivity of common thermoset polymers, which are usually insulating, when these are used as reinforcements.
For this purpose, the main target to be aimed for is the formation of a continuous conductive network of nano-filler inside the polymer matrix. The minimum concentration of filler that allows it is called percolation threshold.
Graphene nano-composites are characterized by percolation threshold values much lower in comparison to other 2-D materials thanks to its high aspect ratio that allows the different nanofiller domains to be in contact with each other even when the loaded mass is very low. As an example, Stankovich et al. [52] studied the effects of graphene addition to polystyrene polymer and showed that the percolation threshold for this composite is as low as 0.1% vol. Increasing the graphene amount also increases the conductivity of the material, that reached values of ≈0.1 S/m at 1% vol loadings, and ≈1 S/m at 2.5% vol loadings.
Bose et al. [61] studied the interaction between graphene oxide and polypyrrole, an already conductive polymer. The addition of 20% weight fraction of GO increased the conductivity of the composite form 0.19 S/cm (conductivity of pure polypyrrole) to 1.64 S/cm. A successive reduction

of the composite to reduce GO to rGO furtherly increased the conductivity to 7.93 S/cm.
In order to decrease percolation threshold, and thus the amount of graphene needed, reinforcement dispersion and lateral size play a crucial role. Both increase the probability for nano-filler domains to be in contact with each other, reducing the minimal loading needed to form a continuous conductive network between graphene sheets.

2.4.3 THERMAL CONDUCTIVITY

Despite the high thermal conductivity of graphene and its related materials, the transfer of this property in polymer composite is usually not easy, and enhancements are often not as outstanding as the ones obtained foe electrical conductivity. This is partly due to the fact that the difference in thermal conductivity between common polymers and graphene is not as high as their difference in electrical conductivity.
GNPs are the most studied graphene-related material as filler for thermally conductive composites. Improving thermal conductivity using GNP was demonstrated for epoxy, polypropylene (PP), polyethylene (PE), polyamide (PA) and other polymers.
Teng et al [62], for example, charged epoxy resin with graphene nanoplatelets, enhancing its thermal conductivity from 0.2 W/mK to 1.6 W/mK.
For the purpose of enhancing the thermal conductivity of nano-composites, different studies highlighted the importance of graphene exfoliation and lateral size, graphene domain orientation inside the composite and polymer-graphene surface interactions.

2.4.4 GAS AND WATER BARRIER

The monoatomic honeycomb lattice of graphene makes it impermeable to water and gases. This interesting property can be exploited in nano-composites for a wide range of different applications.
Many studies acknowledged how GRM-reinforcement in composites can confer hydrophobicity to normally hydrophilic polymers (e.g. PVA) and improve its gas barrier properties to different gases, which is especially interesting for packaging applications [63].
For this latter purpose, graphene dispersion in the composite is of crucial importance, since it helps maximizing the length of the path the gas has to travel inside the polymer matrix.

2.5 APPLICATIONS OF GRAPHENE-BASED COMPOSITES

2.5.1 ENERGY AND ELECTRONICS

The electrical properties of graphene combined with its mechanical flexibility and its huge surface area make graphene-based nanocomposites very interesting for energy harvesting, conversion and storage applications and, in general, for a wide range of electronics applications [64].

Graphene composites are currently studied both as active medium and as electrode material in solar panels. Different studies show how graphene/PEDOT (poly 3,4-ethylenedioxythiophene) composites can substitute usual indium-tin oxide electrodes in organic solar cells (OSC), even improving the overall performances of the photovoltaic devices [65] [66].

Exfoliated graphene and CVD graphene were also deposited on polyacrylonitrile and on a PEDOT-PEG (polyethyleneglicole) block copolymer respectively. These electrodes were applied in traditional and inverted solar cells, improving their overall efficiencies up to 6% and keeping these performances even after hundreds of bending cycles [67].

Even though the lack of a band-gap hinders the possibility to use graphene as channel material for high-performance integrated logic circuits, it can still be exploited for other general electronics applications. Composites made of graphene and conductive polymers (such as PANI and PPy) may improve these polymers' electrochemical properties enough to be used as electrodes in supercapacitors. Devices that exploit these composites show outstanding specific capacitance values that can be higher than 700 F/g and improved cyclic stability [68].

Furthermore, GO is heavily studied as material for new generation flexible transistors, especially in combination with low band-gap semiconductive polymers (such as P3HT). The obtained devices show improved conductivity, good optical transparency and excellent stability to bending cycles [69].

2.5.2 SENSORS

Carbon-based materials, but especially graphene and its derivatives, exhibit outstanding development prospects for sensing applications. In detail, the most recent researches are focusing on strain sensors [70], temperature sensors and electrochemical sensors [71], since these type of applications are the ones that may benefit more from the electrical and mechanical properties of graphene.

Flexible strain sensors are increasingly studied for physiological motion and human-computer interaction applications, mainly because they exhibit excellent performances in the detection of both large body strains (e.g. joint movements) and subtle facial expressions.
These sensors can react efficiently to different types of deformation, such as bending, stretching, pressing and torsion. The main goal at the moment is the production of sensors, or sensor arrays, that are able to respond to different strain simultaneously, while discerning these deformations in different output signals [70]. Strain sensors produced using graphene and its derivatives show outstanding Gauge Factor, sensitivity and reproducibility over thousands of strain cycles.
For electrochemical sensors, on the other hand, GO is the most studied graphene derivative because the presence of oxygen-containing groups on its surface makes it easy to functionalize and improves its interaction with analytes. This, however, compromises its electrical properties. Hence, researchers started using its reduced form, rGO, exploiting its compromise between surface modification availability and good electrical conductivity.
As an example, Sahiner et al. [72] functionalized polyaniline and polypyrrole with L-ascorbic acid reduced graphene oxide to obtain CO_2 sensitive composites with greater performances in comparison to pure polymers.

2.5.3 MEMBRANES AND ENVIRONMENTAL APPLICATIONS

Membrane separation is one of the main technologies used and studied to address environmental problems. For this kind of application, ultra-thin graphene membranes have attracted increasing attention thanks to their nanopore morphology and their feasibility to be functionalised. Thanks to these properties, graphene laminates and composites are suitable materials for the production of high permeate flux and improved selectivity membranes [73].
Cohen-Tanugi et al. [74] showed how nanoporous single-layer graphene is active for water desalination purposes. Its performances are even better than a conventional reverse osmosis membrane. In fact, they both show a similar salt rejection of 99% but nanoporous graphene has an outstanding 66 L/cm^2 water permeability, almost 3 times higher than the one measured for the conventional membrane.
Several studies in recent years showed outstanding results for different membranes applications, such as ion separation, energy storage, water desalination and gas separation.
Among the graphene related materials, graphene oxide is the most studied in industrial scale thanks to its low price, easy functionalization and large surface area. It is especially known as active material for the removal of metal ions, organic compounds and gases from aquatic environment.

Moreover, the high electronic mobility typical of reduced forms of graphene related materials makes them suitable for the production of membranes that can be applied in the fields of energy production and contaminant sensing [73].

3. ELECTROSPUN GRAPHENE-POLYMER COMPOSITES

Electrospinning is widely employed to produce nanostructured graphene-based composites. These materials can exploit the advantages of both their nanometric structure and of graphene reinforcement, leading to a wide range of different composites with unique properties [75] [76].
The main challenge in the production of nanostructured composites is to achieve proper dispersion and alignment of the nanofillers inside the polymeric matrix, which is even more difficult at the nano-scale than in macroscopic composites. The strong Van Der Waals interactions between nanocarbons induce their aggregation and, as a result, compromise their efficient dispersion [77]. To overcome this obstacle, researchers found different technique to obtain well-dispersed electrospun graphene-based composites using as matrix a wide array of polymers.
The obtained composites show enhanced mechanical, electrical and thermal properties when compared to relative electrospun polymers [78]. Furthermore, other properties unique to graphene and other graphene-related materials are observed in these composites, making them suitable for applications in microelectronics, flexible electronics, sensors, biology, energy harvesting, filtration membranes and others.

3.1 MATERIALS FOR ELECTROSPUN GRAPHENE-POLYMER COMPOSITES

Over 100 polymers have already been studied and tested as matrix for electrospun composites. The main constraint for the successful electrospinning of a certain polymer is the possibility to obtain a solution with the appropriate features, such as viscosity, surface tension, polymer concentration and high solvent volatility.
Many polymer commodities satisfy such crucial requirement. Some examples are polyamides, polyethylene terephthalate, polystyrene and polymethylmethacrylate.
In recent years, the increasing requirement for high-performance, sector specific applications shifted the attention of researchers to less common polymers. Bio-polymers and polymers obtained from biological sources, such as polylactic acid, silk fibroin, chitosan and chitin, are attracting a lot of interest [77]. Other interesting polymers include polyacrylonitrile, which is often used as a precursor for the formation of carbon nanofibers, polypyrrole, a conductive polymer, and polyvinylidene fluoride, for its outstanding piezoelectric coefficient.
Among all the possible fillers, nano-structured carbon materials are drawing the interest of scientific community in the latest years for the outstanding properties they can confer to electrospun

composites [79]. Many articles acknowledge the importance of graphene, graphene oxide, graphene nanoplatelets, carbon nanotubes and other nanocarbons in this research field, and successfully obtained superior functional composites with these reinforcements.

The choice of the appropriate filler for a specific matrix depends not only on the final material requirements in term of properties, but also on the interactions between the two phases. These can strongly affect the solution rheology and conductivity, as well as the effective dispersion of the filler. For this reason, an appropriate control over the reinforcement concentration and its chemistry is crucial to determine the morphology of the final material and its properties.

3.2 TECHNIQUES FOR THE PREPARATION OF COMPOSITES

Matrix-filler interactions are often not strong enough to ensure an effective dispersion of the reinforcement. Thus, researchers studied different ways to improve it by modifying the electrospinning process, the interactions in the electrospinning solution or by post-processing the electrospun material [79].

3.2.1 CO-ELECTROSPINNING

The easiest technique to produce composites through electrospinning is the co-electrospinning. In this case, the electrospinning process is performed on a composite solution obtained by accurately mixing the polymeric solution and the filler [80].

The most common filler for successful co-electrospinning processes is GO, since the presence of O-containing groups on its surface increase its interactions with most polymers (usually this occurs via hydrogen bonding), preventing the nanofiller aggregation and improving its dispersion. When required by the target application, a successive reduction to rGO can be performed on the electrospun composite.

Many different polymers and polymeric blends are able to be co-electrospun with GO as a filler. To further improve the interaction between the two phases and the filler dispersion, the electrospinning composite solution is usually sonicated. In alternative, several studies report that the addition of a stabilizer, such as Triton x-100 or sodium dodecyl sulphate, can reduce the surface tension and assist in the dispersion of the nanofiller.

The main advantages of this technique are its simplicity and the optimal adhesion of the nanofiller, which will be dispersed in “bulk” inside of the polymeric matrix. Moreover, the addition of nanocarbons directly inside the polymeric solution can be exploited to modify and finely adjust

important solution parameters such as its rheology and conductivity, improving the overall electrospinning process.

3.2.2 NANOFILLER MODIFICATION

The crucial role that matrix-filler interactions play in electrospinning makes the chemical functionalization of the filler one of the most explored routes for improving the solution dispersion.
GO is the most studied graphene-related material since the hydroxyl and carbonyl groups on its surface are optimal substrates for a chemical modification.
Leyva-Porras et al. [81] modified GO with the insertion of nitroxide groups using an oxoammonium salt (Br-TEMPO). The resulting modified GO showed an improved exfoliation in a PA6 polymeric solution, leading to embedded, well dispersed thin platelets of GO in polymer nanofibers after co-electrospinning.
A different study, by Zhang et al [82][14], obtained similar results not inducing the exfoliation between GO sheets, but improving matrix compatibility of GO domain with the PLA matrix. To achieve this result, they grafted PEG polymeric chains on GO functional groups through an esterification reaction. Results demonstrate that the improved compatibility between PLA and PEG-grafted GO lead to nanofibers with superior mechanical and thermal properties.
Graphene functionalization is more difficult since its oxidation may lead to the formation of defects. However, achieving good dispersion of graphene sheets, as compared to graphene oxide, is extremely challenging due to Van der Waal's forces induced aggregation. For this reason, graphene functionalization is an exciting topic for electrospinning researchers and it may allow to properly produce graphene-polymer composites without the intermediate GO reduction step.
Das et al. [83] used exfoliated graphite using a combination of sonication and polyvinylpyrrolidone grafting, obtaining a PVP-modified graphene. This functionalization improved the graphene interactions with the chosen polymeric matrix, polyvinyl alcohol. The results show that the electrospinning process was improved, resulting in ultrathin, defectless composite nanofibers. Moreover, thanks to the more homogeneous dispersion of graphene inside the polymeric matrix, the electrospun composite exhibited a notable enhancement in thermal properties and crystallinity.

3.2.3 POST-TREATMENT OF ELECTROSPUN POLYMERS

A different approach for the production of graphene-polymer composites is the post-treatment of pure polymer electrospun nanofibers to deposit graphene derivatives on the surface of the nanofibers.

This two-step approach can easily overcome the issue of graphene dispersion inside the electrospinning solution, not needing a graphene/polymer composite solution. Moreover, the deposited graphene layer on top of the nanofibers is completely exposed to the surface and to external stimuli, which is crucial for certain applications.

The downside, however, is that the adhesion of the filler is not as good as for a "bulk" dispersion inside the polymeric matrix. For this reason, the graphene coating may deteriorate or detach from the nanofibers as a consequence of mechanical stresses, such as stretching, bending or etching.

Some of the techniques used for graphene deposition include dip-coating, electrodeposition, hot pressing and vacuum filtering. Among these, dip-coating is by far the most studied for its simplicity, low cost and scalability.

In a typical dip-coating process, the electrospun mat is soaked in a graphene derivative solution to allow the filler particles interaction with the polymer. The dipping solution must be obtained from a solvent that is not a solvent of the electrospun polymer and the graphene derivative concentration must be adjusted based on the morphology and chemistry of the electrospun substrate.

The quality of the deposition in strictly related to the strength of the interaction between the coating and the substrate. The optimization of the deposition allows to obtain composite materials with continuous, homogeneous coatings characterized by improved mechanical resistances.

To strengthen the coating adhesion, GO is often used as coating material in order to exploit its greater affinity with the polymeric substrate and the hydrogen bonds that it forms with the functional groups of the polymer. Moreover, GO is easier to disperse in water, which is a cheap, non-hazardous solvent that does not interact with the majority of common polymers.

Other effective techniques for improving adhesion of both oxidized and reduced graphene derivatives include the use of an adhesive or coupling agent layer between polymer nanofibers and graphene coating, using a graphene composite as coating agent or depositing a graphene-based ink.

Nikolaev et al. [84] produced conductive textiles coating commercial nylon and cotton textiles with GO, then reducing it with hydrazine vapours. The commercial fabric were first functionalized with bovine serum albumin (BSA) as an adhesive layer to improve the strength of the conductive coating. Afterwards, these samples were dip-coated using a 3 mg/mL GO solution and then reduced chemically to rGO. The obtained samples showed good electrical conductivity (from 1 to 9 kΩ/sq

for rGO cotton samples) and, thanks to the use of BSA, a good mechanical resistance to washing (up to 40 washing cycles).

3.3 PROPERTIES OF ELECTROSPUN GRAPHENE-BASED COMPOSITES

3.3.1 MECHANICAL PROPERTIES

To understand the influence of graphene addition in graphene-based composites, several studies were analysed and their results were compared with the properties of pure polymer electrospun nanofibers (Table 3). Moreover, these results were also compared with the properties found in electrospun composites produced using different carbon-based fillers, such as carbon black, fullerene, graphite, nanodiamonds and carbon nanotubes [79].

Graphs in Figure 18 report the collected data for three main values: tensile strength, Young's modulus and elongation.

From the collected data, it is possible to evince that graphene based nanofillers in composites have a great effect in improving the mechanical properties of the material. In particular, tensile strength and Young's modulus are positively enhanced by charging the polymer with nanocarbons, with the only exception of carbon black. Graphene-based nanofillers, in detail, can improve the tensile strength of pure polymer by up to 5000% [85] and its Young modulus by up to 7500%. For comparison, the most effective non-graphenic filler are carbon nanotubes, whose maximum performances are about 5 times lower for tensile strength and 2 times lower for Young's modulus.

The effect of nanofillers on elongation is not always positive, in accordance to the fact that usually materials with greater tensile strength are more brittle and show lower elongations at break. For this reason, only some researches show enhancements in elongation by the addition of nanocarbons. Despite this, graphene-based composite show higher increases and lower decreases in elongation when compared to their respective non-graphenic ones.

The difference in effect between graphene nanofillers and other nanocarbons can be ascribed to their intrinsic properties, which affect the interaction with the matrix and their dispersion. In general, it is possible to observe that strong, well-dispersed nanofillers with strong interactions with the polymer lead to the formation of composites with the best mechanical properties.

The full study conducted by Lee et al. [79] also highlights that the most used and effective technique for the production of mechanically enhanced electrospun composites is co-electrospinning, since the high dispersion and contact area with the polymer matrix improve the effect of graphene fillers on mechanical properties.

Table 3:Enhancement of the mechanical properties of electrospun polymers by graphene-based nanofiller additivation [79]

Nanofiller	Polymer	Nanofiller Treatment	Fabrication Technique	Loading (wt%)	Tensile Strength (MPa)		Young's Modulus (GPa)		Elongation at Break (%)	
					Composite	Control	Composite	Control	Composite	Control
Graphene	PLLA in PBS	–	Co-electrospun + cured	1.3	24.7	22.5	–	–	3.5	4.4
Graphene	Polyvinylidene Fluoride	–	Co-electrospun	1	2.5	0.7	0.72	0.41	–	–
GO	PVA	Glycine grafted + Gold NP deposition	Co-electrospun	0.5	–	–	–	–	–	–
GO	PLA	PEG grafted	Co-electrospun	5	5.2	2.1			84	97
GO	Polyimide	–	Co-electrospun	2	–	–	–	–	–	–
GO	Chitosan/ Cellulose	–	Co-electrospun	1.5	35	21	.73	.34	9.5	16
GO	PVA	–	Co-electrospun	0.02	9.37	0.22	–	–	180	145
GO	PLGA-co-PPF	PGA functional-ized + PPF copolymerized	Co-electrospun with HA	5	79.1	40.9	3.78	1.75	3.78	5.31
GO	PLA	–	Co-electrospun with HA	2	0.57	0.27	0.01673	0.00858	–	–
GO	Poly(carbonate urethane)	–	Co-electrospun	1.5	35.6	11.67	–	–	–	–
GO	Silk	–	Dip coated + in-situ reduction	5 immersion cycles (1 mg/ml)	1.8	1.6	0.023	0.020	9	13.9
GO	PAN	–	Co-electrospun	0.5	171	68	–	–	10.15	12.67
GO	PVDF	–	Co-electrospun	0.7	~9.3	~5.5	–	–	–	–
GO	PLGA/silk tussah	–	Co-electrospun	1	~9	~3	~0.055	~0.010	~150	~275
GO	PVAc	Non covalent PPV bonded	Co-electrospun	0.07	9.52	6.13	0.456	0.513	96.8	12.4
GO	PVAc	PBASE modified	Co-electrospun	0.07	12.39	6.13	0.642	0.513	52	12.4
GO	PVAc	4-(2-(pyridin-4-yl)vinlyl)Phenyl-modified	Co-electrospun	0.07	11.78	6.13	0.598	0.513	82.5	12.4
rGO	Silk	–	Dip coated + in-situ reduction	5 immersion cycles	1.6	1.6	0.0261	0.02	7.1	13.9
rGO	Silk	–	Dip coated + in-situ reduction	5 immersion cycles (3 mg/ml)	1.9	1.6	0.0318	0.020	8.9	13.9
rGO	PVA	–	Co-electrospun	2	5.51	2.97	0.08567	0.06473		
rGO	PCL	Copolymerized with PDDT	Co-electrospun	2	86	1.52	0.394	0.005438	32	54.34
rGO	PCL	Copolymerized with PTet	Co-electrospun	2	56	1.52	0.407	0.005438	45	54.34
Graphite	PAN	–	Co-electrospun	4	–	–	~2	~1	–	–
Graphite	PAN	–	Ultrasonic Embedding	5.1	–	–	–	–	–	–

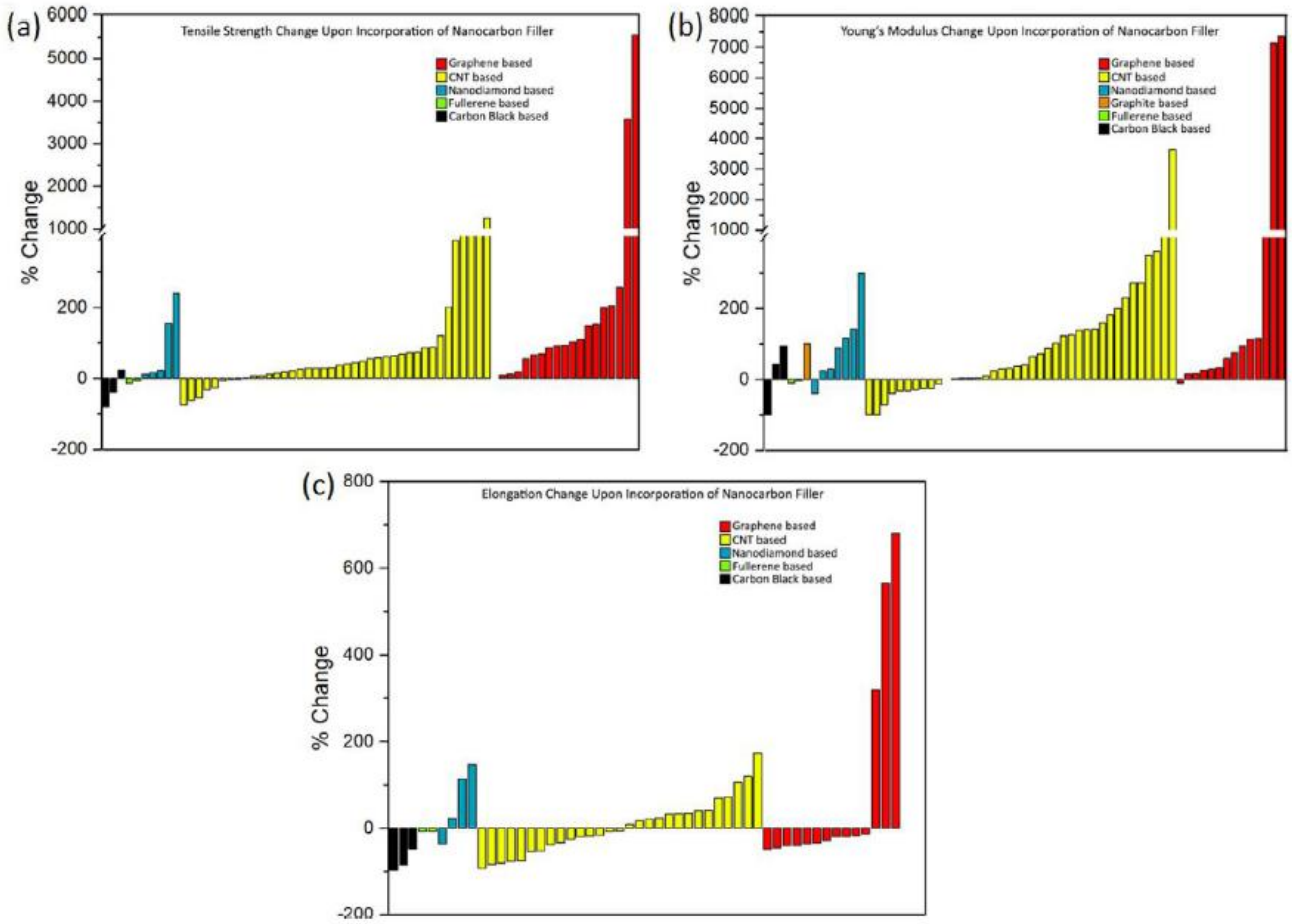

Figure 17: Bar charts comparing the mechanical properties enhancement on a) Tensile strength, b) Young's modulus, c) Elongation caused by additivation of different nanocarbons [79]

As expected, functionalized nanofillers have in most cases a better behaviour than non-functionalized ones. This is mainly because their improved dispersion and stronger interaction with the matrix can enhance the load transferring from the polymer to the strong filler.

Another important conclusion of this study is that in many cases, there exists an optimum loading of the nanofiller for the maximization of the mechanical properties, and interestingly it is usually a low loading. For example, none of the considered studies that used graphene nanofillers worked with a filler loading higher than 5%.

Even though all observations are consistent with the predictions and expectations, it is also important to notice the wide spectrum of results between the various studies. This is strongly due to the high variability among these works when considering other parameters, such as molecular weight and crystallinity of the polymer, aspect ratio of the nanofiller and even diameter and porosity of the electrospun nanofibers.

This should be a remark of the great potential of graphene-based composites but also that each different material and application must be addressed separately and accurately optimized to achieve the best possible result.

3.3.2 ELECTRICAL PROPERTIES

Production of conductive electrospun composites is becoming a crucial topic in the latest years, since the vast majority of conductive polymers (for example polypyrrole, polyaniline and PEDOT) cannot be easily electrospun, if not blended with other polymers, due to their low molecular weight, poor solubility and rigid backbone structure [86].

Incorporation of graphene-based nanofillers in polymeric composites is a well-known solution for the improvement of the electrical properties of the polymer. Electrospun polymers are also suitable for this modification, but their nanometric morphology hinders the formation of a continuous conductive path of nanofiller domains in "bulk" inside the polymeric matrix.

For this reason, graphene-based electrospun composite usually show higher percolation thresholds and lower conductivities when compared to non-nanostructured composites. This is mainly because good reinforcement dispersion, which is hardest to achieve in electrospun composites than in the others, is crucial for decreasing the percolation threshold of a material.

On the other hand, electrospun polymers are appropriate as a substrate for conductive coatings. In this case, by coating with conductive graphene-based materials, the highly interconnected surface of the nanofibers acts perfectly as a scaffold that is able to guide the conductive domains to the formation of a continuous, branched conductive network.

Table 4 summarizes the most interesting articles found in literature using graphene-based fillers and common, industrially known polymers for the production of conductive electrospun composites.

Nanofiller	Polymer	Nanofiller Treatment	Fabrication Technique	Loading (wt%)	Electrical Conductivity (S/cm)		Sheet Resistance (Ω/sq)		Ionic Conductivity (S/cm)		Dielectric Constant		Specific Capacitance (F/g)	
					Composite	Control	Composite	Control	Composite	Control	Composite	Control	Composite	Control
Graphene nanoribbon + mwCNT	Polyimide	partial unzipping of mwCNT	Co-electrospun (aligned parallel)	9	8.3	–	–	–	–	–	–	–	–	–
Graphene nanoribbon + mwCNT	Polyimide	partial unzipping of mwCNT	Co-electrospun (aligned perpendicular)	9	7.2×10^{-6}	–	–	–	–	–	–	–	–	–
Graphene	Polypyrrole/Carbon Nanofiber	–	Electrodeposition	+0.8 V bias (0.1 mg/ml GO, 0.1 M NapTS, 0.1 M Ppy)	–	–	–	–	–	–	–	–	386	–
Graphene	PVA	–	Co-electrospun	1	1.56×10^{-5}	4×10^{-8}	–	–	–	–	–	–	–	–
Graphene	PCL/Gelatin	–	Co-electrospun	2	5.16×10^{-5}	3.7×10^{-6}	–	–	–	–	–	–	–	–
Graphene	PAN	–	Co-electrospun	8	–	–	–	–	3.31×10^{-6}	1.83×10^{-6}	8.5	3.5	–	–
Graphene	PMMA	–	Co-electrospun	8	–	–	–	–	5.52×10^{-6}	3.97×10^{-6}	8.5	3.5	–	–
Graphite	Polyurethane	–	Ultrasonic Embedding	5.1	3.8×10^{-3}	10^{-14}	–	–	–	–	–	–	–	–
GO	Nylon 66	–	Co-electrospun + thermal reduction	5	–	–	2.8×10^{4}	10^{12}	–	–	–	–	–	–
GO	PI	–	Co-electrospun	0.1	1.23×10^{-14}	7.74×10^{-15}	–	–	–	–	–	–	–	–
GO	PANI/PVDF	–	Co-electrospun	18	–	–	–	–	–	–	–	–	170.63	–
GO	PVAc	PBASE modified	Co-electrospun	0.07	2.39×10^{-3}	9.92×10^{-4}	–	–	–	–	–	–	–	–
rGO	PCL	Copolymerized with PDDT	Co-electrospun	2	1.38	–	–	–	–	–	–	–	–	–
rGO	PCL	Copolymerized with PTet	Co-electrospun	2	0.81	–	–	–	–	–	–	–	–	–
rGO	PVC/PLGA	–	Electrospun into GO solution + reduction	1 immersion cycle (0.1 mg/ml)	10	–	–	–	–	–	–	–	–	–
rGO	Polyurethane	–	Dip coated in GO, then Ag nanoparticle solution	9.8	–	–	<10	10^{14}	–	–	–	–	–	–
rGO	Polyamide 66	PVP non covalent attachment	Dip coated in GO-PVP solution + annealing	1 immersion cycle (0.05 wt%)	–	–	8.6×10^{3}	–	–	–	–	–	–	–
rGO	Polyurethane	–	Layer-by-layer assembly + reduction	15 immersion cycles (1 wt% GO solution)	0.168	10^{-14}	–	–	–	–	–	–	–	–

Table 4: Electrical properties enhancement by additivation of common polymeric matrix with graphene-based nanofillers [79]

It can be clearly seen how “bulk” co-electrospun composites reach maximum conductivities around 10^{-3} S/m under these conditions, while coated electrospun mats can outperform them in almost every case, with conductivity values in the order of 1 to 10 S/m.

Another noticeable detail from this research is that the percolation threshold sets around 2% for the majority of the articles that were taken into exam. The main techniques for decreasing this value are the use of GO as graphene-based filler and the functionalization of the conductive nanofiller. These two different approaches both aim to increase the matrix/filler interaction, thus improving the dispersion of the nanofiller.

As an example, Pant et al. [87] produced an rGO/PA6 composite starting from a GO/PA6 solution in a formic acid/acetic acid solvent system. Using GO during co-electrospinning improved the dispersion of the nanofiller, and its good conductivity was later restored by reducing the GO domains to rGO using a hydrothermal process. The resulting mats showed conductivities in the order of 10^{-4} S/m.

Sarvari et al. [85] followed a different approach: rGO was selected as graphene-based nanofiller and added at different concentrations to a Polycaprolactone solution in DMSO.

To facilitate the dispersion of the nanofiller, they functionalized rGO with different thiophenes (3-TAA, 3-DDT and 3-Tet) that can increase its affinity with the polymeric matrix. In this case, the influence of the functionalization was verified by mechanical properties measurement. In detail, Young’s modulus of functionalized rGO/PCL mats was about 400 MPa compared to rGO/PCL mats that reached only 280 MPa. The obtained mats show electrical resistances in the order of 10^{-3} S/m.

Higher conductivities can be achieved by rGO coating on top of the nanofibers. As an example, Huang et al. [88] coated rGO on top of aligned and random electrospun PCL fibres through a vacuum filtration method. The obtained composites showed no increase in conductivity for concentrations of the rGO coating solution lower than 0.1 mg/mL. For higher concentrations, the resistivity of the obtained composites was found to be 0.1 S/m, and for higher concentrations (up to 0.2 mg/mL) it reached 3-4 S/m, although the higher amount of deposited nanofiller compromised partially the surface morphology of the nanofibers.

Apart from conductivity, additivation of polymers with graphene-based nanomaterials may be beneficial also for other interesting electrical properties of the material, such as its capacitive performance.

Ahn et al. [89] demonstrated that the addition of layered graphene oxide sheets could act as charge-trapping sites in a triboelectric nanogenerator, increasing its overall performances in terms of charging current, power output, specific capacitance and cycling stability.

3.3.3 THERMAL PROPERTIES

The intrinsically good thermal conductivity and stability of graphene and of its related materials makes them suitable as nanofillers for the improvement of the thermal properties when incorporated in a composite.

Table 5 collects data from different articles that studied the improvement of thermal properties in an electrospun polymer matrix after its additivation with nanocarbons as fillers.

Several studies reported how electrospun hybrid nanofibers imbued with nanocarbons have shown enhanced thermal behaviour compared to their pristine counterparts. In particular, thermal stability, glass transition temperature and thermal conductivity showed appreciable improvements for almost every tested composite formulation. Also for thermal properties, as it was discussed for mechanical and electrical ones, the dispersion of the nanofiller inside the polymeric matrix plays a crucial role in the effective improvement obtained in the final material.

Wu et al. [90] also demonstrated how, for thermal properties especially, increasing the nanofiller loading above the optimal amount actually leads to a decrease of the properties. In detail, they focused their research on the decomposition onset temperature in a glycine modified GO/PVA nanofibers system. The optimal amount of GO loading was found to be 0.5% w/w; with this composition, the material exhibited a decomposition onset temperature of 288.0°C.

When the filler content was increased to 1.0%, this value decreased to 284.9°C, suggesting a negative effect of the increasing nanofiller content after the optimal value. They suggested this could be attributed to the agglomeration of GO domains when its concentration in the polymer matrix is too high

Table 5: Enhancement of thermal properties of common polymeric matrixes by additivation with nanocarbon fillers [79]

Nanofiller	Polymer	Loading (%)	$T_{decomposition}$ (°C)		T_{glass} (°C)		Coefficient of Thermal Expansion (/°C)		Thermal Conductivity W/(m K)	
			Composite	Control	Composite	Control	Composite	Control	Composite	Control
mwCNT	PAA	3	~260	~225	~260	~260	–	–	–	–
mwCNT	PAN	5	292	268	–	–	–	–	–	–
mwCNT	PAN	10	–	–	94	83	–	–	–	–
mwCNT	PAN	20	–	–	–	–	13×10^{-6}	180×10^{-6}	–	–
GO	PVA	0.5	288	268.5	69.19	66.38	–	–	–	–
GO	PVA	1	284.9	268.5	69.5	66.38	–	–	–	–
mwCNT	PVDF/PANi	10	–	–	~170	160	–	–	–	–
CB	PU	4.58	284.35	276	–	–	–	–	–	–
CB	PU	12.6	269.70	276	–	–	–	–	–	–
mwCNT	PI	10	610	582	–	–	–	–	–	–
Graphene	PVA/PVP	0.5	–	–	73	74	–	–	–	–
Graphene	PLA	0.5	337.9	319.3	–	–	–	–	–	–
GO	PVDF	0.7	466	465	–	–	–	–	–	–
mwCNT	PVDF/HFP	3	–	–	–	–	–	–	0.065	0.052
Graphene	PAN	8	–	–	–	–	–	–	2.7	1
Graphene	PMMA	8	–	–	–	–	–	–	5	1
mwCNT	PCL	5	–	–	56.26	66.5	–	–	–	–
Graphene	PANi/PEO	5	321	285			–	–	–	–
GO	PVA	8mg	245	259	78	69	–	–	–	–
Graphene	PVAc	0.07	335	330	–	–	–	–	–	–
Graphene	PVA	2	281	197	–	–	–	–	–	–
Graphite	PU	5.1	403.4	360.7	–	–	–	–	–	–
GO	PVA	5	283.7	257.7	–	–	–	–	–	–
rGO	PVA	5	273.4	257.7	–	–	–	–	–	–
Graphene	PA	1.5	–	–	58.25	48.73	–	–	–	–
mwCNT	Nylon	7.5	–	–	92	85	–	–	–	–
mwCNT	PI	10	560	501	–	–	–	–	–	–
Graphene	PBS/PLLA	1.3	379	376	–	–	–	–	–	–
GO	PGA-co-PFF	5	356	326	–	–	–	–	–	–
mwCNT	Nylon	0.056	360	320	–	–	–	–	–	–
GO	PLA	3	–	–	62.5	56.2	–	–	–	–
mwCNT	PLLA	4	–	–	60.5	60.3	–	–	–	–
mwCNT	PDLA	4	–	–	60	59.5	–	–	–	–
mwCNT	PCL	0.5	360	316	–	–	–	–	–	–
GO	PVA	0.2	245	295	–	–	–	–	–	–
Graphene	PVA	0.08g	393	383	–	–	–	–	–	–
mwCNT	PBT	5	425	416	–	–	–	–	–	–
rGO	PU	9.8	~400	~375	–	–	–	–	–	–
Nanodiamond	PLA	3	57	52	–	–	–	–	–	–
GO+HA	PLA	8.6+4.3	338.8	228.9	–	–	–	–	–	–
mwCNT	PCL	5	340	310	–	–	–	–	–	–
nwCNT	PCL	1	–	–	62.17	61.68	–	–	–	–
GO	PI	2	603	503	323	317	–	–	–	–
GO	PLA	5	341.9	328.4	–	–	–	–	–	–
mwCNT	PVB	10	290	295	–	–	–	–	16.8	–

3.4 GRAPHENE-BASED COMPOSITE NANOFIBERS APPLICATIONS

Graphene-based composite nanofibers find applications in several fields, thanks to their unique superior properties and their intrinsic multifunctionality [78].

Their enhanced mechanical and electrical properties, coupled with the possibility to produce biocompatible composites, makes them promising as scaffolds for tissue engineering. Further studies are needed to prove the low cytotoxicity of these materials, but they are already showing great potential for bone, cartilage, neural, cardiac and skeletal tissue engineering [77] [91].

Another possible application is environmental remediation, especially for water and air treatment. Their incredibly large contact area and porosity ensure high permeability to fluid streams, while still providing a huge amount of sites for interactions with contaminant molecules. In addition, the presence of graphene-based nanofillers can increase their mechanical stability and the wide variety of possible functionalizations on graphene surface may selectively improve their interaction with specific contaminants. Several studies demonstrated that GRMs addition in electrospun composites significantly increase their performances on the adsorption and filtration of dyes and organic compounds in liquid [79].

In the electronics field, their large surface area, fast response to stimuli and enhanced electrical properties makes them suitable for different applications [92] [93], such as energy harvesting (in the form of dye-sensitized solar cells [94] or triboelectric nanogenerators), energy storage [93] (as components for batteries [95] [75], supercapacitors [96] or fuel cells), sensors [97] and FETs or actuators for nanoelectronics.

For the purpose of this thesis, the main target applications are in the market sector of smart textiles and flexible and wearable electronics.

3.4.1 GRAPHENE-BASED COMPOSITES IN WEARABLE ELECTRONICS

Wearable electronics are small electronics devices worn by a person to provide intelligent assistance. The main components needed for the production and integration of these devices are electronic textiles (e-textiles).

E-textiles are textiles that contain an electrically conductive component. Their combination with miniaturized electronic devices is the core technology for wearable electronics and smart textiles market.

The e-textiles global market is relatively new (around 30 years old) and in 2020 its overall value was estimated around 1 to 4 billion dollars. Despite its study started only in recent times, the market

size is constantly growing every year, reaching billions of people in the world with the market entry of smartphones, smart watches, smart glasses and other similar devices. Many experts think that this growing trend can be foreshadowing a true explosion in this market if a breakthrough technology is able to improve the devices performances and reduce their cost [98] [99].

At the moment, the vast majority of e-textiles are produced using metal-based materials. Although metals are certainly optimal for producing low-resistance materials, many intrinsic problems arises when they are used for wearable applications.

First of all, there are concerns on the safety of metal-based conductive materials when they are in close contact with the human body and with flammable materials. Moreover, metals are notoriously susceptible to chemical corrosion and oxidation (which can be even more important in everyday, environment-exposed applications. Metals are also relatively heavy when compared to common clothing item, and they can be not optimally flexible, hindering the comfort of many wearable devices. Regarding the e-textile end-of-life, the recycle of metals coupled with common fabrics and polymers is trivial and this is a big hurdle that is necessary to overcome for the mass production of e-textiles.

One of the most promising solution to all of these problems could be replacing metals with conductive graphene-based composite and textiles. Graphene and its related materials offer a series of advantages when compared to metals that could overcome the main obstacles that still prevent the widespread diffusion of e-textiles.

Graphene composites can retain the flexibility and comfort of fiber-based polymers and fabrics, their weight is lower than metal-based conductive textiles and easier to recycle since they are all carbon-based materials. Moreover, graphene composites are more resistant to oxidation and corrosion than metals and they could be easier to integrate in electronic devices [100].

The main concerns that still prevent graphene technology to replace metal-based technology are its cost and its mechanical and electrical properties. In fact, despite graphene shows outstanding electrical conductivity and mechanical resistance, these properties are not always easy to transfer composites. In particular, conductive textiles produced using GRMs as fillers usually reach electrical conductivities that are not high enough for their application in e-textiles. Moreover, these materials needs to resist to numerous bending and stretching cycles, caused by the everyday movement of the human body and, more importantly, by the washing of the wearable devices.

Thus, there is a strong interest on innovative technologies for the integration of graphene in wearable textiles that can improve their electrical conductivity and mechanical resistance. When this will be achieved, graphene composites could be exploited for different applications in the wearable electronics market [100].

Recent market studies and forecast indicates that the main possible applications could be for actuators, such as heaters or nanogenerators [101], for sensors [102] [103] or for shielding elements [104].

4. COMPOSITE MATS ELECTROSPINNING: MATERIALS AND APPARATUS

The following paragraph summarizes the materials used in this thesis for the production of electrospun composite mats, with particular focus on the properties that can be beneficial for the target applications. Subsequently, the electrospinning apparatus that was used for the production of these materials will be explained in detail

4.1 POLYMERIC MATRIX

Polymer matrixes are selected in view of different requirements of the final composites for the targeted applications, which may include mechanical properties as well as the recyclability and environmental impact. Some polymers may also confer the final composite other interesting properties, such as tribo- or piezo-electric properties or affinity towards specific analytes, and this also has to be taken into account when selecting the most suitable polymeric matrix for a specific application.

The polymers were also selected considering their processability with the electrospinning process. Ideally, a polymer suitable for electrospinning needs to be easily soluble in a highly volatile solvent and its solution, after the filler addition, must possess suitable rheological properties.

4.1.1 POLYVINYLIDENE FLUORIDE

Polyvinilydene fluoride (PVdF) is a fluorine-containing thermoplastic polymer with high performances in terms of chemical resistance to acids and oxidation, high UV resistance and large thermal application range (-40°C to 150°C).

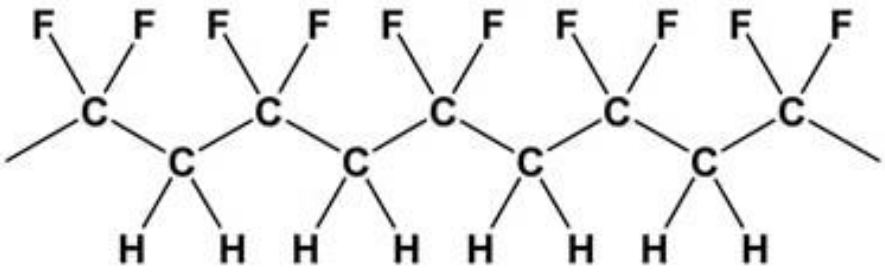

Figure 18: Chemical structure of Polyvynilidene fluoride

Moreover, its high solubility in polar solvents makes it suitable for electrospinning applications.
PVdF shows five different crystalline polymorphs, namely α, β, γ, δ and ε phases, and their relative amount depends on the production method that was used for its production [105]. Among these crystalline phases, α-phase and ε-phase are characterized by an anti-parallel packing of the dipoles, which makes them non-polar. Other phases are polar instead, and they all possess remarkable piezo- and tribo-electric properties, especially its β-phase.

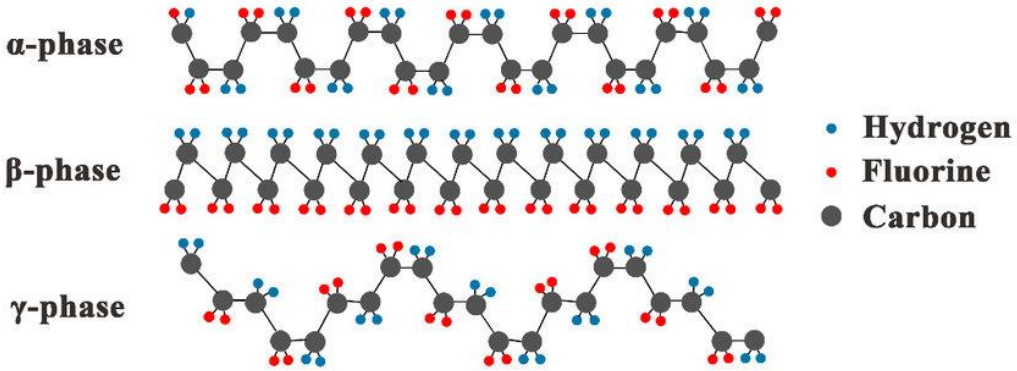

Figure 19: Chemical structures of the most common crystalline phases of PVdF

Many different articles highlight how the strong electrical field and the stretching conferred to the polymeric solution during electrospinning can increase the relative amount of the piezoelectric β-phase [106]. For this reason, electrospun PVdF is mainly studied for applications that can take advantage of its piezoelectric properties, such as nanogenerators [107] or actuators .
Non-electrospun PVdF, instead, finds many applications in anti-corrosion paints, ultrafiltration membranes, lithium batteries and medical supplies thanks to its biological inertia.

4.1.2 POLYAMIDE 6

Polyamide 6 (or Nylon 6 or polycaprolactam) is a semicrystalline thermoplastic polymer usually obtained by ring-opening polymerization of caprolactam.

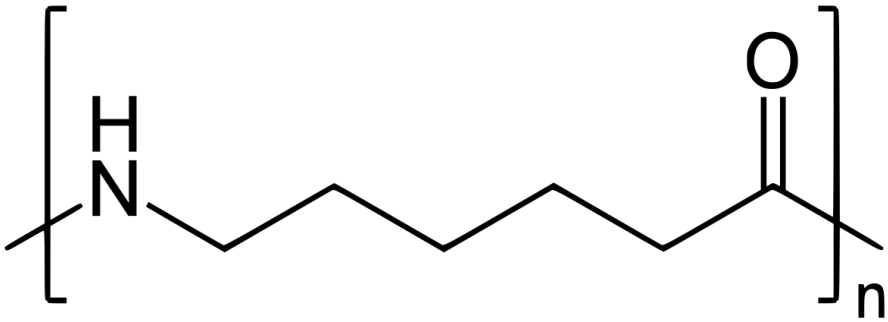

Figure 20: Chemical structure of polyamide 6 monomer

The entire family of polyamides (especially polyamide 6,6, polyamide 6 and polyamide 11) is extensively exploited in industrial processes and applications, making these polymers some of the cheapest and most common polymers in the world (annual demand only in Europe is over 1 million tonnes).

Polyamide 6 fibres possess strong mechanical properties, in particular they show an outstanding resistance to abrasion. For this reason and for its high flexibility when produced in the form of fibres, PA6 is one of the principal materials used in textile industry.

Moreover, it shows a good tenacity of 6 - 8.5 gf/D, and a good temperature resistance since its melting point sets at around 220°C.

Polyamides are in general also easy to electrospin and different solvents and solvent mixture have been studied for the preparation of electrospinning solution [76] [108].

4.1.3 POLYLACTIC ACID

Polylactic acid (PLA) is an amorphous thermoplastic polyester obtained by condensation of lactic acid. It also exists in a crystalline form, which is only obtainable by using stereospecific catalysts to produce a heterotactic polymer.

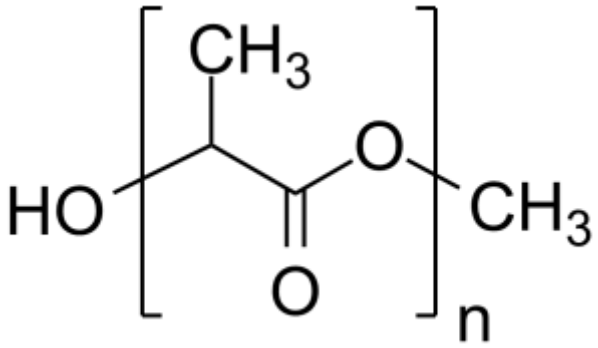

Figure 21: Chemical structure of PLA monomer

PLA became a popular material in the latest years since it can be y produced starting from renewable sources with an economically sustainable process. For example, lactic acid monomers are often industrially produced from fermented plant starch from different agricultural products (such as corn, cassava, sugarcane and others).

PLA has poor temperature resistance (melting temperature is about 60-65°C), but it shows strong mechanical properties, with a Young's modulus ranging from 2.7 to 16 GPa depending on the degree of crystallinity. These properties makes PLA the most widely used polymer material for 3D printing applications.

In industrial applications, the thermal and mechanical properties of PLA can be further increased by annealing, crosslinking of the polymeric chains or formation of composites using fibres or nano-fillers.
PLA is soluble in many different organic solvents and can be electrospun in different conditions.
Its low environmental impact and high biodegradability and biocompatibility make electrospun PLA suitable for many different applications, ranging from filtration [109] and environmental remediation to medical implants and scaffolds.

4.2 FILLERS

Nanofillers used in this research activity were selected based on the specific functionalities they can confer to the electrospun composites. Nevertheless, their addition to the polymeric matrix could also enhance its mechanical and thermal properties and this may be useful for many of the proposed applications.

4.2.1 GRAPHENE RELATED MATERIALS

Graphene related materials as composite reinforcements were comprehensively discussed in Chapter 3: Electrospun graphene-based composites.
In this work, GO, rGO and GNPs were selected as possible additives mainly for their positive effect on the enhancement of the electrical properties.
GO was chosen for its high affinity with many of the polymer matrixes that were used. Moreover, its electron-trapping effect may be useful for energy harvesting applications [101] and the possibility to reduce it into highly conductive rGO can be exploited in the production of high-performance conductive composites.
On the other hand, rGO and GNPs were selected for their intrinsic high conductivity and mechanical properties. They were tested without any modification for the production of conductive e-textiles.

4.2.2 NANOCELLULOSE

Cellulose is the most abundant biopolymer on earth and it can bio obtained starting from several plant resources and biomasses.

Cellulose is attracting much interest in the latest years because it is renewable, recyclable and biodegradable, thus it can be defined as environmentally sustainable and "green" polymer [110].
An amorphous (or para-crystalline) region and a crystalline one compose cellulose as found in nature. The latter can be isolated in through different chemical or mechanical processes to obtain cellulose nanocrystals or nanofibers [111]. They only difference between these two materials is their aspect ratio and length.
These nanomaterials possess surprisingly high mechanical properties [112] (such as flexibility, elasticity and toughness), good chemical compatibility and large surface area. For these reasons, they are intensively studied for applications in the field of composites.
The increasing interest towards nanotechnologies shifted the attention to nanocomposites, and cellulose nanocrystals and nanofibers found many interesting applications in electrospinning studies, especially in the fields of biomedicine and filtration [113] thanks to its non-toxicity and biocompatibility.
The main advantages in the use of nanocellulose fillers in electrospun composites is the enhancement of the mechanical properties even at low loadings. The oxygen-containing groups present on the surface of cellulose are also good substrates for chemical reactions, thus nanocellulose can be easily functionalized to confer new properties to the composite or to increase its affinity towards the polymeric matrix.
All of these interesting properties come with the advantage to use a sustainable filler. Nanocellulose is therefore often used coupled with bio-based polymers to produce composites completely derived from sustainable sources or with high biodegradability and biocompatibility.

4.3 COMPOSITE FORMULATIONS FOR SPECIFIC APPLICATIONS

Several applications were hypothesized for electrospun composites based on market needs that were reported in market studies and literature reviews.
The aforementioned matrixes and fillers were coupled in different composite formulations based on their properties and their interest for every specific application and market sector.

4.3.1 ENERGY HARVESTING

Energy harvesting devices can strongly benefit from the electronic properties and large contact area of electrospun graphene-based composites. In particular, their flexibility, lightweight and strong

adhesion on the substrate can make electrospun composites interesting for wearable applications, such as TENGs (triboelectric nanogenerators).

TENGs are energy harvesting devices that can convert mechanical energy into an electrical signal by exploiting the triboelectric effect.

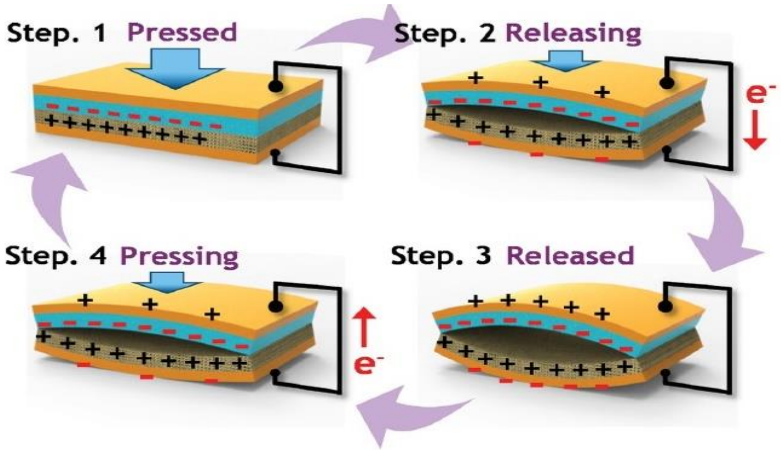

Figure 22: Schematic representation of the working principle of a TENG

When two different materials come in contact with each other, their friction can cause a charge transfer between their surfaces. This charge transfer directly depends on the contact frequency, the surface area of the two materials and on their relative position on the triboelectric series, a list that ranks different materials based on their tendency to gain or lose electrons upon friction. Thus, the further two materials are on this list the higher triboelectric charge transfer can be expected when they come in contact with each other.

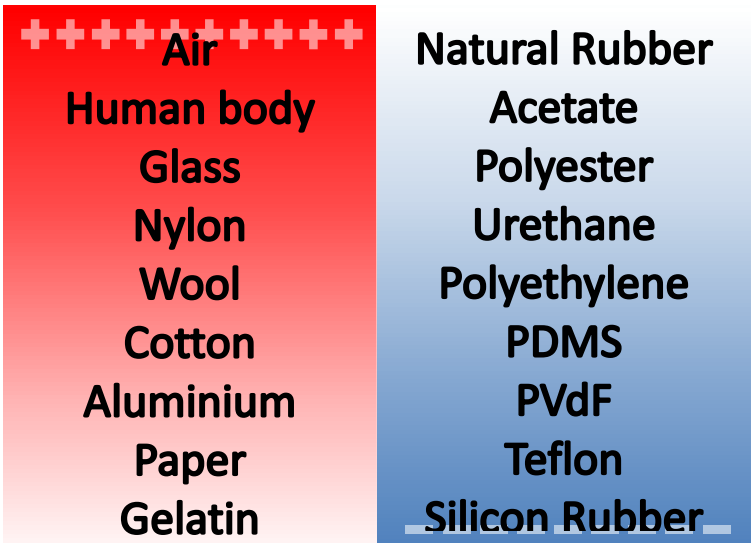

Figure 23: Triboelectric series reporting some common triboelectrically active materials and their relative tendency to transfer charges upon friction.

The working principle of TENGs is relatively straightforward. Two active layers of triboelectric materials are deposited on metal electrodes that are connected through an electrical circuit separated

by a small air gap. When an external force causes these materials to touch each other, charges will be transferred from the surface of the most tribo-positive material to the surface of the tribo-negative one. When the external force is removed, the layer will separate again and the charge difference on the electrodes will cause electrical current to flow through the circuit.

TENGs are currently intensively studied since they can represent a safer and environmentally friendly alternative to traditional batteries in wearable devices. As a matter of fact, the vast majority of traditional batteries (such as lithium batteries) are considered dangerous for applications that require a close contact with the human body and they are usually difficult to recycle and reuse.

They main obstacle that needs to be overcome for TENGs to become a suitable alternative is their power output, which is usually not high enough for the power supply of standard wearable electronic devices.

In this scenario, electrospun composites could be very interesting since their outstanding surface area could drastically increase the charge transfer between the triboelectrically active layers, thus increasing the power output of the TENG. Moreover, as different studies highlighted, GO domains inside the polymeric matrix can act as electron trapping sites, further increasing the amount of charge that can be stored in the triboelectric material and the performances of the TENG.

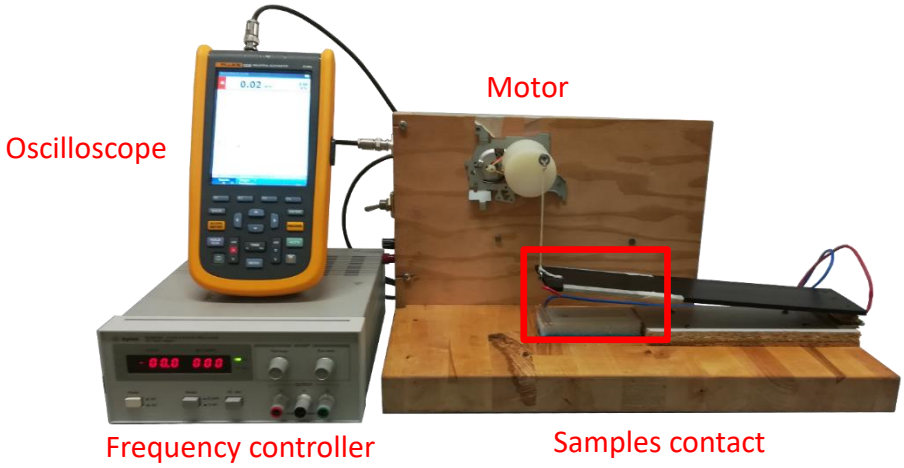

Figure 24: Home-made TENG prototype used for preliminary tests

In this study, PVdF was chosen as triboelectric layer for energy harvesting application in a TENG prototype for its unique triboelectric properties and piezoelectric constant. GO was used as a filler to exploit its electron-trapping effect [101]. For this specific application, the nanofiber morphology and diameters were especially important in order to obtain the higher power output possible for the TENG prototype.

4.3.2 CONDUCTIVE TEXTILES

Innovative, high-performance e-textiles are crucial for the development of the market sector of wearable electronics, as previously discussed in paragraph 3.4.1.

For this type of application, graphene-based composites can represent a potential alternative to metal-based conductive textiles which, at the moment, represent the vast majority of products on the market.

Metal-based conductive textiles are cost-effective and easy to produce but they present some major concerns when applied to wearable devices. In particular, they are susceptible to oxidation and corrosion, they are difficult to recycle when coupled with polymers in a composite and they could cause safety issues to the end-user.

Graphene-based composites can overcome all of these major problems. Compared to metal, they are more resistant to oxidation and corrosion and more compatible with polymers in composites. Moreover, they are more flexible and lightweight, thus more comfortable for the end-user.

Nanofiber morphology, in addition, can be exploited in these materials to improve charge transfer and electrical conductivity. Furthermore, it can speed up the material response to external stimuli, which could be a crucial advantage for chemical sensor and strain sensors applications [102] [93].

PA6 was chosen as polymer matrix for this application considering it is a cheap polymer, which is also well known in the textile industry, facilitating the integration of the material for wearable devices. In addition, PA6 is interesting for its strong mechanical properties and its relatively high melting point, which are important properties for textile applications [76].

The main property needed from the filler for this application is the enhancement of the conductivity of the material. For this reason, GO, rGO and GNPs were selected as fillers for the PA6 matrix.

rGO and GNPs are characterized by an intrinsically good conductivity and will be added directly in the composite solution.

On the other hand GO has a poor electrical conductivity and GO-based composites will need to undergo a reduction process to achieve the conductivities that are needed for e-textiles applications. Despite this disadvantage, GO was selected as possible filler for its great affinity with the polymeric matrix [76], that could allow to obtain well-dispersed composite solution and mechanically strong coatings.

4.3.3 FILTRATION MEMBRANES

Electrospun membranes are attracting much interest for air filtration, water remediation and adsorption membranes applications.

The main advantages they can bring to these sectors derive directly from their nanoscale morphology. In particular, the small diameter of electrospun nanofibers allows air to pass smoothly through the polymeric mat while their high surface to volume ratio can increase the active area for the adsorption of analytes such as dyes and small molecules. Thus, membranes obtained by electrospinning have the potential to replace traditional technologies if they could simultaneously ensure high filtration efficiency and low pressure drop.

PLA was studied in several works for this application since it is hydrophobic, non-toxic, highly biocompatible and quite stable in the typical condition in which filtration is performed. Moreover, PLA nanofibrous mats possess excellent mechanical properties, can be produced from green sources and are easily recyclable after their use [114].

In this work, PLA matrix will be charged with nanocellulose as a filler. Cellulose nanofibers were selected to further improve the active surface for adsorption purposes and the mechanical resistance of the material. Moreover, cellulose can easily be surface functionalized in many different ways, allowing to tune the selectivity of the final composite towards a wide range of different analytes.

PLA/cellulose electrospun composites also show enhanced mechanical properties and stability when compared to pure PLA nanofibrous mats [115].

PLA/nanocellulose mats could ideally be completely prepared from bio-based sources and be easily recyclable, reducing the environmental impact deriving from the large-scale production of these materials.

4.4 ELECTROSPINNING APPARATUS

The electrospinning apparatus used for the production of these materials is completely home developed by CNR-ISOF institute. Figure 25 is a picture of the electrospinning setup.

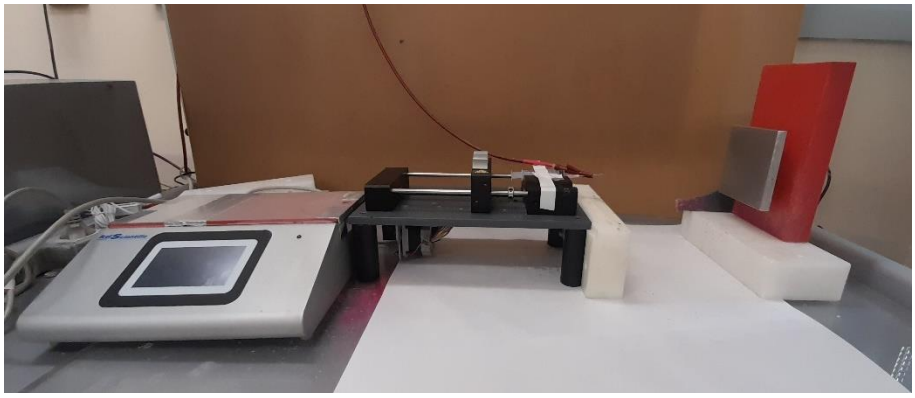

Figure 25: Electrospinning equipment used for the production of nanostructured composites

A software-controlled syringe pump (LEGATO 200, KD Scientifics) ensures a precisely defined, steady extrusion of the polymeric solution through the thin needle (20 Gauge internal diameter). The power supply is a custom-made electrical generator (developed by Alintel) which can generate high voltages up to several tens of kilovolts.

High-tension suitable electrical wires connect the generator to the tip of the needle and to the flat, square-shaped aluminium collector, which is free to be moved and set to different distances from the tip of the needle.

The entire equipment is confined in a Faraday cage to ensure safety to the user, regarding both risks related to the high-voltage and to the evaporating solvent.

Humidity and temperature are measured but cannot be modified. Other electrospinning parameters, instead, can be set to the appropriate values. Optimization of extrusion flow, voltage and tip-to-collector distance was crucial for the entire research that will be described in this thesis.

5. CHARACTERIZATION TECHNIQUES

The following chapter summarizes the main techniques that were used for the characterization of the materials produced in this research.

5.1 RHEOLOGICAL ANALISYS

At discussed in previous chapters, the viscosity of the composite solution is crucial for its behaviour during electrospinning and also influences the final morphology of the nanofibers [116].
In general, in order to be electrospinnable, a composite solution should be a non-Newtonian, shear-thinning fluid, displaying both plastic and elastic behaviour to withstand acceleration, stretching and whipping [117].
A shear rheometer is a laboratory device that can measure the viscosity and other related parameters by analysing the way a fluid flows in response to forces applied to it. In particular, these measurements can be performed in either controlled shear stress or shear rate.
The way the viscosity changes in function to the applied forces defines the Newtonian behaviour of the fluid and thus its plastic or elastic response to deformations.
In detail, three main rheology parameters are important for the good behaviour of a solution during electrospinning:

- The power-law index, n. The smaller the value of n is, the more shear thinning is the material.
- The consistency index, m. The higher m is, the more viscous is the solution.
- tan δ. Quantifies the relative weight of viscous and elastic contribution on the behaviour of the fluid.

The tan δ value can be easily obtained by equation 1:

$$\tan\delta = G''/G' \qquad \text{EQ. 1}$$

Where G'' is the loss modulus of the fluid and G' its storage modulus. These values are directly related to the elastic and plastic behaviour of the fluid and can be obtained by the frequency sweep rheological analysis of the solution. For the electrospinning process, a relatively lower elasticity of the polymer solution with respect to the plasticity is preferable to obtain a stable jet and to confer

the polymer chains stretching. This is because the elastic force tends to contract the polymer jet reducing the polymer chains elongation.
The two indexes, m and n, can be found by fitting the Ostwald-de Waele power law equation:

$$\sigma = m(\dot{\gamma})^n \qquad \text{EQ. 2}$$

Where σ is the shear stress imposed to the solution and $\dot{\gamma}$ is the shear rate of the fluid.
In this case, the electrospinning process benefits from a small value of n (high shear-thinning behaviour). A higher shear thinning behaviour indicates a higher viscosity reduction with increasing the shear rate, thus the polymer chains undergo lower shear resistance and are more prone to align with their main chain axis along the shear rate direction.
On the other hand, a higher m value is beneficial for electrospinning since it indicates that the solution has higher apparent viscosity. This is needed to efficiently stretch the polymeric chains during the jet formation, thereby obtaining thinner nanofibers.
In this work, an Anton Paar Compact Rheometer MCR 102 equipped with a PDT 200/56/l Peltier temperature control device, set at 25 (± 0.1) °C, using a cone plate geometry (75 mm diameter, 1° angle and 45 μm truncation). Steady shear measurements were performed in a shear rate range between 0.1 and 100 s^{-1}. In order to define the elastic and loss modulus G' and G'', oscillatory tests were performed at an amplitude sweep within the linear region and with a frequency ranging from 0.1 to 100 s^{-1}.

5.2 SEM ANALISYS

In Scanning Electron Microscopy (SEM) a finely focused electron beam scanned across the surface of the sample generates different types of interactions such as secondary electrons, backscattered electrons, and characteristic X-rays. Detectors collect these signal to form a digital image of the sample. SEM is typically used to observe morphological, structural and surface properties of the electrospun nanofibers.
In this work, the electrospun nanofiber morphology was observed using a Zeiss EVO LS 10 LaB6 scanning electron microscope (SEM), with an acceleration voltage of 5 kV and a working distance of 5 mm. Samples were gold-sputtered for 1 min before the analysis when non-conductive. The nanofiber diameters distributions were analysed by means of the software GIMP 2.8 (GNU Image Manipulation Program), from 100 measurements randomly gathered from several SEM photos of different electrospun samples.

5.3 X-RAY PHOTOELECTRON SPECTROSCOPY (XPS)

Photoelectron spectroscopy (PES) is schematized in Figure 26. It involves the energy analysis of electrons photo emitted from matter by incident radiation. The technique allows quantitative chemical characterization of surfaces and thin films.

The use of soft x-rays radiations (XPS; 0.4 keV < $h\nu$) with energies comparable to the ones of atomic core states is necessary to completely determine the material composition. The only exceptions are hydrogen and helium for which the photoionization cross-sections are too low to make the emission possible with lab-scale instrumentation.

In this thesis, and electrospinning in general, XPS is useful to verify the absence of solvent after the electrospinning process and to investigate the efficiency of post-treatments such as surface functionalization or coating of the materials.

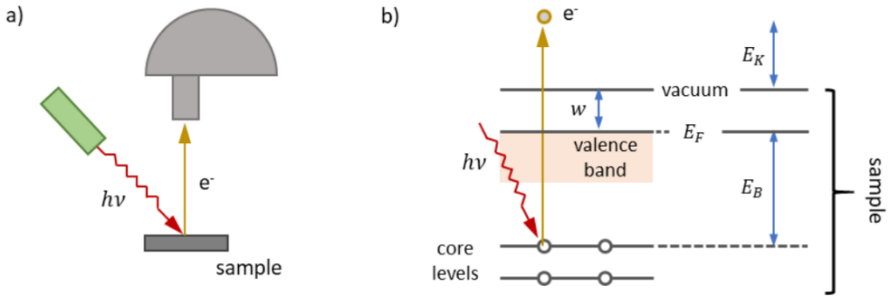

Figure 26: Schematization of the basic principle of XPS operation. a) Incident radiation impinges the sample surface and causes the emission of an electron; b) energy diagram representing the electron emission

5.4 ATOMIC FORCE MICROSCOPY (AFM)

Atomic Force Microscopy (AFM) is a wide-spread scientific tool which provides information on the nanoscale. An AFM image is constructed by probing the forces felt by a solid sharp tip while it is scanning the sample surface. Based on the tip characteristics and the way it is made to interact with the sample, different signals can be retrieved from the studied surface/nanostructures: morphological, mechanical, electrical, magnetic, electro-chemical, etc…

AFM is one of the most useful techniques for the analysis of 2-d materials and is widely used especially for graphene and its related materials. In this work, measurements were performed with a commercial microscope Multimode 8 (Bruker) operated in air in tapping mode (Figure 27),

employing doped Si probes with mechanical constant k = 40 N/m and oscillating frequency f0 ~ 300 kHz . The average size of GO sheets was measured by automatic image processing.

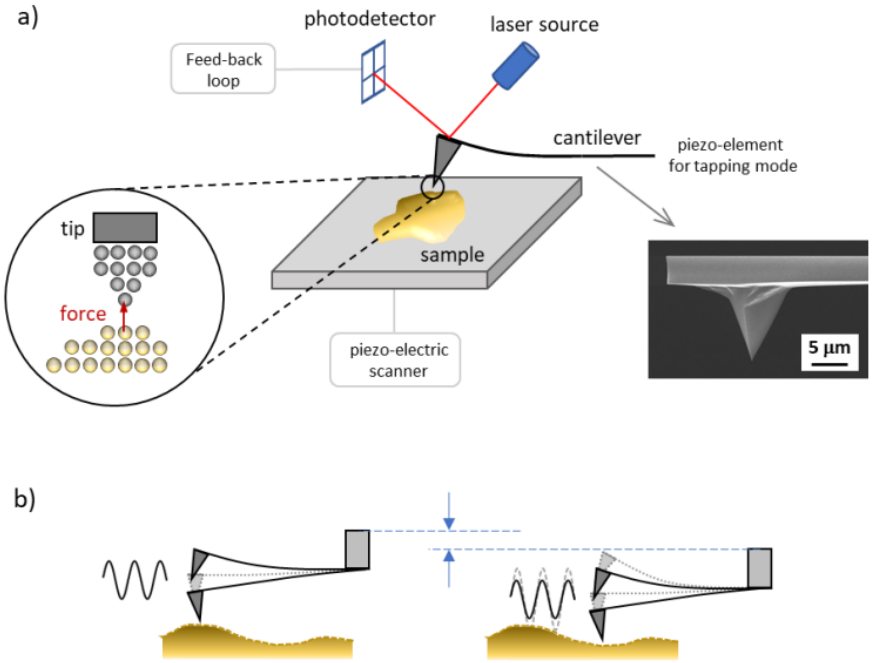

Figure 27: a) Schematic representation of a typical AFM setup. b) focus on the working principle of the tapping mode: the imaging mechanism relies on the interactions between the oscillating tip and the surface of the sample

5.5 OTHER TECHNIQUES

Additional information on the samples were collected through different techniques.

IR spectroscopy and X-ray diffraction are useful techniques for qualitative and quantitative analysis of materials. In this work, these techniques were used in particular for the determination of the crystallinity of the electrospun composites.

DSC and TGA are wide-spread techniques used for the thermal analysis of polymers and composites.

4-point probe conductivity measurements were used for the determination of the electrical conductivity of the coated electrospun mats. For this specific analysis, we used a KEITHLEY SourceMeter 2450 multimeter (Figure 28).

Figure 28: The Keithley multimeter used for the acquisition of electrical conductivity measurements

6. ELECTROSPINNING PARAMETERS OPTIMIZATION

The following chapter highlights the optimization process that was followed for the production of PVdF and PVdF/GO electrospun mats for energy harvesting applications.

The study and setting of the electrospinning parameters is not only necessary for the production of nanostructured materials, but can also be exploited for finely tuning the nanofiber diameters, modifying the final properties of the material.

In particular, the main electrospinning parameters that influence the morphology of the nanofibers are extrusion flow, applied voltage and tip-to-collector distance. Moreover, the composite solution viscosity is crucial and can be modified by polymer concentration and addition of specific additives. For this reason, the effects of GO addition on the final morphology of the nanofibers was also tested.

Every different sample was electrospun at room conditions. Typical relative humidity values were around 60 ± 5 % and temperatures of 25 ± 2 °C. Tests in different conditions showed that these parameters in these ranges did not influence the feasibility and reproducibility of the electrospinning process for the tested samples.

The main results reported in this chapter are also contained in the scientific publication “Enhancing triboelectric performances of electrospun poly(vinylidene fluoride) with graphene oxide sheets” [118].

6.1 MATERIALS

Graphene oxide was prepared from graphite flakes by a modified Hummers method [119]. The GO water dispersion (2.5 g/L) was sonicated 40 h and used for the next phases.

The dispersions for electrospinning were prepared starting from PVDF pellets (Sigma Aldrich, MW ≈530,000) and from the freeze-dried GO powder.

Pure PVDF solutions were obtained by solubilizing PVDF pellets at a concentration of 10% w/w in a solvent mixture composed of dimethylformamide (DMF) and acetone at a 2:3 ratio. The complete dissolution was obtained by stirring the solution at 100 °C for an hour and keeping it stirred overnight at room temperature.

For the preparation of PVDF dispersions doped with the GO, the GO powder was dispersed into DMF at a concentration of 2.5 mg/mL and sonicated for two hours.

This dispersion was then used to prepare the DMF:acetone mixed solvent to obtain a GO concentration ranging from 0.1 to 1% w/w compared to the PVDF. The polymer is then added to the GO dispersion at a concentration of 10% w/w. Afterwards, the PVDF/GO dispersions were treated as the pure PVDF one.

The pure PVDF dispersion and the one of PVDF doped with 0.5% of GO were electrospun using different voltages (15, 20, 25 kV), flow rates (0.01, 0.02 0.05 mL/min) and tip to target distance (12, 15, 18 cm).

6.2 GO CHARACTERIZATION

Figure 29 shows AFM images of GO sheets deposited onto silicon oxide (SiO2) substrates by spin coating. Sheet thickness and lateral sizes amount to 1.1 ± 0.2 nm and 120 ± 30 nm, respectively, as calculated by statistical analysis of the acquired AFM images.

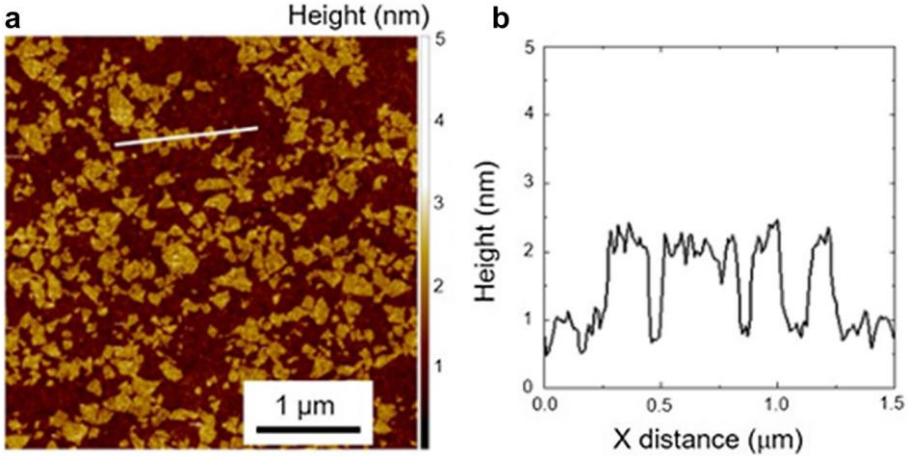

Figure 29: AFM images (a) and thickness profile (b) of GO nanosheets deposited onto silicon oxide

6.3 RHEOLOGY OF ELECTROSPINNING SOLUTIONS

The rheological behaviour of polymeric solutions of pristine PVdF and PVdF/GO using an acetone/DMF mixture as solvent was analysed. GO loadings in the composite solution were set between 0.1% and 1%. In particular, we were interested in the dependency of viscosity and shear stress from the shear rate (Amplitude sweep analysis) to gather information on the shear-thinning behaviour of the solutions. Figure 30 shows the results of the amplitude sweep analysis for the tested solutions. The shape of all the viscosity curves clearly shows a decrease of the viscosity values with increasing the shear rate, thereby indicating that all the dispersions behave as non-

Newtonian shear thinning fluids. The addition of GO in the polymer solution caused an increase of viscosity (figure 30 a) as GO loading increased up to 0.3%.

A further increase in filler content slightly decreases the dispersion viscosity over the entirety of the range of loadings that were tested. This is probably due to an issue related to the agglomeration of GO sheets when their concentration is increased, thus hampering their good dispersion in the polymer dispersion.

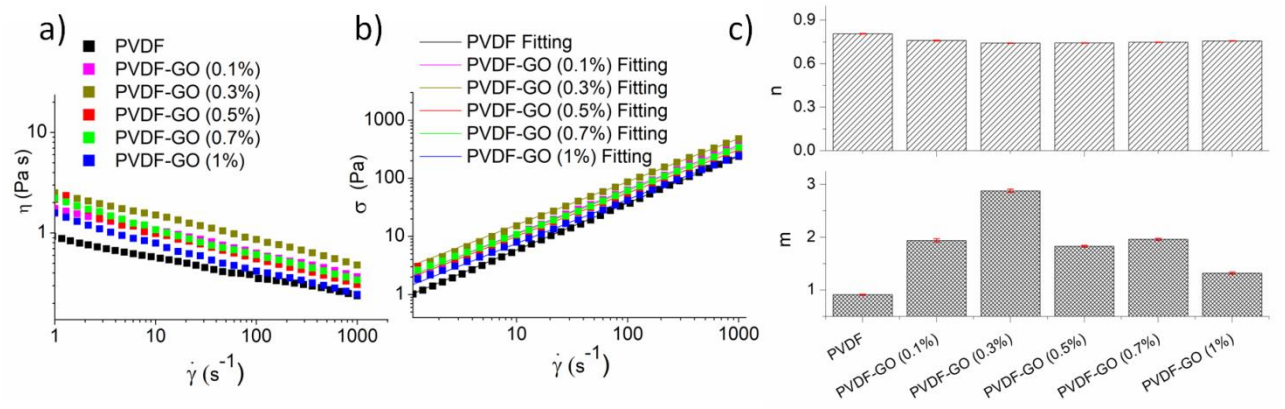

Figure 30: Amplitude sweep analysis of PVdF solution and PVdF/GO dispersions with different GO loadings. a) dependency of solution viscosity on shear rate b) dependency of shear stress on shear rate c) Values of power-law index and consistency index obtained from Ostwald-de Waele power law

Figure 30 c shows the values of the power-law index n and of the consistency index m calculated by fitting the Ostwald-de Waele power law equation (Equation 2) with the shear stress and shear rate values that can be found in Figure 30 b.

The n value of PVDF–GO dispersions was smaller than the PVDF one, thereby indicating higher shear thinning behaviour of PVDF–GO dispersions compared to PVDF solution. The PVDF–GO (0.3% wt) dispersion displayed the highest shear thinning behaviour (lowest n value). The consistency index and the viscosities showed the same trend, i.e., it increased with increasing the GO amount up to 0.3% and 0.5% w/w and it decreased with increasing the GO amount from 0.5% up to 1% w/w. A higher shear thinning behaviour indicates a higher viscosity reduction with increasing the shear rate.

This probably occurs because in the presence of GO the polymer chains undergo a lower shear resistance, thus being more prone to align with their main chain axis along the shear rate direction.

Moreover, the storage (G') and loss (G'') modulus of the PVdF solution and PVdF/GO dispersions were analysed through a frequency sweep analysis (figure 31 a and figure 31 b). The ratio between these values was then calculated and plotted as tan δ in figure 31 c.

It can be clearly seen how GO addition strongly decreases the storage modulus of the dispersion, which reflects in a less strong elastic behaviour in response to the application of an external shear stress. Also the loss modulus (which is an index of the viscous behaviour) of the dispersion decreases after addition of GO, but in a less significant amount.

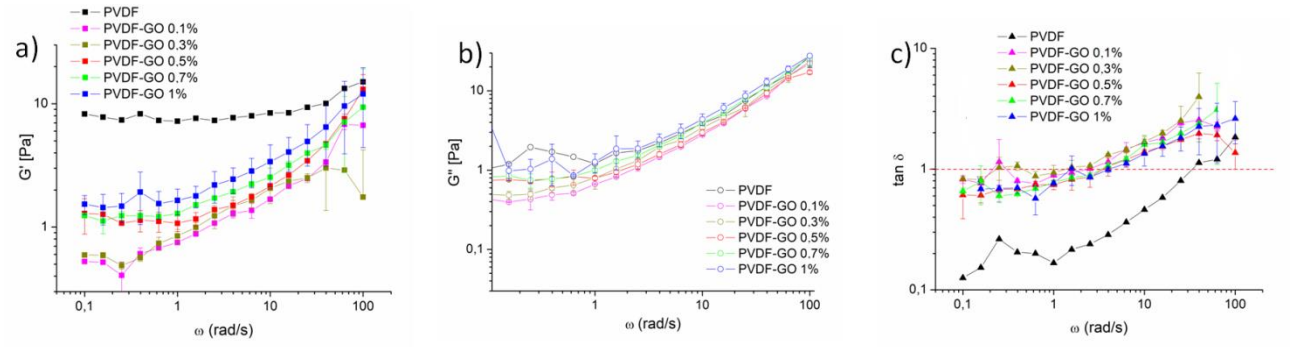

Figure 31: Frequency Sweep analysis of PVdF solution and PVdF/GO dispersions with GO loadings up to 1%. Dependency of a) storage modulus, b) loss modulus and c) tan δ on the frequency of the applied shear stress

This reflects directly in the tan δ values calculated for the dispersions. In particular, all the PVdF/GO dispersions shows tan δ values much higher than the value found for pristine PVdF solution. This is a promising result for the electrospinning of GO composite solutions, since high tan δ values are preferable to obtain stable jets and confer stretching to the nanofibers.

In particular, taking into consideration that the typical ω values for electrospinning are approximately 1 rad/s, the 0.3% PVdF/GO dispersion and the 0.5% PVdF/GO dispersion show the best suitable rheological properties for a good electrospinning process.

Considering these results and that, specifically for energy harvesting applications, a high content of GO is preferable in order to have a higher number of charge trapping sites, the 0.5% PVdF/GO dispersion was selected for electrospinning tests and for the production of the material.

6.4 MORPHOLOGY OF THE ELECTROSPUN NANOFIBERS

The pristine PVdF solution and the 0.5% PVdF/GO dispersion were electrospun at different electrospinning conditions to test their behaviour, optimize the setup and finely tune the diameter of the resulting nanofibers.

Electrospinning was possible in every tested condition. Results were analysed through SEM imaging and size distribution of the electrospun nanofibers were plotted based on the acquired images. Nanofiber diameters were collected using an image manipulation software (GIMP), collecting the length in pixels of different sections of the nanofibers and converting it to nanometers using the scale bar as a reference. 50 different data were collected in randomly chosen spots for

every SEM image. At least three SEM images were produced for each sample. In the case of beaded samples, data were collected only on sections of nanofibers and not on beads that were considered as defects.

6.4.1 EFFECT OF APPLIED VOLTAGE

Figure 32 shows the optical images obtained by SEM of PVdF and PVdF/GO electrospun mats obtained at different applied voltage values (15, 20 and 25 kV) while setting the extrusion flow at 0.02 mL/min and the tip-to-collector distance at 15 cm.

As shown, all the nanofibers displayed the highly roughened beads-on-string structure, typical of PVDF and attributed to its crystallization process [120]. The addition of GO reduced the amount of beads-on-string structures, as well as the fibres diameter, and increased their homogeneity.

Probably, the effect of the GO filler on the electrical conductivity of the PVDF–GO dispersions is negligible since both PVDF and GO have similar dielectric properties [121]. Therefore, the reason for obtaining decreased diameters and reduction in beads-on-string structures with the addition of the GO could be mainly attributed to the pronounced shear thinning of the PVDF–GO compared to pure PVDF, thereby playing a contribution to promote the elongation of polymer chains.

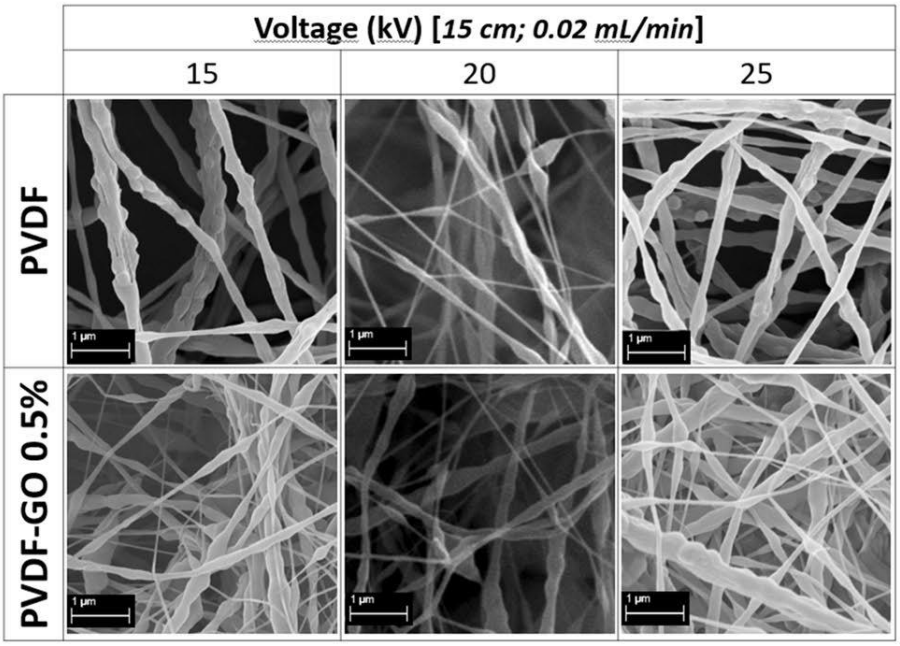

Figure 32: SEM images of electrospun nanofibers of PVdF and PdF/GO 0.5% obtained at different electrospinning voltages

Figure 33 shows the graphs collecting data on the size distribution of the nanofiber diameter. Both for pristine PVdF nanofibers and for composite PVdF/GO 0.5% w/w nanofibers, an increase in the voltage applied to the electrospinning causes a subsequent increase in the mean diameter of the

nanofibers. This trend probably occurs because the application of higher voltages seems to favour the formation of bead-on-strings defects along the length of the nanofibers.

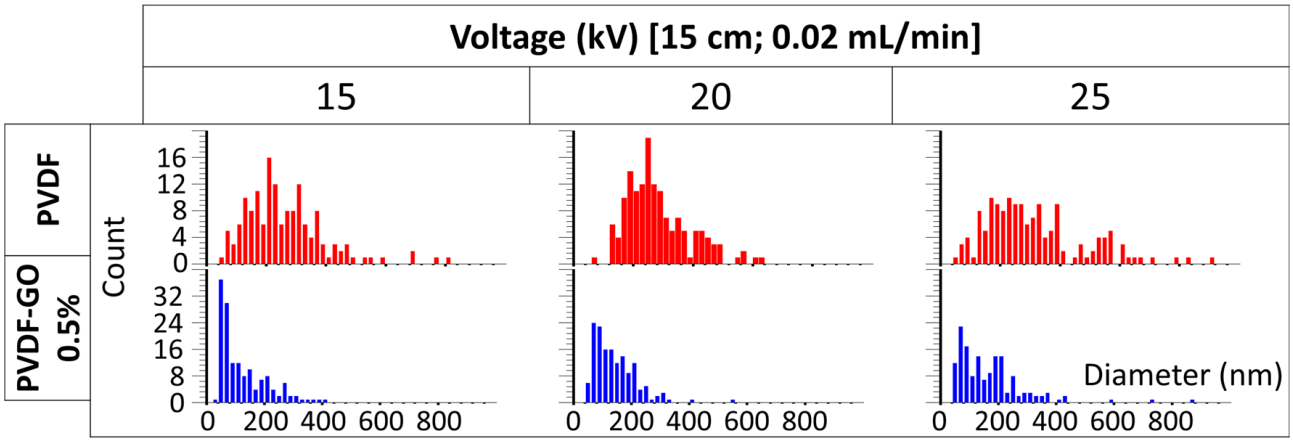

Figure 33: Size distribution of the diameter of PVdF and PVdF/GO 0.5% nanofibers obtained at different electrospinning voltages

6.4.2 EFFECT OF COLLECTOR-TIP DISTANCE

Figure 34 shows the optical images obtained by SEM of PVdF and PVdF/GO electrospun mats obtained at different tip-to-collector distances (12, 15 and 18 cm) while setting the extrusion flow at 0.02 mL/min and the applied voltage at 15 kV.

As evidenced by the size distribution of the nanofiber diameter (figure 35), an increase in the collector-tip distance causes a sharp decrease in the mean diameters of the electrospun nanofibers. This behaviour is probably due to the increased stretching time that is applied to the polymeric jet when it travels longer distances before the complete solvent evaporation.

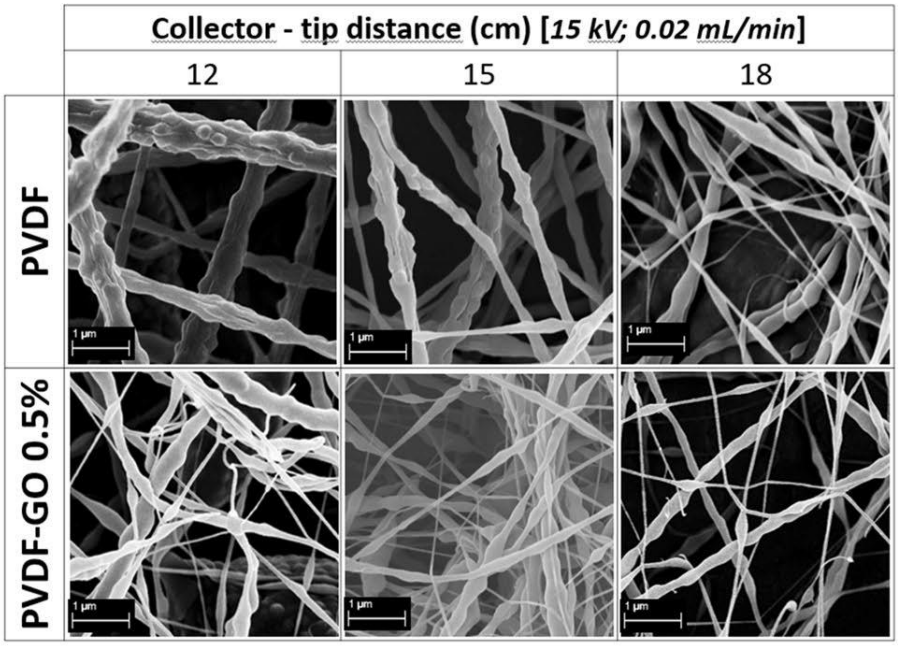

Figure 34: SEM images of electrospun nanofibers of PVdF and PdF/GO 0.5% obtained at different tip-to-collector distances

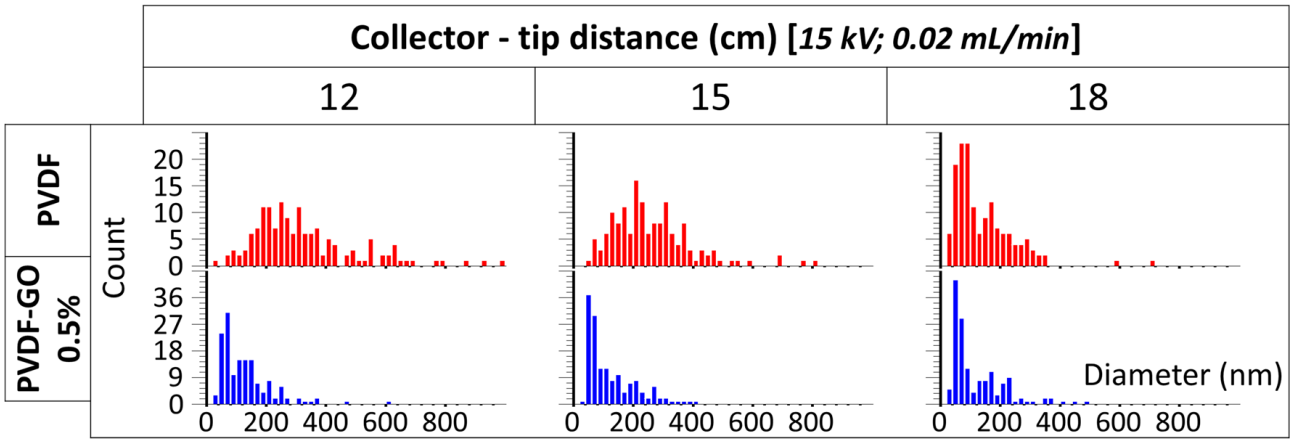

Figure 35: Size distribution of the diameter of PVdF and PVdF/GO 0.5% nanofibers obtained at different tip-to-colector distances

6.4.3 EFFECT OF EXTRUSION FLOW

Figure 36 shows the optical images obtained by SEM of PVdF and PVdF/GO electrospun mats obtained at different extrusion flows (0.01, 0.02 and 0.05 mL/min) while setting the tip-to-collector distance at 15 cm and the applied voltage at 15 kV.

The size distribution of nanofibers obtained at slower extrusion flows is more shifted to thinner diameters in comparison to the one found at faster rates (figure 37). This trend is explained by the dimensions of the electrospinning solution droplet that forms the Taylor cone at the beginning of the electrospinning process. At faster extrusion flows, this droplet will be bigger in size, generating nanofibers with a larger mean diameter.

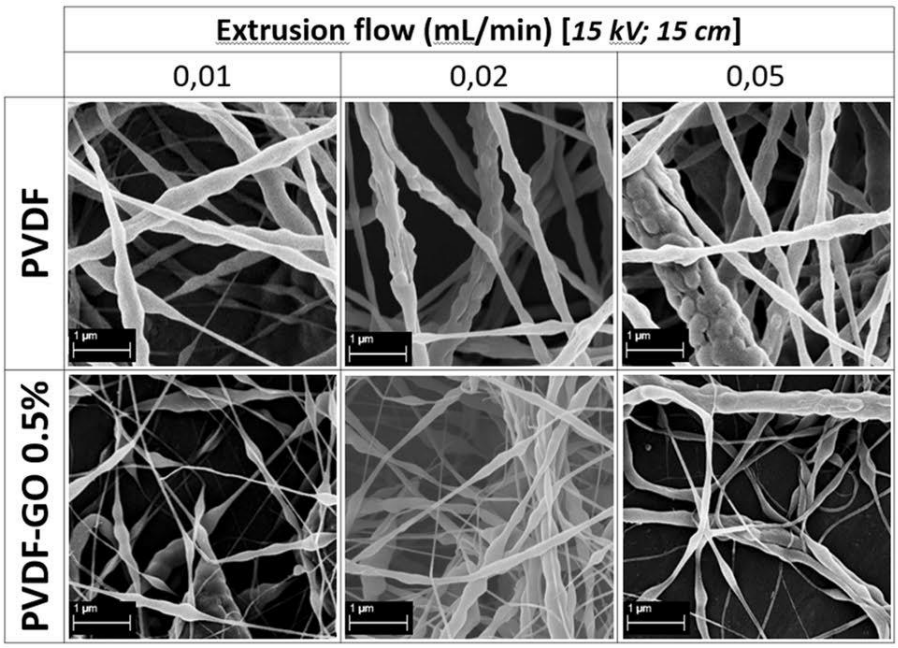

Figure 36: SEM images of electrospun nanofibers of PVdF and PdF/GO 0.5% obtained at different extrusion flows

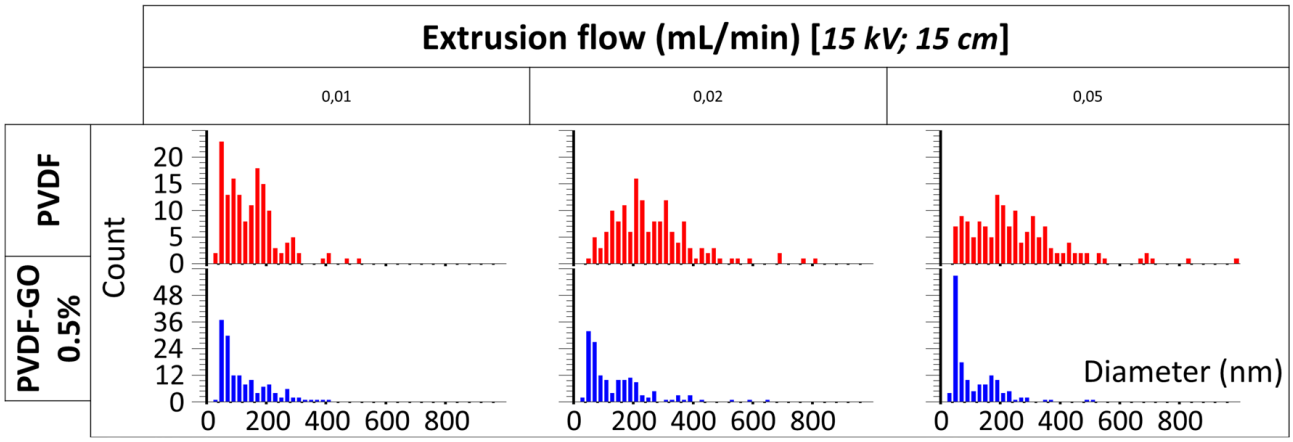

Figure 37: Size distribution of the diameter of PVdF and PVdF/GO 0.5% nanofibers obtained at different extrusion flows

6.5 CONCLUSIONS

Experimental data showed evident trend in the variation of the diameter of PVdF and PVdF/GO electrospun nanofiber while modifying different electrospinning parameters, such as voltage, extrusion flow and tip-to-collector distance.

The complete understanding of these effects and the possibility to control all of these parameters makes it possible to finely tune the diameters of the electrospun nanofibers as long as these remains in the electrospinnability range of the polymeric solution.

This approach and this knowledge were used for all the materials shown in this thesis.

Moreover, this study evidenced how GO addition to the PVdF polymeric solution drastically decreased the mean nanofiber diameter and allowed the production of thinner, more homogeneous nanofibers with less bead-on-string defects.

Thus, GO addition to polymeric solutions can be an easy approach to improve the overall process and optimize the morphology of the resulting nanofibers even with very low loadings of nanofiller in the polymeric dispersion.

7. PRODUCTION OF TRIBOELECTRIC ELECTROSPUN COMPOSITES FOR ENERGY HARVESTING APPLICATIONS

7.1 MATERIALS

The materials used for the production of electrospun mats that can be exploited as active layers in triboelectric nanogenerators (TENGs) were already discussed in paragraph 6.1.

The electrospinning process parameters were selected based upon the optimization shown in the previous chapter. By taking into consideration the requirements of the final application and the homogeneity and mechanical resistance of the produced materials, the electrospinning voltage was set at 15 kV, the tip-to-collector distance at 15 cm and the extrusion flow at 0.02 mL/min.

The obtained materials were named ES-PVdF, indicating the electrospun pristine PVdF mats, and ES-PVdFGO, indicating the electrospun PVdF/GO composite with GO weight fraction of 0.5%.

The electrospun mats were directly deposited on an electrode obtained by gold-sputtering a flexible PET substrate. This electrode was kindly supplied by IIT of Genova, Italy.

The resulting nanofiber covered electrode was directly tested on a TENG prototype to test the performances of the material in energy harvesting applications.

Figure 38: Optical images of PVdF and PVdF/GO 0.5% electrospun mats

7.2 PRODUCTION OF ELECTROSPUN MATS

Low-thickness homogeneous mats were obtained by electrospinning both PVdF solution and PVdF/GO 0.5% w/w dispersion.

Figure 38 shows the evident difference in colour between samples of the two different materials, which gives a first hint on the effective presence of GO in the polymeric matrix even after electrospinning.

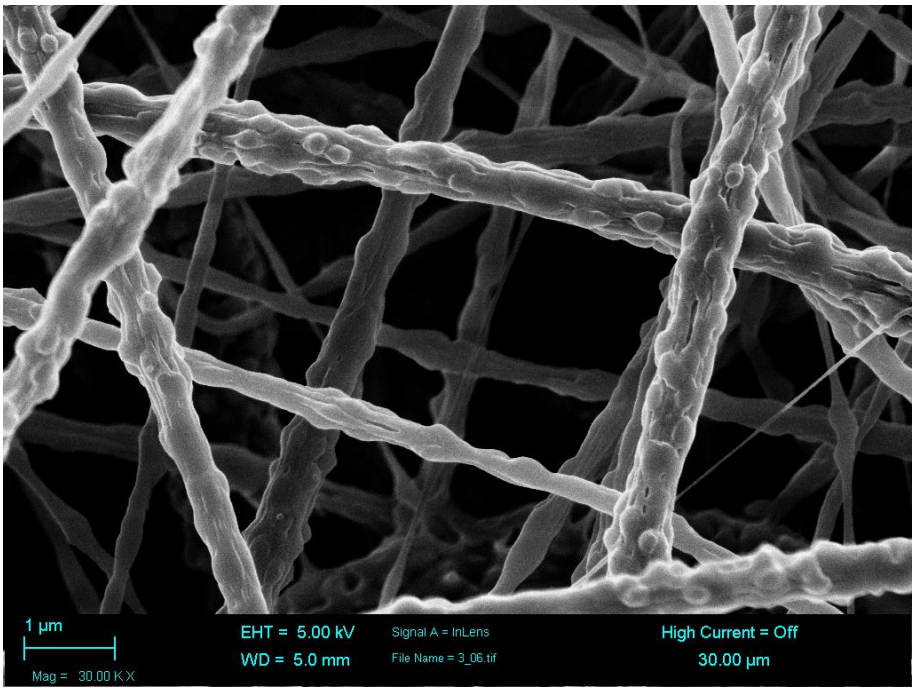

Figure 39: SEM image of the electrospun PVdF triboelectric mat

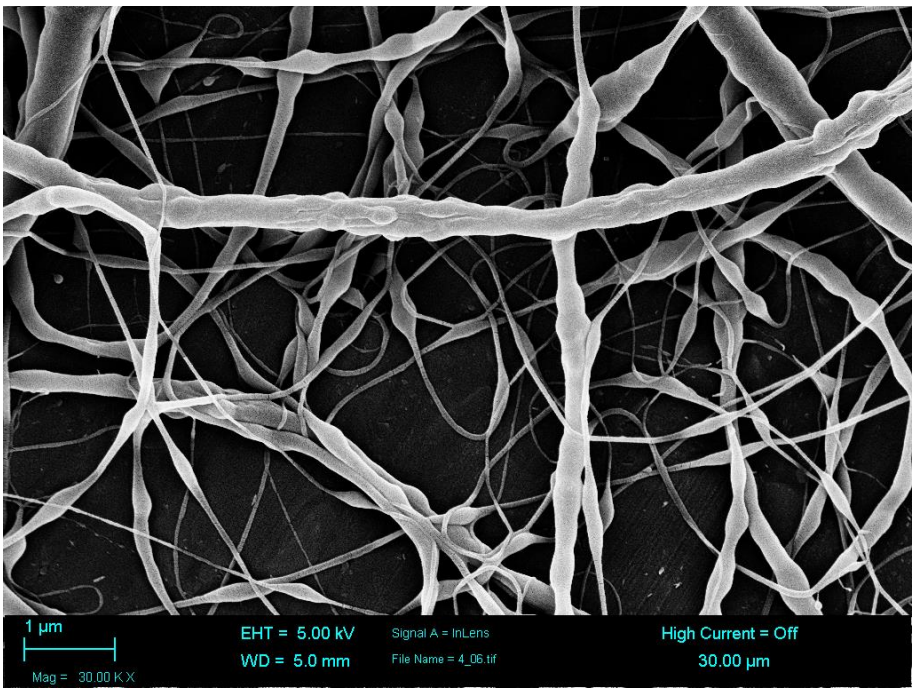

Figure 40: SEM image of the electrospun PVdF/GO 0.5% triboelectric mat

SEM images collected on the two samples (figures 39 and 40) confirmed that the nanostructured fibres morphology was effectively obtained in both cases. As expected, the GO containing composite was characterized by thinner nanofibers with a smoother surface morphology.
The mean nanofiber diameter for ES-PVdF samples was (350 ± 100) nm, while for ES-PVdFGO composites this value decreased to (120 ± 40) nm.

7.3 XPS ANALYSIS

XPS analysis was performed to verify the effective presence of GO inside the polymeric matrix even after the electrospinning process. Moreover, since XPS can only gather information on the surface composition of the material, being sensitive only to the first 10 nm in depth, this analysis can also determine whether GO domains are in the bulk core of the material, on its surface or both.
The main obstacle in this case was the low amount of GO loaded inside the composite. To overcome this hurdle, a PVdF/GO composite solution with higher GO loading (1.0% w/w) was also prepared and electrospun.

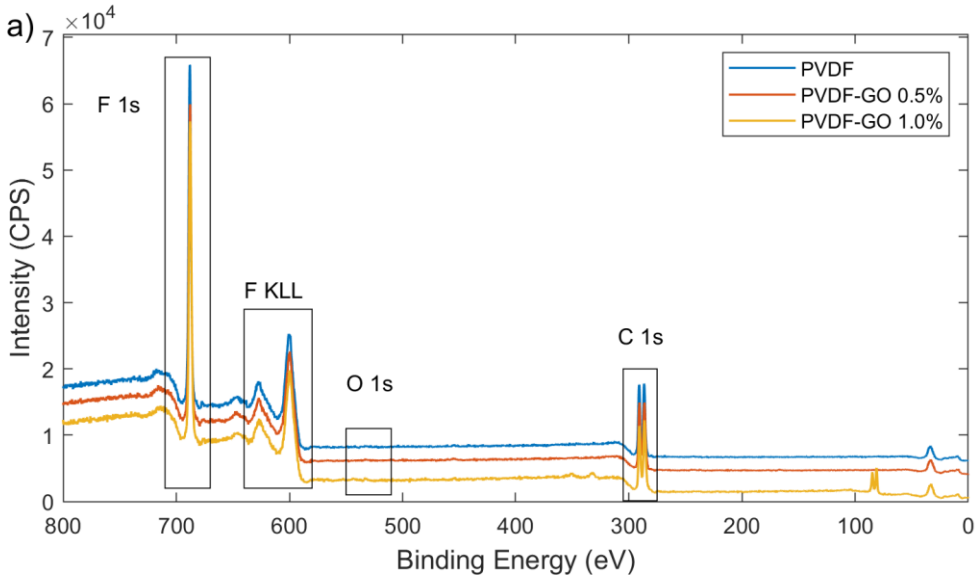

Figure 41: XPS survey spectra comparing the chemical composition of PVdF, PVdF/GO 0.5% and PVdF/GO 1.0% electrospun mats

The comparison of the XPS spectra of the three electrospun samples is shown in figure 41.
Table 6, instead, collects the relative amount of the elements composing the surface of the materials. Analysis and mathematical fitting of the XPS spectra was performed to obtain this information on the chemical composition.

Elements	C 1s (286.4 – 289.9 eV)	O 1s (532.1/ 530.6 eV)	F 1s (688.1 eV)
PVDF	57.0 ± 1.0	< 0.1	43.0 ± 0.9
GO*	70.1 ± 1.0	28.9 ± 1.0	-
PVDF-GO 0,5%	56.2 ± 1.0	0.2 ± 0.05	43.6 ± 0.9
PVDF-GO 1,0%	55.8 ± 1.0	0.5 ± 0.1	43.7 ± 0.9

*Table 6: Comparison between the relative chemical composition (at. %) of PVdF, PVdF/GO 0.5%, PVdF/GO 1.0% electrospun mats and GO powder. * 0.4% N 0.6% S.*

The first result that can be extracted by XPS analysis is the absence of the solvents that were used during electrospinning, due to the absence of nitrogen signal at 400 eV in the XPS spectra, that could be deriving by residual N,N-DMF.

This is a clear sign of the correct behaviour of the electrospinning process and of the complete evaporation of the solvent.

Furthermore, the oxygen relative amount (O1s, at ≈ 530 eV) increases whit the GO loading in the polymeric solution. This confirms the effective presence of GO in the electrospun composite.

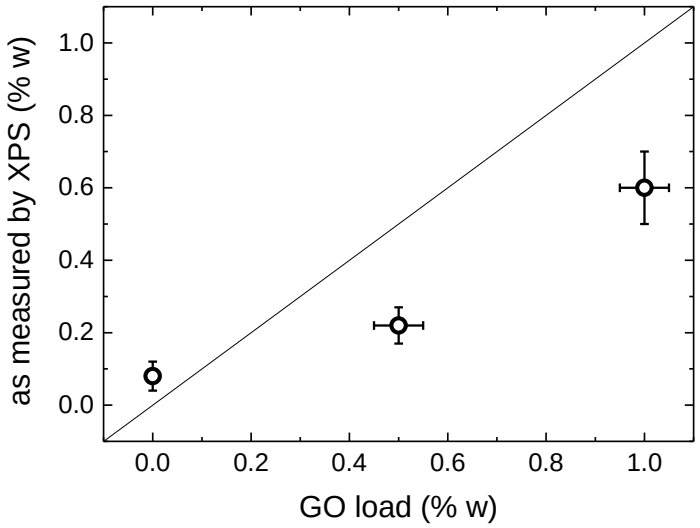

Figure 42: Plot comparing the GO relative amount as measured by XPS to the GO loading in the composites

The comparison between the amount of GO loaded in the electrospinning solution and its relative composition as measured in XPS analysis is shown in figure 42. The relative GO composition was found by the direct XPS measurement of the oxygen amount in electrospun samples and the relative oxygen composition in pure GO powder.

This graph highlights how the GO amount present on the surface of the sample is much lower than what expected by its loading in this electrospinning solution. This is a clear hint that the majority of the GO domains remain in the core of the nanofibers after the electrospinning process. The non-zero

value of measured GO at 0% GO loading is due to the presence of environmental contamination on the surface of the sample. Even so, the Oxygen signal measured in this sample is comparable to the low sensitivity limit of the instrument, hence it could be neglected when analysing the collected data.

This result is promising for TENGs applications, since having the surface of the material composed primarily by triboelectric PVdF has a positive effect on the performances of the material in energy harvesting.

7.4 IR ANALYSIS

As discussed in paragraph 4.1.1, PVdF is a semicrystalline polymer whose crystalline structure can arrange in different possible crystalline phases. The most common among those phases are α and β. The relative fraction determines the properties of the material, in particular it is well known that a higher fraction of β-phase improves the triboelectric and piezoelectric performances.

ATR-IR analysis was used to obtain structural information on the relative content between these two phases in ES-PVdF and ES-PVdFGO. A PVdF membrane obtained by solution casting was used as a comparison to evaluate also the effect of the production technique.

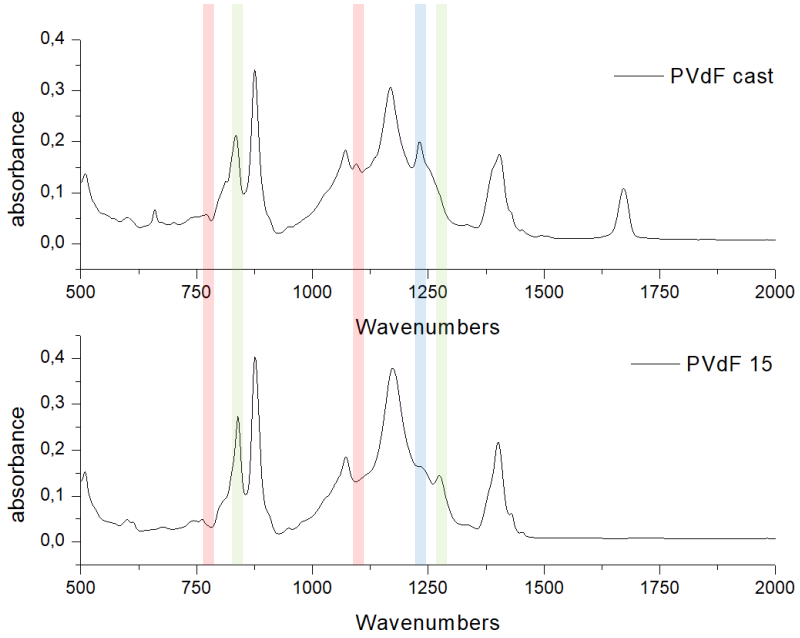

Figure 43: ATR-IR spectra of cast PVdF and electrospun PVdF.

Figure 43 compares the ATR-IR spectra of electrospun PVdF and cast PVdF. The spectra were normalized in correspondence with the 1400 cm^{-1} band, assigned to wagging vibration of CH_2 groups.

The main peaks associated with the α-phase are found at 763 cm^{-1} and 1071 cm^{-1} (highlighted in red in the spectra). β-phase, instead, is usually identified by the peak at 1275 cm^{-1} and 838 cm^{-1} (highlighted in green in the spectra) [105]. By the comparison of the two spectra, it is evident how the triboelectrically active β-phase increases in relative amount when the polymer is produced by electrospinning instead of casting. This can be extract by the graph by noticing the simultaneous decrease in height of the α-phase associated peaks and the formation of a β-phase associated peak at 1275 cm^{-1}. Moreover, the β-phase associated peak at 838 cm^{-1} increases in height.

In addition, a peak at around 1234 cm^{-1} is only present in the cast spectra. This peak can be attributed to the normally less abundant γ-phase that is instead produced in cast samples thanks to the long time necessary for the solvent evaporation in this technique.

By ATR-IR analysis, we can safely assert that electrospinning has a positive effect on the formation of the wanted β-phase in PVdF, since its relative abundancy is higher than in cast samples. The β-phase forms thanks to the strong stretching imparted by electrospinning and also because of the fast evaporation time that does not allow a reconfiguration of the polymeric chains. In electrospun samples, β-phase takes place both of α-phase and of γ-phase.

Figure 44 a) instead compares two electrospun samples: ES-PVdF and ES-PVdFGO.

The characteristic peaks used for quantitative analysis of α and β phases are magnified in the spectra. Peaks at 614 and 762 cm−1 were assigned to the α-phase and specifically to the bending and the wagging vibration of the CF_2 and the rocking of the main PVDF chain, respectively. The aforementioned adsorption peaks shifted to 838, 876, 1172 and 1234 cm^{-1} in the β-phase conformation.

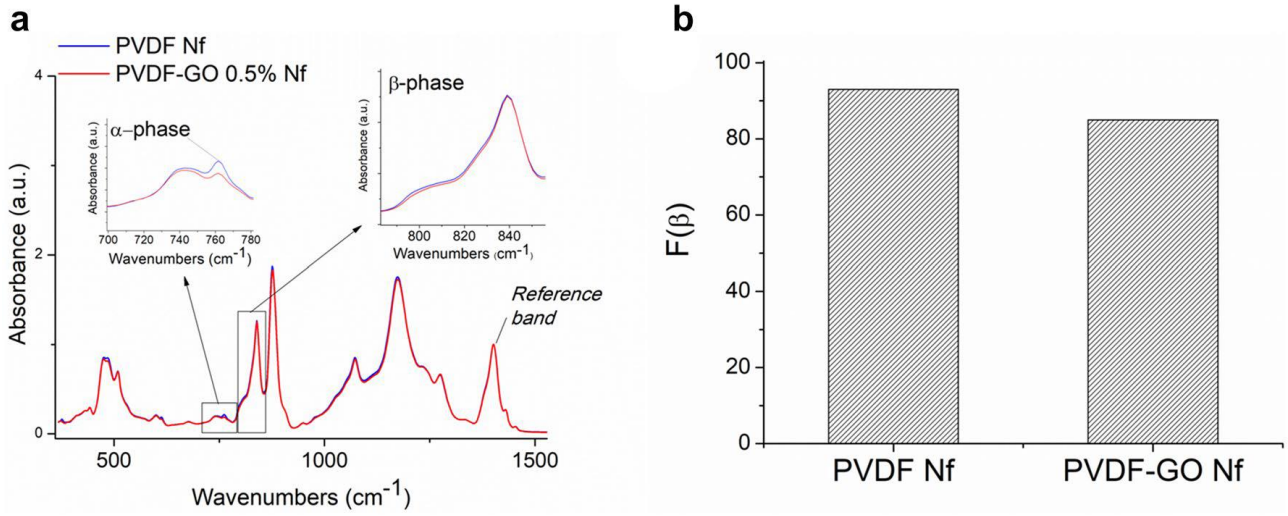

Figure 44: a) comparison between ATR-IR spectra of electrospun PVdF and PVdF/GO mats. Magnifications show details on the bands and peaks used for crystalline morphology determination. b) Comparison between the calculated β-phase relative amount in PVdF and PVdF/GO nanofibers

The effect of GO in the crystalline morphology of electrospun PVdF can be determined by the relative abundancy of these two crystalline phases. It can be evaluated using Equation 3:

$$F(\beta) = \frac{A_\beta}{\left(\frac{k_\beta}{k_\alpha}\right) A_\alpha + A_\beta} * 100 \qquad \text{EQ. 3}$$

In which k_α and k_β are the adsorption coefficients and they are $k_\alpha = 6.1*10^4$ and $k_\beta = 7.7*10^4$.
A_α and A_β are the absorbance values at, respectively, 763 and 838 cm^{-1}.
As shown in figure 44 b), the addition of GO slightly reduced the amount of β-phase fraction. Nevertheless, the calculated β-phase fraction was higher than 80% for all samples, high enough for energy harvesting applications.

7.5 XRD ANALYSIS

X-ray diffraction analysis was performed on the same samples used for IR analysis to further confirm the effect of electrospinning on the crystallinity of the polymer.
As reported in literature, the main peaks relative to the α-phase of PVdF are two major peaks found at 18.4° and 20.0° and a medium peak at around 26.6°. These peaks correspond respectively to 020, 110 and 021 reflections of the monoclinic α-phase crystal [105].
All these peaks can be clearly seen in the cast PVdF spectra.
In electrospun samples, the strong peak at around 20.0° shifts to 20.6° and increases in intensity. According to literature, this is a hint that β-phase is dominating in this sample, confirming the positive effect of electrospinning that was already investigated in IR analysis.
The spectra of ES-PVdF and ES-PVdFGO show negligible differences, as can be seen in Figure 45, indicating that GO addition has no effect on the preferential formation of β-phase crystals.

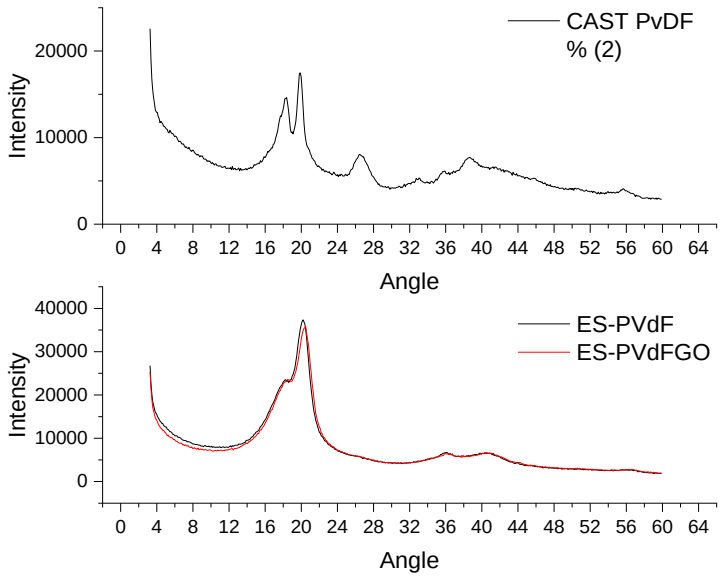

Figure 45: Comparison between XRD spectra of cast PVdF membranes, PVdF electrospun mats and PVdF/GO electrospun composite mats

7.6 TESTS ON TENG PROTOTYPE

The electrospun materials deposited on Au-sputtered PET electrodes were tested on a TENG prototype in collaboration with IIT-Genova, Italy. The illustration of a typical TENG configuration is reported in Figure 46.

The TENG prototype was working on contact-separation mode with an applied force of 10 N. The maximum air gap between the two triboelectric layers was of 5 mm and their active area was set at 2.5 x 2.5 cm^2.The operating frequency was set at 4 Hz to simulate the typical frequencies of human body movements.

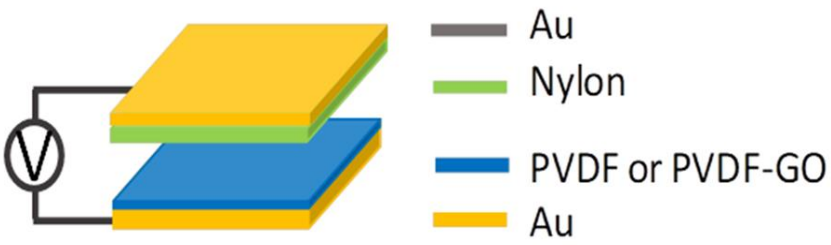

Figure 46: Schematic ilustration of the composition of triboelectric layers and electrodes in the TENG prototype

Continuous open-circuit voltage tests were performed with a 40 MΩ probe, while power output scans were performed using a variable resistance scanning from 1 kΩ to 1 GΩ.

Since PVDF has a strong tendency to attract negative charges, we electrospun the PVDF nanofibers on Au-sputtered PET electrodes and used it as the negative triboelectrode. As positive tribomaterial,

we selected nylon membranes commercially available, which have been interfaced with a second Au electrode to fabricate the positive triboelectrode.

Energy conversion performance of the TENG prototype are shown in figure 47.

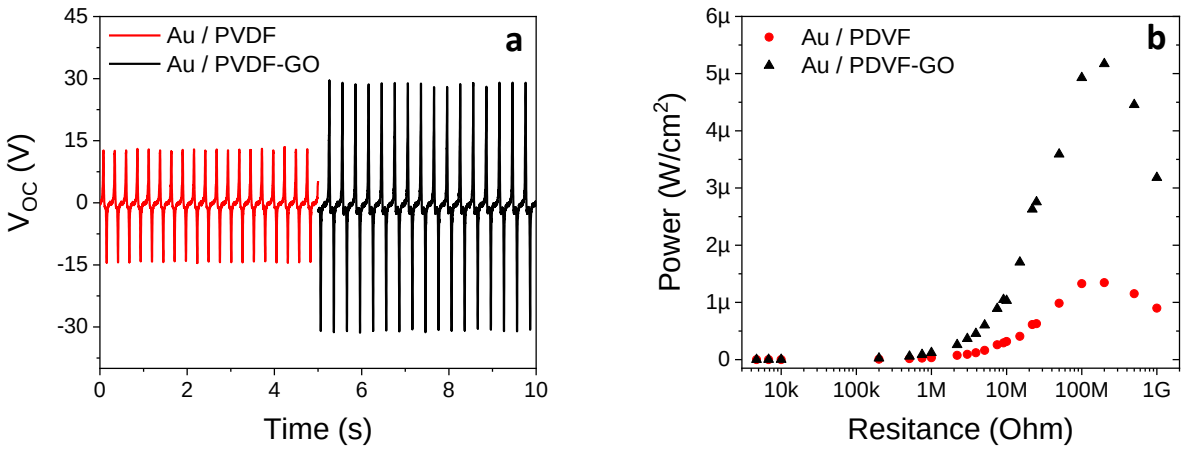

Figure 47: Comparison of the performances of the TENG prototype using as trioelectric negative material electrospun PVdF or electrospun PVdF/GO 0.5%. a) Open-circuit voltage test b) Output power test in function of the external resistance

The introduction of the GO into the electrospun PVDF nanofibers led to an increase in open-circuit voltage (V_{OC}) measured with a 40 MΩ probe (figure 47 a) and in the power efficiency of a factor 3.5 (figure 47 b).

Since IR analysis showed no significant change in the crystallinity of PVdF after GO addition, the increased TENGs' performances observed when employing PVDF–GO fibres can be attributed to the increased surface area of the PVDF–GO membrane, as a consequence of the thinner diameter of its fibres with respect to the pristine PVDF membrane.

However, previous work has also shown the possible influence of the charge trapping centres present at the GO sites, which may contribute to increase the negative charges transferred from the nylon membrane to the PVDF [101].

7.7 CONCLUSIONS

PVdF and PVdF/GO mats composed by nanofibers have been successfully produced by electrospinning. The presence of GO in the final composite was confirmed by XPS and IR analysis.

The produced composites showed high triboelectric performances when tested in a TENG prototype, leading in an increase of its power output and open-circuit voltage in comparison to non-nanostructured materials. This was attributed to the high surface contact area of the electrospun membranes that lead to a higher charge transfer during the contact of the two active layers in the

device. Moreover, electrospinning can increase the amount of the crystalline β-phase, which possess high piezo- and tribo-electric coefficients.
GO addition was proved to further increase the triboelectric performances of the electrospun composite. ATR-IR and XRD analysis proved that this effect is not related to changes in the crystalline morphology of the material, since the β-phase amount is comparable in pristine PVdF mats and PVdF/GO composite mats.
The main advantages of GO addition were found to be:

- Nanofiber-thinning effect: GO addition allows to tune the morphology of the nanofibers, reducing their mean diameter. This way, we were able to produce electrospun mats with an enhanced surface area and porosity. The increased surface area can generate a higher charge transfer between the materials during the operation of the TENG

- Electron-trapping effect: the presence of GO domains in the core of electrospun nanofibers during the operation of the TENG can partially trap the electrons transferred from a triboelectric layer to the other. This can enhance the total charge transfer during the TENG operation.

We found an optimum in the GO loading in the composite dispersion at around 0.5%. This concentration was selected since it offered a good compromise between a stable electrospinning process and a sufficiently high GO loading to maximize its electron-trapping effect.
With this composition, composite mats performed over 3 times better than pristine PVdF mats in the TENG prototype, that exhibited an open circuit voltage of ≈ 60 V and a peak power output of ≈ 5 $\mu W/cm^2$.
Nonetheless, according to literature [122] [123], the performances that were reached are not sufficient for a direct application of these materials in a wearable TENG device. Some improvement in the performances are still needed.
The main possible improvements that could make these materials suitable for industrial applications could be researched in the geometry of the device. Complex TENG geometries are currently being studied in literature and the results show a great improvement in terms of performances when compared to the commonly used contact-separation mode.
The combination of such geometries and the effect of nanostructured graphene-based composites can open the doors to the use of TENG for the energy supply of many wearable devices.

8. PRODUCTION OF CONDUCTIVE ELECTROSPUN COMPOSITES FOR WEARABLE ELECTRONICS

I strongly acknowledge the EU for funding the research activity that is resumed in the next chapter in the context of Graphene Flagship Core 3 (Work Package 9: Flexible Electronics).

8.1 MATERIALS

Graphenea supplied the graphene oxide as water dispersion (4 g/L). It was diluted to the appropriate concentrations and sonicated 40 h prior its use. After sonication, the average lateral size of GO sheets was ≈ 100 nm (figure 48)

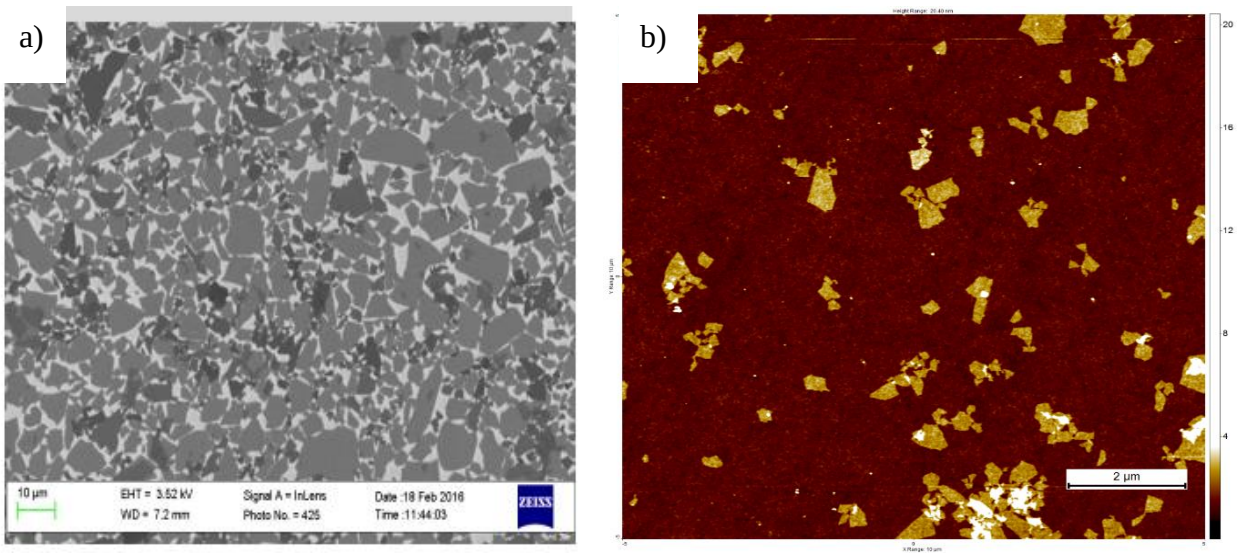

Figure 48: AFM image of GO nanosheets deposited on silicon oxide. a) material as supplied b) after 40 hours sonication

Avanzare supplied GNPs (AVA-18) as pure powder. The average lateral size of GNP flakes was ≈ 50 µm (figure 49)

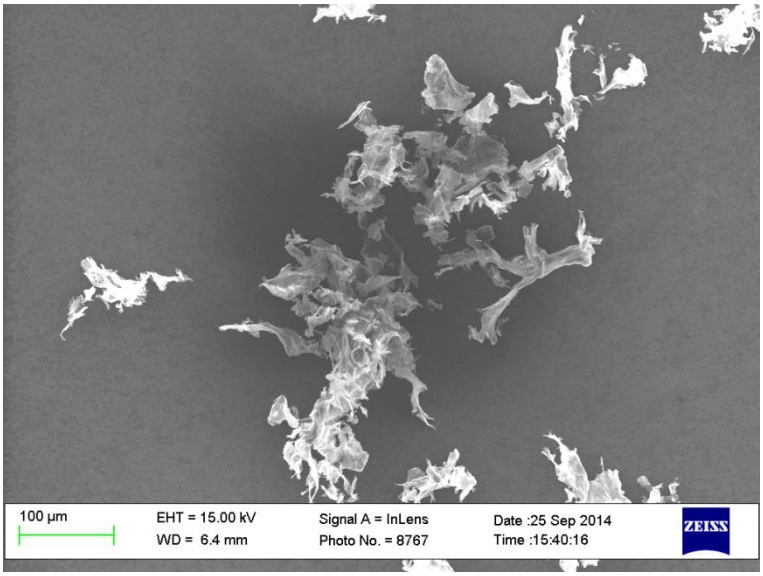

Figure 49: SEM image of AVA-18 GNPs supplied by Avanzare

The dispersions for electrospinning were prepared starting from PA6 pellets (Sigma Aldrich, 181110) and from the freeze-dried GO powder.

Pure PA6 solutions were obtained by solubilizing PA6 pellets at a concentration of 10% w/w using 1,1,1,3,3,3-hexafluoroisopropanol (HFIP) as solvent. The complete dissolution was obtained by stirring the solution at room temperature overnight.

For the preparation of PA6 dispersions doped with GRMs, GO powder was obtained by freeze-drying. GO and GNP powders were then dispersed in HFIP at appropriate concentrations and sonicated 2 hours before adding the PA6 pellets.

Composite dispersions were produced maintaining the same polymer concentration used in pristine polymer solutions. The relative GO concentration compared to the polymer was selected in a range from 0 to 2 % w/w. The relative GNPs concentration compared to the polymer was instead selected in a range from 0 to 10 % w/w.

All the dispersions (pristine PA6, PA6/GO and PA6/GNPs) were electrospun using the same electrospinning parameters. After electrospinning optimization, the voltage was set at 22 kV, the tip-to-collector distance at 30 cm and the extrusion flow at 0.03 mL/min.

8.2 RHEOLOGY OF ELECTROSPINNING SOLUTIONS

Before electrospinning, the rheology of the produced polymeric dispersions was evaluated to understand the effects of the addition of GO and GNPs on PA6 solutions.

The plot that reports viscosity values of the solution in function of the applied shear rate is shown in figure 50.

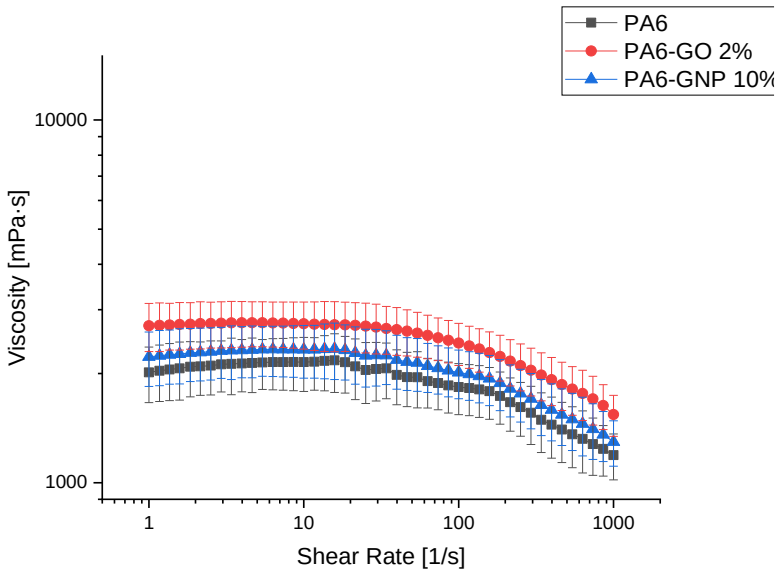

Figure 50: Rheological analysis of electrospinning dispersions of pristine PA6, PA6-GO 2% and PA6-GNP 10%

As it can be seen by this graph, the viscosity of all the solutions decreases at higher shear rates. This is typical of a non-Newtonian shear thinning behaviour, which is the most suitable rheology for electrospinning solutions.

Furthermore, as expected by the results shown in paragraph 6.3, the addition of GO as nanofiller increases the overall viscosity of the solutions. Despite the higher loading, the addition of GNP does not influence much the viscosity of the solution. This is probably due to the higher agglomeration and weaker affinity with the polymeric matrix that characterizes GNPs in comparison with GO.

The rheological results suggests that electrospinning of the polymeric dispersions should be possible and that GO-modified electrospun mats should be composed by thinner diameter nanofibers.

8.3 PRODUCTION OF ELECTROSPUN COMPOSITES

8.3.1 CO-ELECTROSPINNING OF GRAPHENE-BASED PA6 COMPOSITES

Pristine PA6 solution, PA6/GO dispersions and PA6/GNPs dispersion were all suitable materials to successfully produce electrospun mats.

10 cm x 10 cm PA6 electrospun mats with an average thickness of 100 µm are shown in Figure 51.

Figure 51: Optical image of electrospun PA6 mats highlighting its flexibility

The thickness of each single mat can be easily controlled by setting the appropriate deposition time. These mats are very flexible and lightweight (around 0.2 grams per mat), two important properties for wearable applications.

SEM image of the produced nanofibers (figure 52) proved the effectiveness of the electrospinning process in obtaining the researched nanostructured fibre morphology.

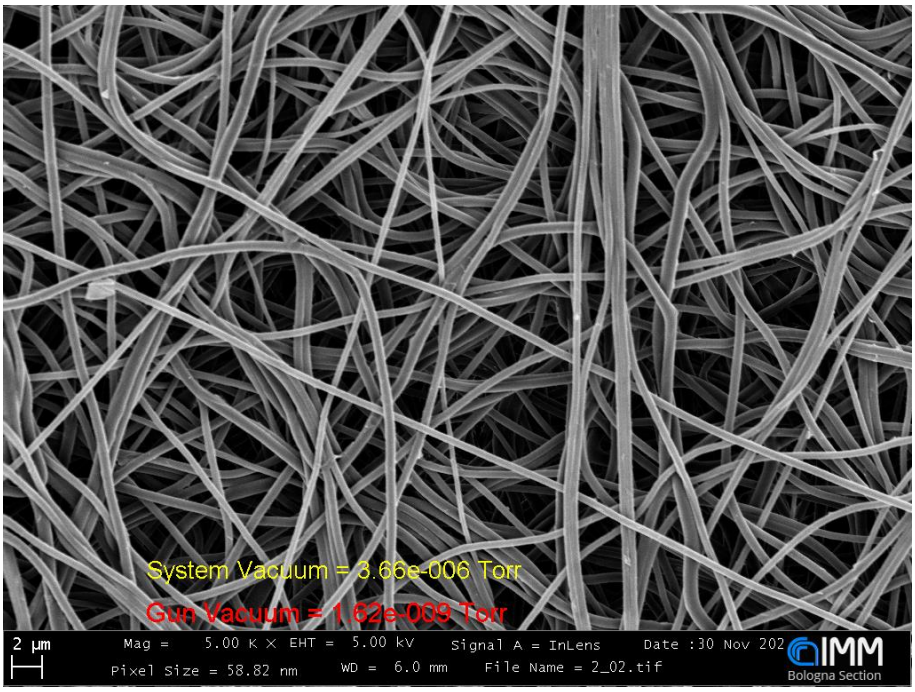

Figure 52: SEM image of pristine PA6 electrospun nanofibers

Further analysis on the SEM images was needed to estimate that the mean diameter of the obtained nanofiber is (520 ± 120) nm.

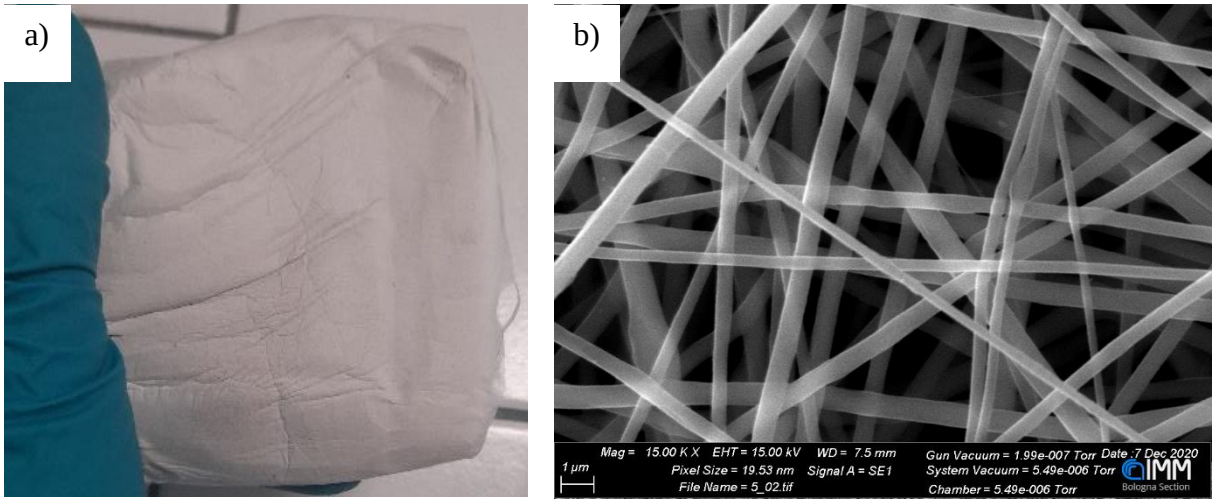

Figure 53: a) optical image and b) SEM image of electrospun PA6/GO 2% mats

As observed in chapter 5 for PVdF textiles, the addition of just 2 % of GO changed macroscopically the colour of the electrospun mat (figure 53 a) and drastically reduced the diameter of the nanofibers, as it can be seen from the SEM image (figure 53 b)

In this case, the average nanofiber diameter is approximately (400 ± 80) nm.

PA6/GNPs composite electrospun mats were successfully obtained even at higher nanofiller loadings, up to 10%. This is mainly due to the higher stacking and density of GNPs in comparison to GO and to their lower interaction with the matrix. These properties favours the aggregation of GNPs domain inside the polymeric matrix. This has a negative effect on the properties of the final material but allows to add a higher amount of filler since also the dispersion properties (such as its viscosity) are less affected by its concentration.

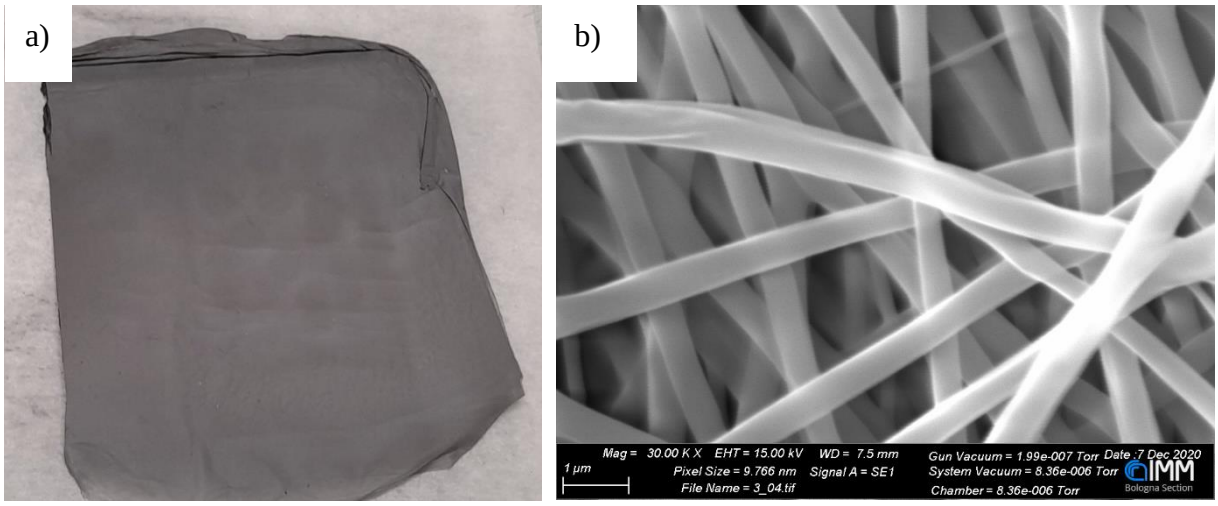

Figure 54: a) optical image and b) SEM image of electrospun PA6/GNP 10% mats

Figure 54 a) shows an optical image of the electrospun PA6/AVA18 composite and its dark grey colour is a good index of the presence of the filler in the electrospun material.
In this case, despite the high filler concentration, the weak matrix/filler affinity reduces its diameter-thinning effect on the nanofibers.
As shown by the SEM image (figure 54 b), the mean nanofiber diameter in this case (510 ± 100 nm) is comparable with the one of pristine PA6 nanofibers.

8.3.2 PRODUCTION OF GO COATED ELECTROSPUN COMPOSITES

Conductivity in polymeric composites is achieved when a fully interconnected network of conductive material is formed inside the polymeric matrix. In bulk composites, this happens when the concentration of the filler is higher than a threshold value called percolation threshold.
In nanostructured composite with fibre-like morphology, the complex network of intersecting nanofibers can be used as a scaffold for the formation of the conductive network. However, to allow conductive domains to be connected one another, they must be found on the surface of the nanofibers.
SEM images of electrospun composites show no evidence of conductive domains on the surface of the nanofibers. For this reason, and to explore a different approach on the production of nanostructured electrospun composites, we produced new materials exploiting a simple coating technique.
To exploit the advantages of the nanofiber morphology on the finale properties of the material, pristine PA6 electrospun mats were used as substrates. GO was used as coating agent for two main reasons.
First, it is known for its superior affinity with polyamides, and this could be crucial for improving the adhesion on the surface of the nanofibers and the overall mechanical stability of the coating.
Furthermore, GO is highly dispersible in water, while other GRMs are more easy to disperse in organic solvents. In this case, performing the coating process in aqueous solution is crucial since water is a non-solvent of PA6, thus the mechanical integrity and the nanofiber morphology of the electrospun mats will not be compromised by the GO dispersion.
A sonication-assisted dip-coating technique was used for the production of coated electrospun textiles.
This simple method consists in the immersion of the substrate in the coating dispersion. The whole system is then sonicated for 1 hour after a 15 minute degas step. The sonication helps the GO nanosheets to pass through the small pores in the nanofibrous mat, allowing to coat the entirety of

the nanofibers. Moreover, the energy that is provided to the system by sonication helps the GO sheets to wrap around the nanofibers in an effective way.

After the sonication, the sample is left drying in the air overnight.

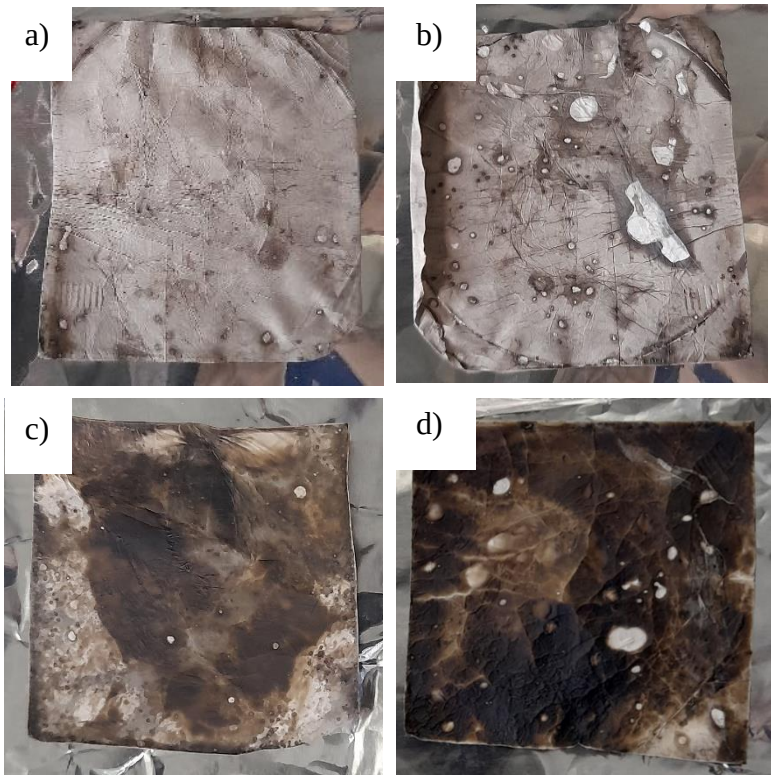

Figure 55: Optical images of GO-coated PA6 mats. Concentration of the coating soution was a) 0.025 mg/L b) 0.25 mg/L c) 2.5 mg/L and d) 4 mg/L

5 cm x 5 cm PA6 electrospun mats have been successfully coated with GO (figure 55). Different samples with different concentrations of the coating solution were produced to optimize the process conditions in order to obtain coatings that are both mechanically resistant and electrically conductive. The concentrations of the coating solution that were tested are 0.025 mg/L, 0.25 mg/L, 2.5 mg/l and 4 mg/L (solution as supplied).

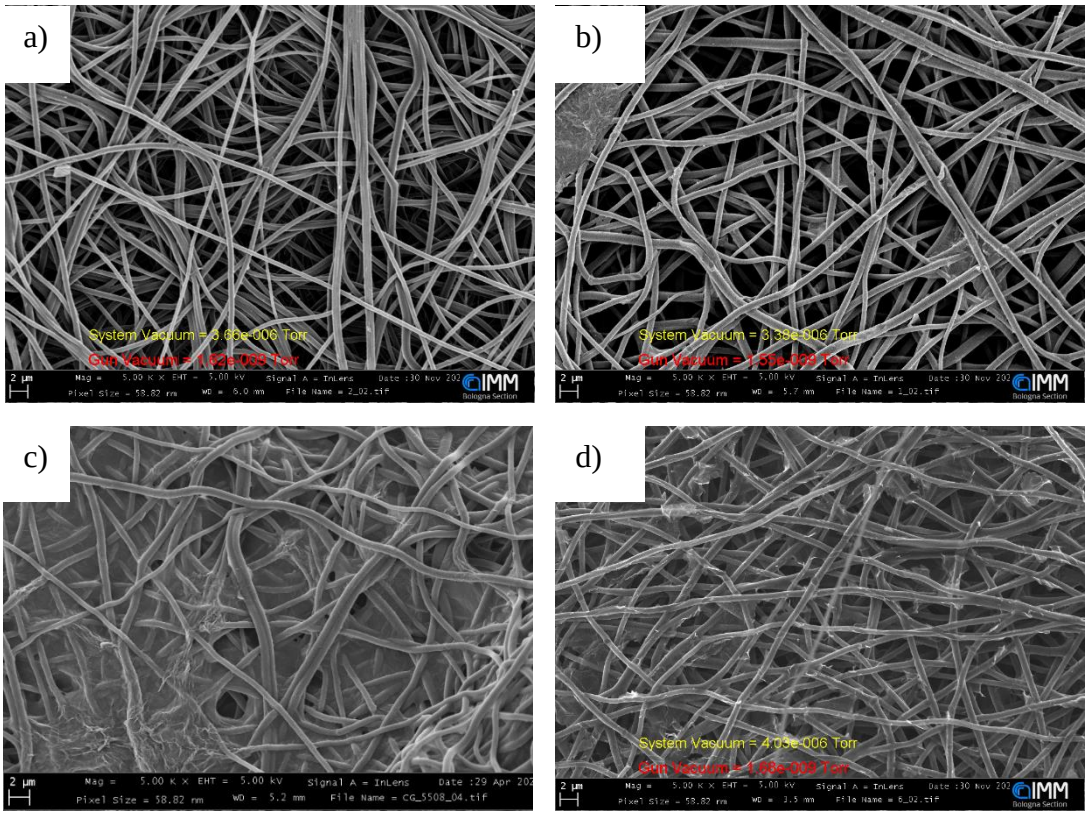

Figure 56: SEM images of GO-coated PA6 nanofibers obtained using coating dispersions with different concentrations: a) 0.025 mg/L, b) 0.25 mg/L, c) 2.5 mg/L and d) 4 mg/L

SEM images (figure 56) proves that the nanofiber morphology was retained even after the dip-coating step. A higher magnification (figure 57) also shows the presence of tiny wrinkles on the surface of the nanofibers. These were attributed to the presence of GO sheets wrapped around the surface of the polymer.

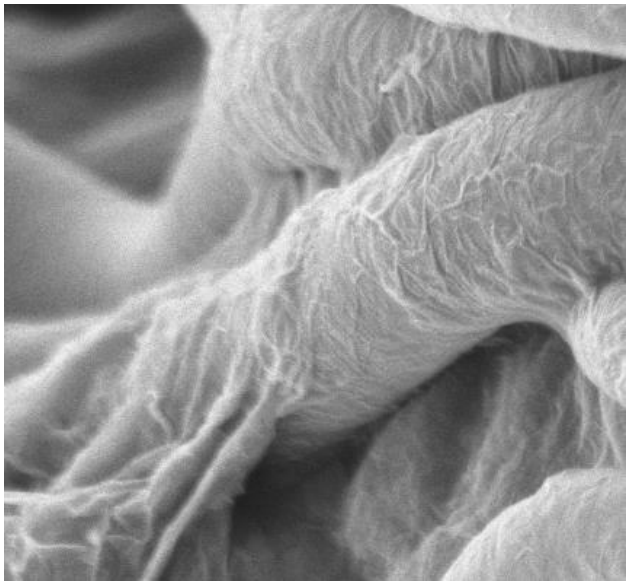

Figure 57: High-magnification SEM image showing the formation of wrinles on the surface of a PA6 nanofiber attributed to the coating with GO nanosheets

8.3.3 REDUCTION OF GO-CONTAINING COMPOSITES

As previously discussed, GO is widely used for composite production for its large surface area and affinity with many polymeric matrix, such as polyamides.

While this important advantage allows to obtain well-dispersed bulk composites and mechanically strong coatings, pristine GO is not suitable for the production of e-textiles and conductive polymers because of its poor electrical conductivity.

To partially restore the electrical properties typical of graphene and graphene-related materials, GO can be reduced in different ways to the more electrically conductive rGO (as schematized in Figure 58).

In this work we reduced GO containing composite (both co-electrospun and coated) using an environmentally friendly technique that involved no harmful solvents and reducing agents.

First, composite mats were chemically reduced in an L-Ascorbic acid aqueous solution. The concentration of the reducing solution was 5 mg/mL and the system was kept at 90°C using a hot plate.

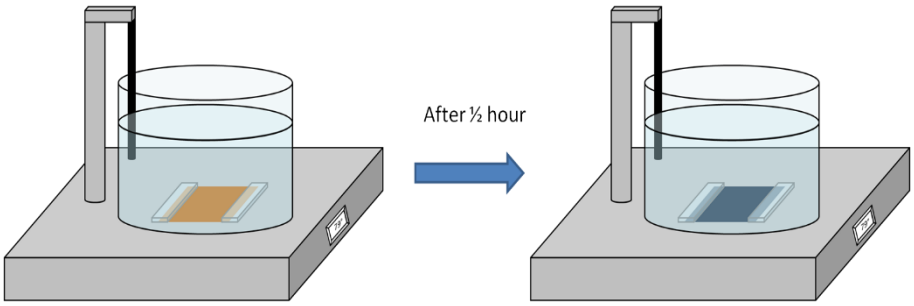

Figure 58: schematic representation of the process used for the reduction of GO coatings to rGO coatings

After 30 minutes, we removed the sample from the reducing bath and carefully rinsed it with warm distilled water (≈ 50°C) and room temperature distilled water. The washing step is crucial to prevent recrystallization of L-ascorbic acid on the surface of the composite that could compromise its conductivity.

After the chemical reduction, the samples were dried overnight in air and then underwent a thermal annealing step to conclude the reduction of GO domains. This thermal annealing step was conducted in an oven (ArgoLab TCF120) at 180°C for 30 minutes. Usually higher temperatures are needed to efficiently reduce GO to rGO. In our case, the thermal stability of PA6 (melting temperature ≈ 200°C) does not allow its thermal annealing at higher temperatures without compromising the nanofiber morphology. For this reason, we used this specific two-step chemical and thermal reduction process.

Figure 59 shows optical images of the reduced samples.

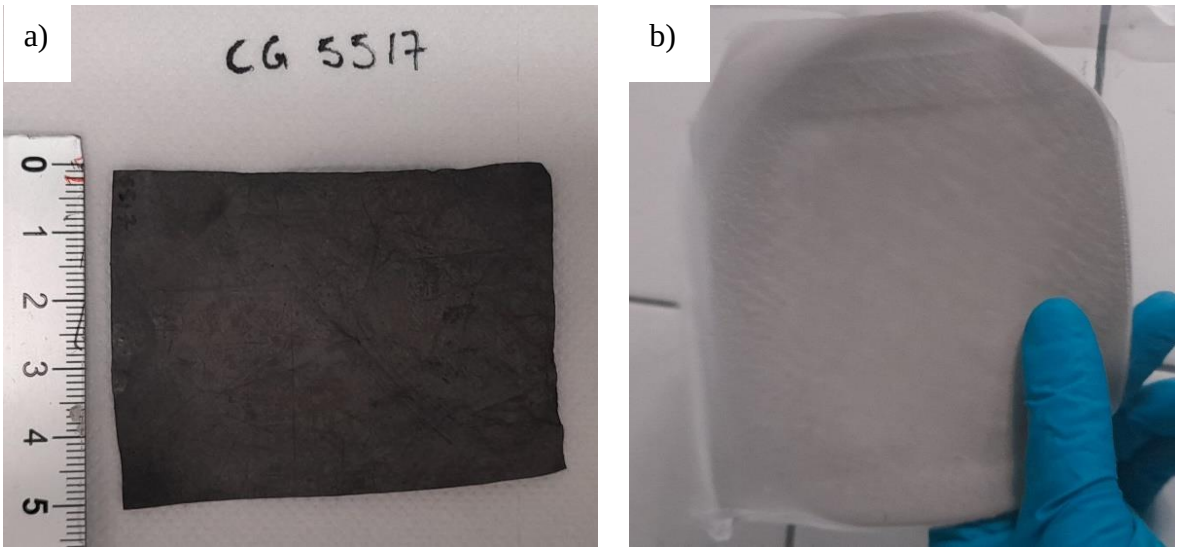

Figure 59: Optical image of reduced PA6/rGO mats. a) coated PA6/rGO mat and b) co-electrospun PA6/rGO 2% mat

The change of colour from brownish to dark grey/black is a first hint that the reduction of GO to rGO was successful. The coated sample (Figure 59 a) changed more in colour, probably caused by the fact that GO domains are exposed on the surface of the nanofibers so a large part of the GO nanosheets were reduced. On the other hand, the co-electrospun PA6/GO composite changed only slightly in colour, suggesting a non-complete reduction of the GO domains.

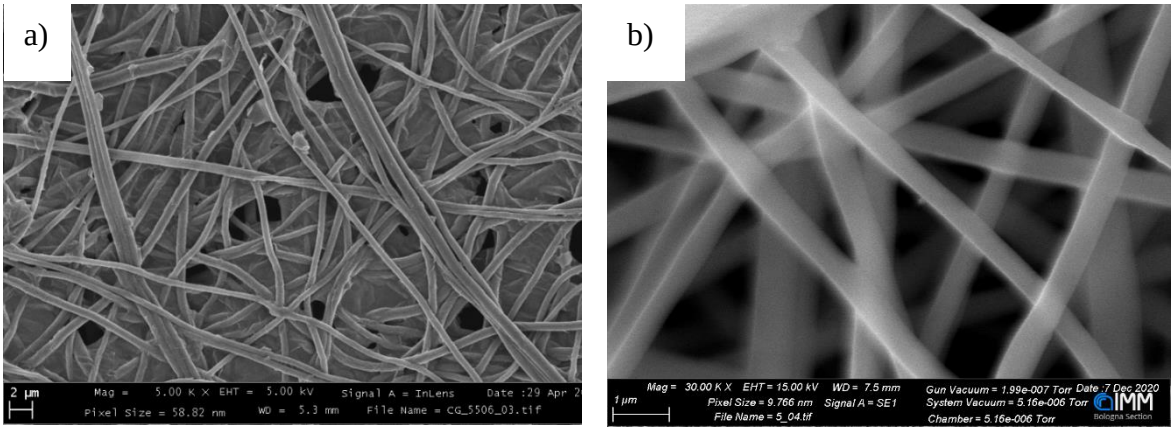

Figure 60: SEM images of a) reduced PA6/rGO coated electrospun mats and b) reduced PA6/rGO 2% co-electrospun mats

This is probably due to the fact that many GO domains in this sample are in the core of the nanofibers, hence not available for the reduction.

SEM images (figure 60) show that the two-step reduction process did not compromise the nanostructured morphology of the electrospun materials. In particular, coated samples continued to

show rGO wrinkles on the surface of the nanofibers, while co-electrospun mats are characterized by smoother nanofibers, as before reduction.

8.3.4 LIST OF GRAPHENE-BASED ELECTROSPUN COMPOSITES

To clarify the difference between the produced materials, they have been collected in Table 7. Column 5 contains the name that they will be referred to for the rest of this thesis.

MATRIX	**ADDITIVE**	**TECHNIQUE**	**POST-TREATMENTS**	**SAMPLE NAME**
PA6	---	electrospinning	---	ES-PA6
PA6	GO 2%	Co-electrospinning	---	COES-PA6GO
PA6	GO 2%	co-electrospinning	Chemical and thermal reduction	COES-PA6rGO
PA6	GNPs 10%	Co-electrospinning	---	COES-PA6GNP
PA6	GO (from water solution 2.5mg/mL)	Coating of electrospun PA6 mats	---	ES-PA6-c-GO
PA6	GO (from water solution 0.025mg/mL)	Coating of electrospun PA6 mats	Chemical and thermal reduction	ES-PA6-c-rGO1
PA6	GO (from water solution 0.25mg/mL)	Coating of electrospun PA6 mats	Chemical and thermal reduction	ES-PA6-c-rGO2
PA6	GO (from water solution 2.5mg/mL)	Coating of electrospun PA6 mats	Chemical and thermal reduction	ES-PA6-c-rGO3
PA6	GO (from water solution 4mg/mL)	Coating of electrospun PA6 mats	Chemical and thermal reduction	ES-PA6-c-rGO4

Table 7: Summary of produces graphene-based electrospun composites

8.4 XPS ANALYSIS

Coating is a process that involves a surface modification of the material. For this reason, XPS is particularly suited for coating analysis, since it gives information on the first 10 nanometres of the surface of the material.

Therefore, XPS was used to analyse coated composites to prove the effectiveness of the coating and reduction steps.

Figure 61 shows the XPS survey spectra of ES-PA6, ES-PA6-c-GO3 and ES-PA6-c-rGO3. These samples were selected among the rGO-coated ones for the homogeneity of their surface coating.

Numerical data on the relative abundance of C 1s, O 1s, N 1s and S 2p in the different samples and in a sample of the GO powder are collected in Table 8.

XPS analysis confirmed the effectiveness of the coating process, by looking at the variations in chemical composition of the samples ES-PA6 and ES-PA6-c-GO3.

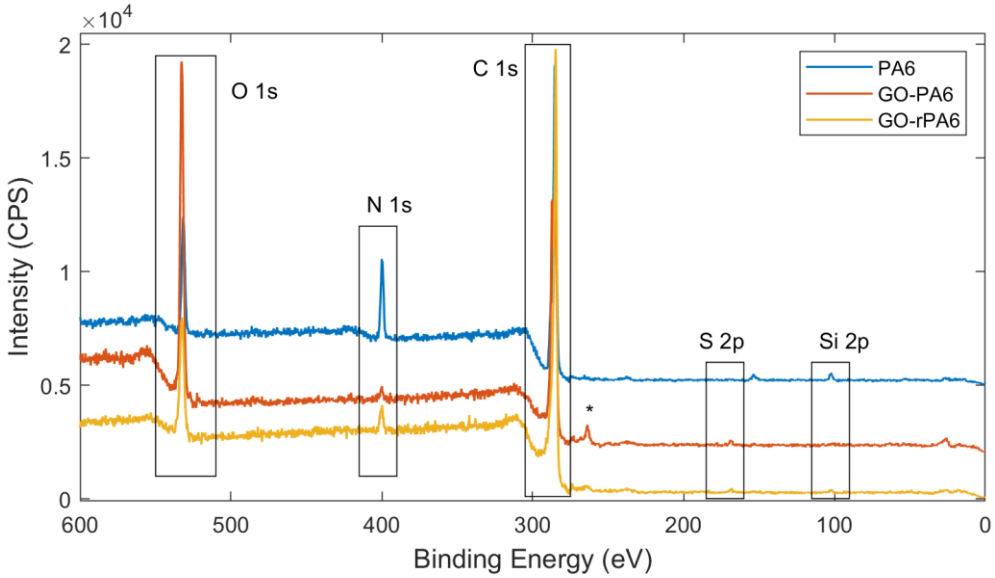

Figure 61: XPS survey spectra comparing the chemical composition of ES-PA6, ES-PA6-c-GO and ES-PA6-c-rGO

Elements	C 1s 285 eV	O 1s 532.1/ 530.6 eV	N 1s 399.8 eV	S 2p 168 eV
PA6	76.9 ± 1.0	11.2 ± 0.5	10.0 ± 0.3	-
GO*	72.1 ± 1.0	26.1 ± 1.0	0.4 ± 0.1	0.4 ± 0.1
GO/PA6	69.5 ± 1.0	28.6 ± 0.5	1.6 ± 0.2	0.5 ± 0.1
rGO/PA6	83.3 ± 1.0	13.6 ± 0.5	2.6 ± 0.2	0.4 ± 0.1

*Table 8: Comparison between the relative chemical composition of PA6, PA6-c-GO, PA6-c-rGO electrospun mats and GO powder *0.15% Mn and 0.9% Si.*

The sample coated with GO, in particular, shows a lower content in C 1s (from 76.9% to 69.5%) and a higher content in O 1s (from 11.2% to 28.6%). This information, alongside the presence of traces of S 2p that is a contaminant found in GO powder, confirms that the surface of the nanofibers is composed by a large majority by GO sheets. Furthermore, the N 1s relative amount drastically drops, suggesting that the polymer composes a small portion of the exposed surface, since nitrogen is mostly found in PA6.

XPS analysis also confirmed that the two-step reduction process was sufficiently effective. In particular, the main differences between the GO-coated sample and the rGO-coated one are the C 1s and O 1s relative compositions.

The reduction process caused an increase in the amount of C 1s on the surface of the material (from 69.5% to 83.3%) while simultaneously reducing the amount of O 1s (from 28.6% to 13.6%).
This is a clear evidence that the chemical/thermal process effectively reduced the coating material. A further evidence can be extracted by C 1s XPS spectra (figure 62)

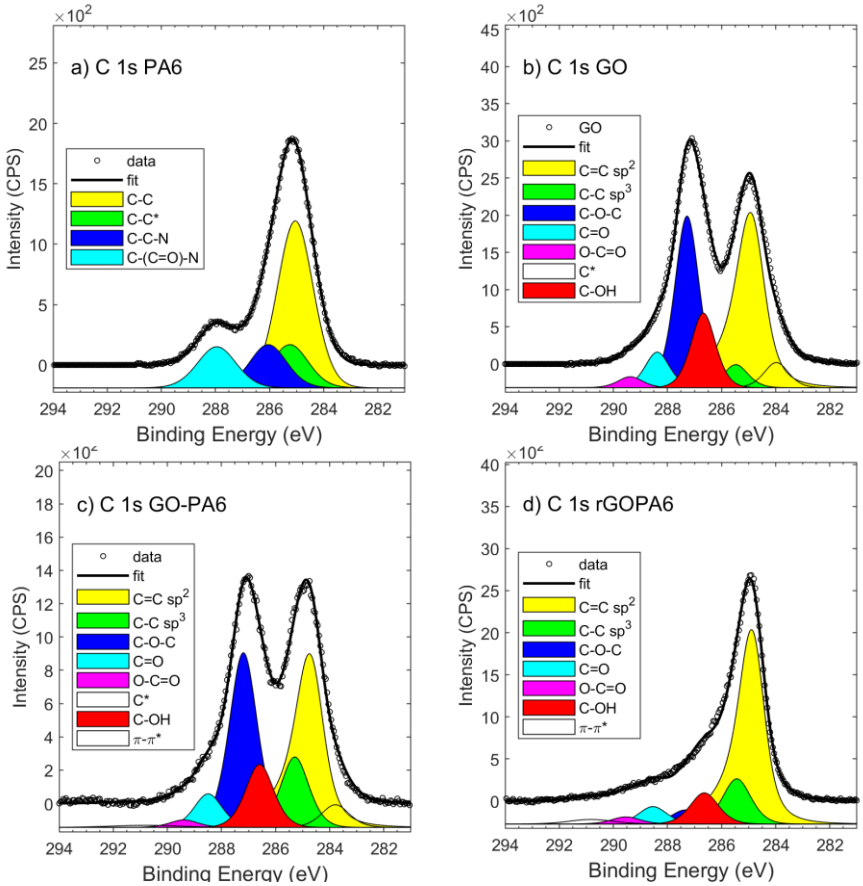

Figure 62: Comparison of Carbon 1s XPS spectra of a) electrospun PA6, b) GO powder, c) GO-coated PA6 electrospun mats and d) rGO-coated PA6 electrospun mats

8.5 THERMAL ANALYSIS

Thermal properties of electrospun composites were evaluated by TGA and DSC analysis.
The resulting plots are shown in figure 63.
Since all the composites showed similar behaviour, ES-PA6 and COES-PA6GO were selected to discuss the influence of graphene-based composites on the thermal properties of electrospun PA6 nanofibers.

TGA analysis clearly shows that GO addition has negligible influence on the thermal stability of the material. In detail, the onset for the thermal degradation temperature sets at 428.89°C for pristine PA6 mats and only slightly increases up to 431.02°C for GO-charged composites.

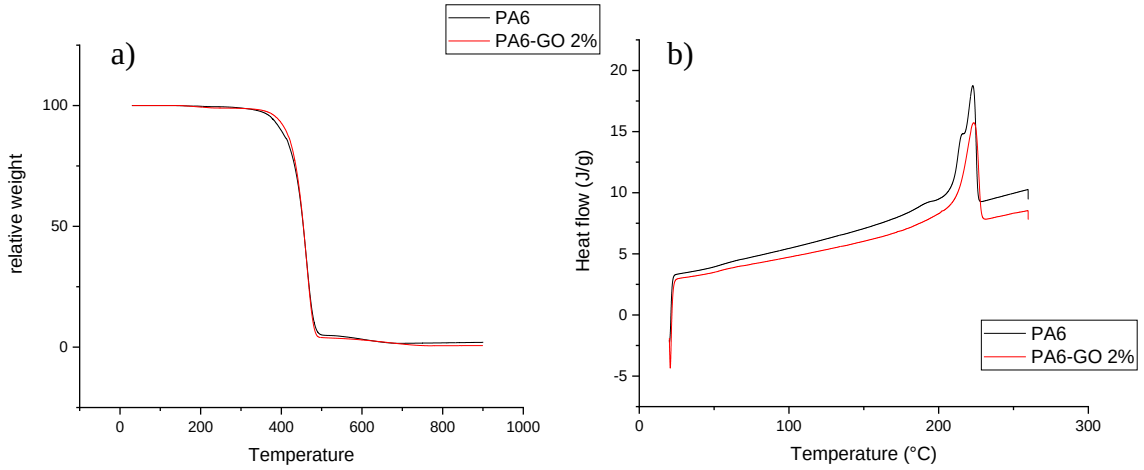

Figure 63: Comparison of a) TGA analysis and b) DSC analysis plots of electrospun PA6 mats and co-electrospun PA6/GO 2% mats

Also DSC analysis show the negligible effect of GO addition on thermal properties, since the glass transition temperature shifts from 222.79°C (with a ΔH of 75.6 J/g) for pristine PA6 to 223.29°C (with a ΔH of 73.6 J/g) for GO-charged PA6 electrospun mats.

The thermal degradation temperatures and glass transition temperature obtained in these analyses are coherent with the typical values found in literature for PA6 polymers. This gives us information on the good behaviour of the polymer during electrospinning and on the fact that the addition of nanofillers does not compromise the already good thermal properties of the matrix.

8.6 ELECTRICAL CONDUCTIVITY OF THE ELECTROSPUN COMPOSITES

To test their possible applications in wearable electronics applications and to study in which devices the electrospun composites could be exploited, we tested their electric conductivity.

All measurements were conducted after contacting the samples to ensure a better charge transfer between the tips of the analysing probes and the sample. The typical contacts were made by applying a conductive paint containing silver nanoparticles on the surface of the material and using this as an adhesive to paste a thin copper foil on top of it. An image of a contacted sample is shown in figure 64.

Figure 64: Optical image of rGO-coated PA6 electrospun mat with silver paint/copper foil electrical contacts

The electrical conductivity analysis consisted in a measurement of the voltage that forms between the two sensing probes at different set current intensities. The collected I/V plots were then used to obtain the mean sample resistance in this range of current intensities by applying Ohm's law (Equation 4)

$$R = \frac{V}{I} \qquad \text{EQ. 4}$$

where R is the electrical resistance of the sample expressed in Ω, V is the voltage measured across the conductor and I is the current passing through the conductor.

A typical obtained I/V plot is shown in figure 65

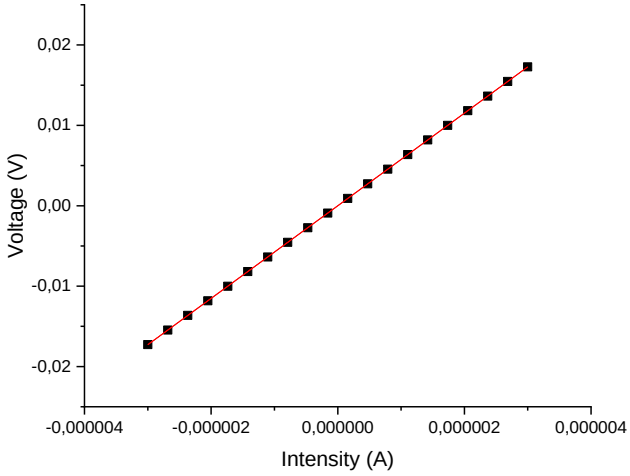

Figure 65: Example of a I/V plot otained by 4-point probe electrical measurements

Since the obtained resistance values do not take in consideration the geometry of the samples, for textiles or film-like materials in general the sheet resistance is usually considered. When the thickness of the material is negligible in respect to its other two dimensions, the sheet resistance is simply found by equation 5

$$SR = R * \frac{W}{L} \qquad \text{EQ. 5}$$

where the sheet resistance (SR, expressed in Ω/sq) is calculated starting from the measured resistance (R, expressed in Ω), the width of the sample (W, expressed in mm) and the length of the sample, or the length of the channel between the two sensing contacts (L, expressed in mm).

8.6.1 CONDUCTIVITY OF CO-ELECTROSPUN MATS

Co-electrospun samples COES-PA6rGO and COES-PA6GNP were contacted and their electrical conductivity was measured. Their sheet resistances were compared to electrospun pristine PA6 that, as expected, was completely electrically insulating.

Both COES-PA6rGO and COES-PA6GNP showed very high sheet resistance in the range of tens of GΩ/sq. This poor electrical conductivity was not expected, especially since the loading of both nanofillers is higher than the percolation threshold values found in literature for non-nanostructured composites.

To verify that these poor electrical performances only depended from the production method, PA6/rGO and PA6/GNP samples were produced starting from the same dispersions used for electrospinning but using a blade casting process. This further test was necessary to exclude issues in the nanofiller dispersion or the poor electrical conductivity of the nanofiller themselves.

The blade casting process was performed using an Erichsen CoatMaster 510 blade casting equipment, which consists in a rigid blade that is able to move above a flat surface, homogeneously spreading a viscous mass of polymeric solution on top of it.

The gap between the blade and the surface can be adjusted to obtain polymeric films with a controlled thickness, while setting the speed of the blade allows a defectless and homogeneous spreading of the polymer solution. After obtaining a polymeric dispersion film, it was left overnight and a thin film of composite material was obtained

For the formation of PA6/rGO and PA6/GNP mats, the blade/surface gap was set appropriately to obtain films with a final thickness of ≈ 100 μm. Optical images of the obtained materials can be seen in Figure 66.

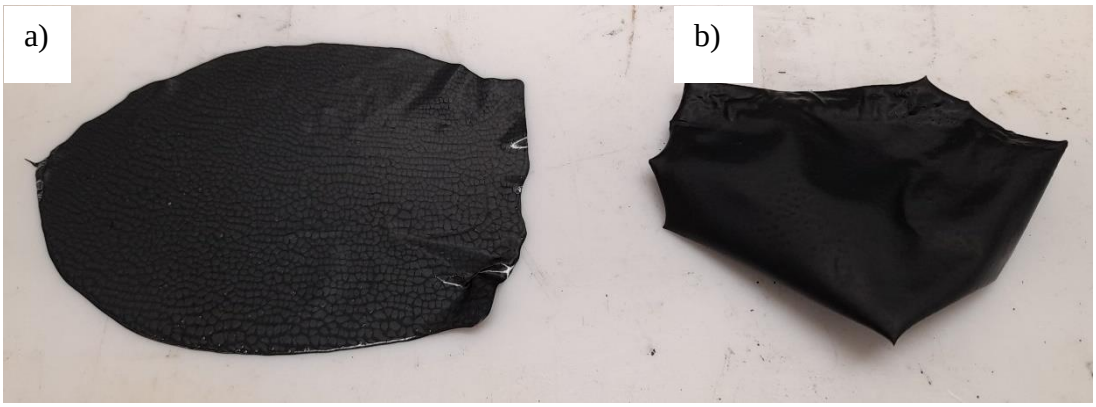

Figure 66: Optical image of composite films of a) PA6/GNPs 10% and b) PA6/rGO 2% obtained by blade casting

5 cm x 5 cm samples were cut from this polymeric films and contacted using the same technique used for electrospun composites.

The mean sheet resistance of the rGO-charged PA6 cast samples was estimated in (3.0 ± 0.4) MΩ/sq, while the GNPs-charged PA6 cast samples showed a mean sheet resistance of approximately (5.8 ± 0.4) kΩ/sq.

These results suggest that producing a graphene-based composite through co-electrospinning technique has a negative effect on the electrical conductivity of the final material. This is probably due to the nanofiber morphology that hinders the formation of a fully-connected network of the conductive reinforcements when these domains are present in bulk in the polymeric matrix and to the presence of GO domains in the core of the composites, that makes them non-available for the reduction.

8.6.2 CONDUCTIVITY OF COATED MATS

The electrical conductivity of the coated samples after reduction (ES-PA6-c-rGO) was tested with the same procedures used for co-electrospun samples.

ES-PA6-c-rGO1 and ES-PA6-c-rGO2 (obtained from GO coating solutions with concentration 0.025 mg/L and 0.25 mg/L respectively) remained electrically insulating even after coating and reduction of the PA6 electrospun mats.

ES-PA6-c-rGO3 and ES-PA6-c-rGO4 (obtained from GO coating solutions with concentration 2.5 mg/L and 4 mg/L respectively) showed instead a remarkable enhancement in electrical

conductivity. The mean values of sheet resistance measured for these samples are respectively (650 ± 100) Ω/sq and (120 ± 20) Ω/sq.

The obtained results suggest that at lower concentrations of the coating solution, the coted mass of GO is not enough to form a conductive network on the surface of the nanofibers. On the other hand, when the concentration is higher than 2.5 mg/L a conductive path is effectively formed on the surface of the nanofibers, improving the electrical conductivity of the material.

Despite the better conductivity, the rGO coating on the surface of the nanofibers of ES-PA6-c-rGO4 was thick and mechanically weak. Probably, the high viscosity of the coating solution caused a thick layer ("cake") of GO to deposit on the surface of the sample, forming a mechanically weak layered system.

For this reason, ES-PA6-c-rGO3 samples were selected for mechanical tests and for their testing for wearable devices application. Numerous samples were prepared (Figure 67) and their sheet resistances ranged from 500 to 800 Ω/sq.

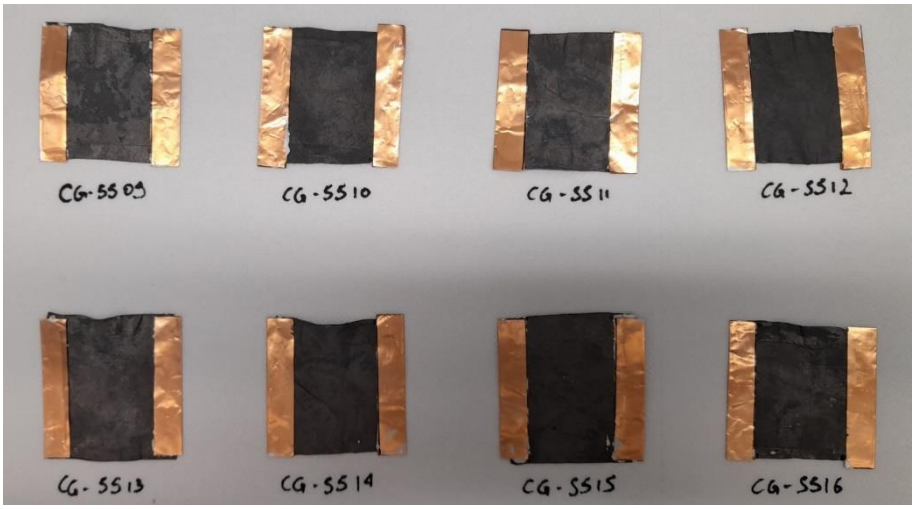

Figure 67: rGO-coated PA6 electrospun samples

To verify the effect of the nanostructured morphology on the coating process, rGO-coated textiles were produced starting from commercial textiles composed by fibres with diameters in the order of tens of µm. Commercial textiles were purchased by MAEKO tessuti (Milano,Italy). For these coating tests, we used a 100% cotton textile, because cotton is a widespread material in clothing industry, and a 96% bamboo/4% elastan textile for its high stretchability. Since electrospun mats are not stretchable, this material could expand the application fields of graphene-based coated textiles.

Both commercial textiles were GO-coated and reduced exploiting the same techniques that were used for electrospun PA6 mats. An optical image of the rGO-coated commercial textiles is shown in Figure 68.

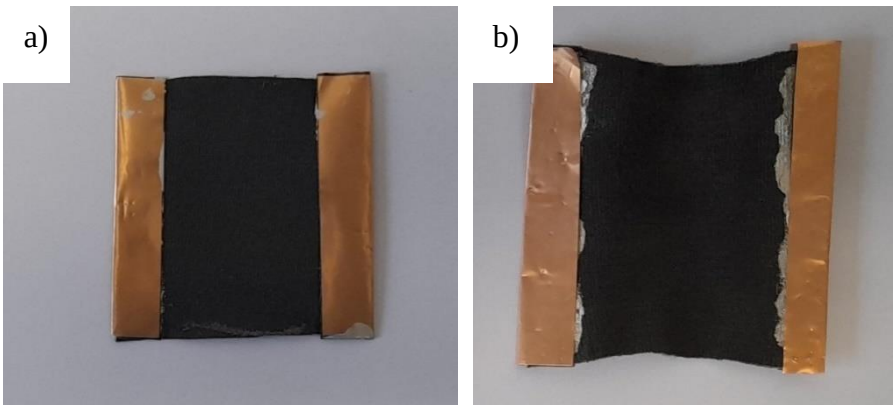

Figure 68: Commercial tetiles coated with rGO. a) cotton-c-rGO and b) bamboo/elastan-c-rGO

After contacting, the sheet resistances were measured as for coated electrospun mats.
The rGO-coated cotton textiles show a mean sheet resistance of approximately 10 kΩ/sq, while the rGO-coated bamboo/elastan textiles show a mean sheet resistance of approximately 50 kΩ/sq.
These results confirm the positive effect of the nanometric morphology of the materials on their electrical conductivity when they are coated with a graphene-based material. This positive effect is probably due to the thin diameter of the nanofibers, which confers them a high interconnectivity and reduces the size of the pores between each fibre.

8.7 MECHANICAL TESTS

To prove the mechanical stability of electrospun coated mats, the variation of their sheet resistance after mechanical stress was analysed.
A crucial parameter for e-textiles and wearable electronics is their washing cycle resistance. For this reasons, ES-PA6-c-rGO3 samples were tested following the method AATCC-135 for home laundering tests of textiles materials. This test was performed in collaboration with University of Strasbourg.
The samples underwent a 30 complete washing cycles at 40°C with a total load of 2 kg in a commercial washing machine. After completing the standard method, the electrical conductivity of the samples was tested and confronted to the one registered before their washing.
All the coated samples showed a strong mechanical resistance and the washing cycles did not deteriorate their morphology. The mean sheet resistance variation after washing was negligible (< 1%), suggesting that also the conductive coating on the surface of the nanofibers is characterized by a strong mechanical resistance.

The results of these tests are very promising towards a possible application of these materials in wearable devices.

We also performed a sharp-corner folding test to prove the resistance of the materials to bending and folding.

After measuring the pre-test sheet resistance, the samples were folded in half at a sharp corner (180°C) and a determined weight was applied on the top of the fold. Afterwards, the samples were folded backwards (-180°) and the same weight applied on the backwards fold. This concluded the folding cycle (figure 69).

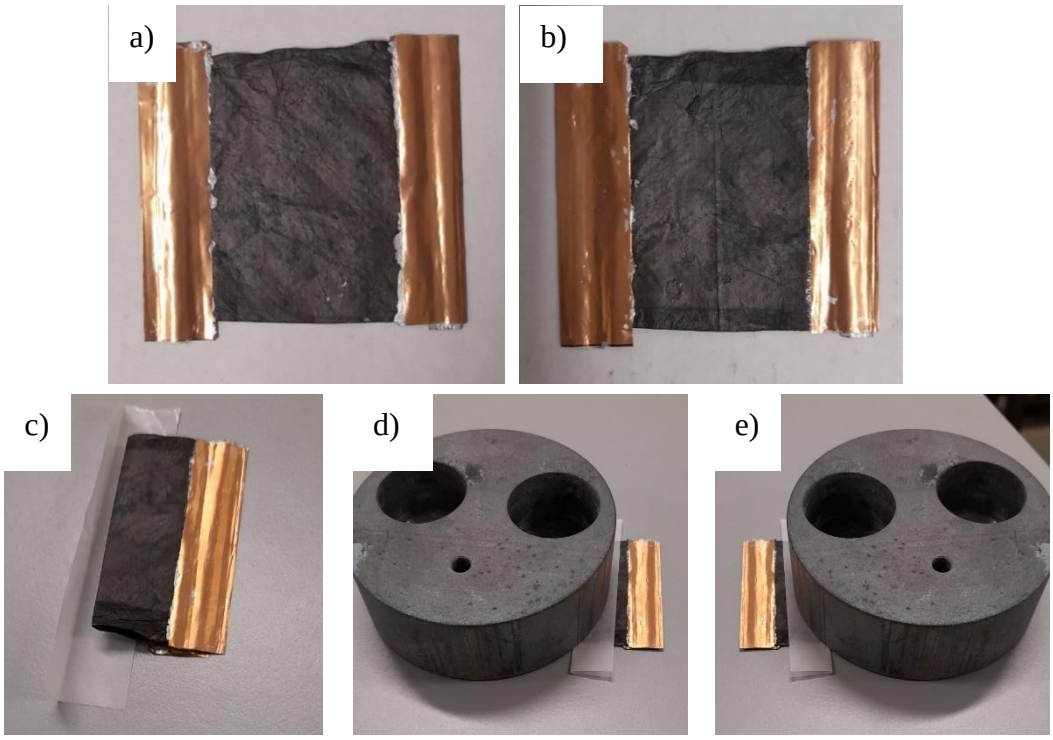

Figure 69: Optical image of the sample a) before and b) after 50 folding cycles. c), d) and e) show different stages of a single folding cycle

The variation in sheet resistance of the samples was registered after 50 folding cycles. As it is possible to see in the graph (figure 70), also in this case the sheet resistance variation for the samples is negligible (< 1%), suggesting that the material has a strong mechanical resistance to bending and folding.

For this reason, one of the possible applications that can be foresaw for these materials is in the field of strain sensing, in detail as sensing elements in bending and pressure sensing devices.

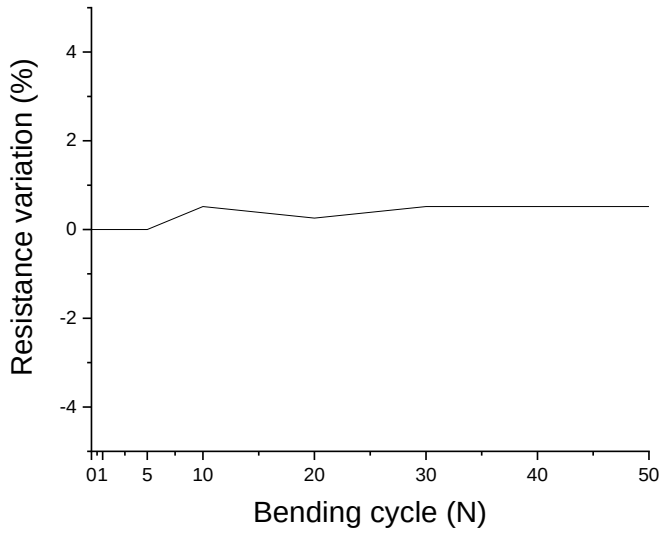

Figure 70: Plot showing the sheet resistance variation in an rGO-coated electrospun sample during 50 folding cycles

8.8 CONCLUSIONS

Electrospun mats of pristine PA6 and PA6/GRMs composites were successfully produced and the obtained morphology was positively tested through SEM imaging.

Moreover, a simple, environmentally friendly coating and reduction process was fine-tuned and used for the production of electrospun PA6 mats coated with reduced graphene oxide. XPS analysis confirmed the effectiveness of both the coating sand the reduction steps.

The electrical conductivity of the produced materials was tested using a 4-point probe method.

Co-electrospinning of bulk GRM-PA6 composites produced textiles with a high sheet resistance that are not suitable for e-textiles applications. This is probably due to the electrospinning technique that hinders the formation of a conductive path in the core of the polymer matrix due to the high orientation of the nanofiller domains during the process.

An alternative way was found in the coating of electrospun mats with conductive GRMs. The best results were achieved by GO-coating a PA6 electrospun mat and subsequently reducing the obtained composite.

The coated composites showed sheet resistances of ≈ 500 Ω/sq, which are promising for their possible application in wearable electronic devices. The advantages of using an electrospun textile as substrate for the coating process was proven by comparison with commercial textiles that were coated using the same technique.

Moreover, mechanical tests of washing and sharp-corner bending proved the mechanical strength of the electrospun polymer and the strong adhesion of the coating. This allows the materials to retain their electrical properties even after several washing and bending cycles.

The obtained composites could be used for different applications in the field of smart textiles and flexible electronics. In particular, some of the produced textiles were tested as strain sensors sensible to pressure, bending and stretching deformations. Preliminary tests show their sensibility towards this mechanical stresses and are promising for their possible application in this sort of devices.

According to literature, though, the conductivity of these materials is not good enough to be exploited in wearable heating elements [124] [125]. The following steps in this research will focus on further enhance the electrical properties of these materials. One possible way of achieving this result is to perform a multi-layered coating of conductive GRMs on the surface of the electrospun nanofibers. Preliminary tests already showed the feasibility and promising results of this approach even when only a second coating is applied on the top of the first.

9. PRODUCTION OF ELECTROSPUN COMPOSITES FOR FILTRATION AND ADSORPTION APPLICATIONS

9.1 MATERIALS

Graphene oxide was prepared from graphite flakes by a modified Hummers method [119]. The GO water dispersion (2.5 g/L) was sonicated 40 h and used for the next phases.

Cellulose nanofibers produced at Innventia AB (Stockholm, Sweden) and labelled CNF G1 were used in this study. For their manufacture a commercial bleached sulphite softwood pulp (Domsjö ECO Bright, Domsjö Fabriker AB, Sweden) consisting of 40% pine (Pinus sylvestris) and 60% spruce (Picea abies) with a hemicellulose content of 13.8% and a lignin content of 1% was used. The pulps were thoroughly washed with deionized water before use.

CNF G1 was processed using a combined refining and enzymatic pre-treatment followed by high-pressure homogenization. CNF G1 microfibrils have diameters of ~17–30nm

The dispersions for electrospinning were prepared starting from amorphous PLA pellets (Natureworks INGEO 4060D), from the freeze-dried GO powder and from CNF G1

Pure PLA solutions were obtained by solubilizing PLA pellets at a concentration of 10% w/w using 1,1,1,3,3,3-hexafluoroisopropanol (HFIP) as solvent. The complete dissolution was obtained by stirring the solution at room temperature overnight.

For the preparation of PLA dispersions doped with GRMs, GO powder obtained by freeze-drying was dispersed in HFIP at appropriate concentrations and sonicated 2 hours before adding the PLA pellets. CNF G1 instead was used starting from a 2.1% w water dispersion. The solution underwent a solvent exchange process by multiple centrifugation steps to disperse the CNFs in HFIP.

Composite dispersions were produced maintaining the same polymer concentration used in pristine polymer solutions. The relative GO concentration compared to the polymer was 0.5% w/w, while the relative CNF concentration was up to 10% w/w.

All the dispersions (pristine PLA, PLA/GO and PLA/CNF) were electrospun using the same electrospinning parameters. After electrospinning optimization, the voltage was set at 18 kV, the tip-to-collector distance at 20 cm and the extrusion flow at 0.03 mL/min.

9.2 PRODUCTION OF ELECTROSPUN MATS

Pristine PLA electrospun mats were successfully obtained in the already discussed conditions.
A 10 cm x 10 cm PLA electrospun mats with an average thickness of 100 µm is shown in Figure 71 a). The thickness of the mat can be easily controlled by setting the appropriate deposition time.

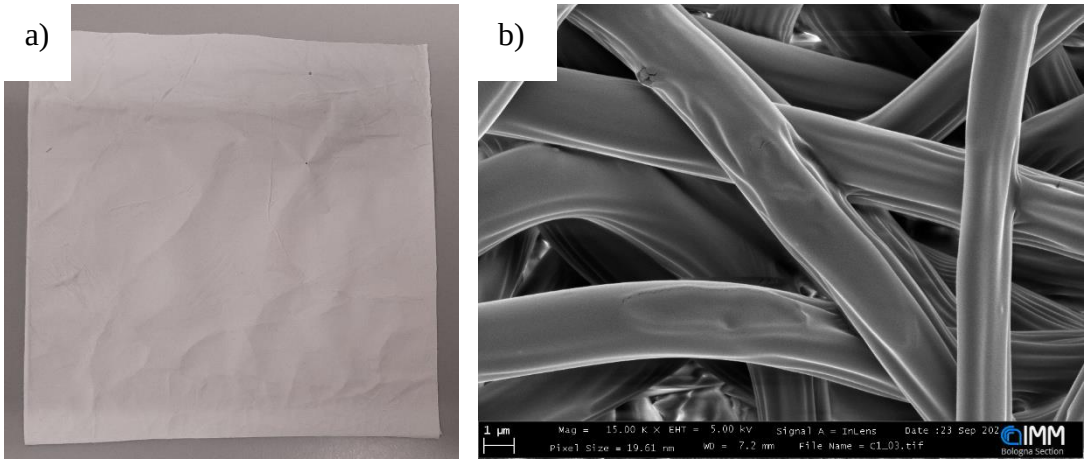

Figure 71: a) Optical image and b) SEM image of electrospun PLA mat

SEM analysis (figure 71 b) shows clearly the typical grooved morphology and large diameter of the PLA fibres produced thorugh electrospinning. In particular the mean diameter of these microfibers was found to be (2100 ± 300) nm.
GO-charged electrospun PLA mats were also successfully prepared with GO loading up to 0.5%. Optical and SEM images can be seen in figure 72.

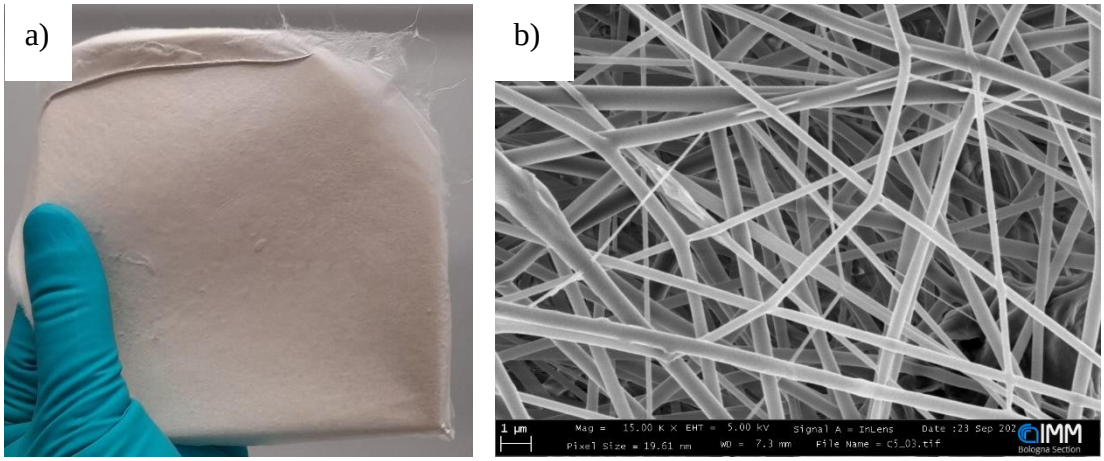

Figure 72: a) Optical image and b) SEM image of PLA/GO 0.5% co-electrospun mat

The effects of GO addition on the nanofiber morphology is evident by analysing the SEM image. PLA/GO 0.5% nanofibers obtained through electrospinning are smooth and their diameter is thinner than the pristine PLA ones. By analysing the SEM images we found that the mean nanofiber diameter sets at (400 ± 120) nm, proving once again the strong nanofiber-thinning effect of GO when used in co-electrospinning processes.

Despite the low affinity between hydrophobic PLA and hydrophilic CNFs, by optimizing the production of the electrospinning dispersion we were also able to successfully obtain PLA/CNF electrospun mats with CNF loadings up to 10%.

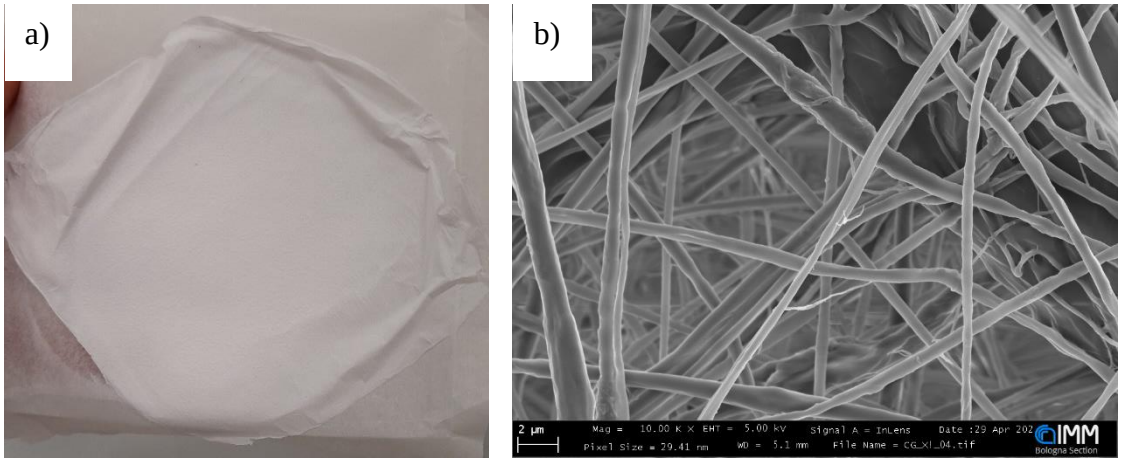

Figure 73: a) Optical image and b) SEM image of co-electrospun PLA/CNF 10% mats

Optical image (figure 73 a) and SEM images (figure 73 b) of PLA/CNF electrospun mats show that the electrospinning process was successful. The resulting material show enhanced mechanical properties when compared to pristine PLA mats and the mean nanofiber diameter is (630 ± 180) nm, comparable with the one obtained by GO addition.

9.3 SURFACE AREA AND POROSITY ANALYSIS

The main advantage of GO addition in PLA electrospun mats is the reduction of the nanofibers diameter.

For this reason it is crucial to understand the effect that GO addition has on the active surface area and on the porosity of the final electrospun material. These properties were analysed both with instrumental BET analysis and with a liquid displacement method.

BET analysis is based on the adsorption and desorption of an inert gas (N_2) on the surface of the material at low temperature conditions. The resulting plots for electrospun PLA and PLA/GO 0.5% mats are shown in figure 74.

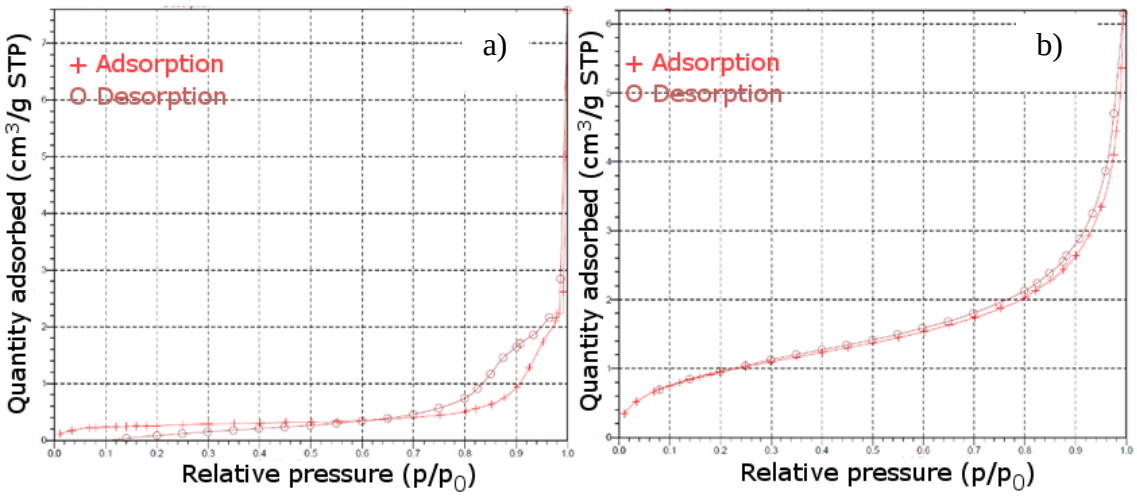

Figure 74: BET desorption plots of a) electrospun PLA mat and b) co-electrospun PLA/GO 2% mat

The BET analysis highlights the increase in the surface area of the material after GO loading as low as 0.5%. In detail, by data analysis, the results show an increase in surface area from (0.9 ± 0.2) m^2/g to (3.6 ± 0.5) m^2/g. This is due to the reduction of the average diameter of the pores that forms between nanofibers from ≈ 54 nm to ≈ 11 nm. The intersecting adsorption and desorption curves in Figure 74 a) are due to the very low surface area of the material, that falls around the sensitivity limit of the instrument.

The liquid displacement method used for the determination of the porosity is based on the difference in mass when a known-dimensions textile sample is weighted in air or in a fluid with known viscosity [126]. The material must not be soluble in the selected solvent and its swelling ratio in the solvent must be negligible. In this work, for PLA mats, n-hexane was selected as a solvent.

The density of the sample can easily be calculated from equation 6

$$\rho = \frac{(m_{air} * \rho_{hex})}{(m_{air} - m_{hex})} \qquad \text{EQ. 6}$$

Where m_{air} and m_{hex} are the measured masses in air and hexane, respectively, and ρ_{hex} is the density of hexane at room temperature (0.659 g/cm^3).

The relative porosity of the sample (ε%) can then be found applying equation 7

EQ. 7

$$\varepsilon(\%) = \frac{V_{tot} - V}{V_{tot}} * 100$$

Where V_{tot} is the apparent volume of the sample calculated geometrically by approximating it to a parallelepiped with low height and V is the "real" Volume occupied by nanofibers obtained by the multiplying the density of the sample found in equation 6 by m_{air}.

By this liquid displacement method it was possible to discover that the addition of GO increased the porosity of the nanofibers from ≈ 85% to ≈ 95%.

These results are very promising for adsorption and filtration applications where high surface areas are crucial for a high interaction with the contaminants and a high porosity allows to produce mats with lower pressure drops and able to withstand a higher permeate flux.

9.4 ADSORPTION TESTS

Electrospun PLA, PLA/GO and PLA/CNF mats were tested in the adsorption of methylene blue.

Methylene blue was selected as analyte for its low cost and the possibility to analyse data through UV-VIS spectrophotometry.

The direct measurement of the surface area of the samples has been performed exploiting the principle of dye adsorption. In analogy with the adsorption of N_2 molecules from gas (a.k.a. BET method) – the standard technique used for nanomaterials [ISO 9277:2010] – we generalized such approach investigating the adsorption isotherms of Methylene Blue (MB) in isopropanol (IPA). [127]

The BET model describes a multilayer adsorption mechanism in the gas–solid and liquid–solid equilibrium systems described by equation 8 [128]:

$$q_e = q_m \cdot \frac{K_S \cdot C_e}{(1 - K_L \cdot C_e)(1 - K_L \cdot C_e + K_S \cdot C_e)} \qquad \text{EQ. 8}$$

where q_e is the number of molecules adsorbed corresponding to the equilibrium concentration Ce and q_m is the amount of molecules needed to cover the entire adsorbent surface with a monolayer (i.e. the monolayer saturation capacity). K_S and K_L are the thermodynamic equilibrium constants of the first layer and the upper ones, respectively.

In the case of monolayer adsorption (K_L=0) the eqn.1 assumes the form described by Langmuir model (equation 9):

$$q_e = q_m \cdot \frac{K_S \cdot C_e}{1 + K_S \cdot C_e}. \quad \text{EQ. 9}$$

Then, we converted the quantity of molecules adsorbed (q_m) in the SA ideally occupied by those molecules using equation 10:

$$SA = q_m \cdot \frac{N_A \cdot A_{MB}}{M_w} \quad \text{EQ. 10}$$

where N_A is the Avogadro number, Mw = 373.87 g/mol is the molecular weight of MB and A_{MB} = 1.30 nm^2 [129] is the estimated "footprint", i.e. the amount of substrate ideally occupied by a single adsorbed MB molecule.

Unfortunately, due to time issues and COVID-19 restrictions the analysis is still ongoing at the moment I am writing this thesis.

9.5 CONCLUSIONS

PLA fibrous mats were successfully produced through electrospinning technique. SEM analysis showed the high diameter of the produced microfibers (> 2 μm).

The addition of a nanofiller, such as GO and cellulose nanofibers, was proved to be effective for controlling the morphology and dimensions of the obtained nanofibers. In detail, both PLA/GO and PLA/CNF electrospun composites were composed by sub-micrometrical fibers with diameters in the order of 500-600 nm.

BET analysis and liquid displacement proved that the composite mats are characterized by a higher surface area (≈ 3.6 m^2/g) and porosity (≈ 95%) than the pristine PLA mats. Many articles in literature show that these values are suitable for adsorption membranes applications [130] [131].

Adsorption tests are currently being performed using methylene blue as analyte. If these tests will be promising enough, the next step will be the functionalization of the CNFs domains inside the electrospun mat. Literature shows the effectiveness of nanocellulose modification to improve its affinity and selectivity towards specific analytes [132] [133].

This research could present a cost-effective and simple method for the production of completely bio-based adsorption membranes characterized by high adsorption capacity and low pressure drops thanks to the nanostructured morphology. Moreover, the vast array of possible functionalization of nanocellulose could improve their selectivity towards specific contaminants or analytes.

10. CONCLUSIONS

This thesis highlighted the possibility to produce nanostructured polymeric composites containing graphene-based nanofillers by exploiting the electrospinning technique to confer these materials a nanofiber morphology.

The reinforcements can be added to the polymeric matrix in bulk, using a co-electrospinning approach, or as coatings. The proper method is selected based on the properties required by the purposed application of the material.

Co-electrospun membranes were obtained after the optimization of the electrospinning setup for every different composite material. In this context, the present work shows the positive effect that the addition of nanocomposites (especially graphene oxide) has on the stability of the overall electrospinning process. This effect is probably due to the modified rheology of the dispersion, which can be finely tuned to produce nanofibers characterized by a thinner and controlled mean diameter.

GO-coated membranes were produced using a sonication assisted dip-coating technique followed by a chemical and thermal reduction step to restore its electrical conductivity. Washing and folding tests proved the strong mechanical resistance of the material and the strong adhesion of the coating on its surface.

In particular, during this research work we focused on three different application fields: energy harvesting, wearable electronics and adsorption membranes.

- We proved that co-electrospun PVdF/GO nanostructured composites could be a promising material to be used as active layer in a wearable triboelectric nanogenerator. Both the nanoscale morphology and the GO addition improved its performances in a TENG prototype up to ≈ 60 V open-circuit voltage and ≈ 5 $\mu W/cm^2$ peak power output.

- rGO-coated PA6 electrospun mats were successfully produced and we proved their mechanical resistance to washing and electrical conductivity (≈ 500 Ω/sq sheet resistance). Comparative tests coated commercial textiles proved the importance of the nanoscale morphology on the final conductivity of the materials. The fast response to external stimuli provided by the nanofiber morphology makes these materials interesting for mechanical sensors applications, while a further enhancement of the final conductivity could open the doors for their use as heating elements in flexible and wearable devices.

- Completely bio-based composites were produced by co-electrospinning a PLA/CNF dispersion. This work proved the effectiveness of the nanofiller addition on the reduction of the diameters of the obtained nanofibers. This grants the produced materials enhanced surface area and porosity. Thus, such composites are particularly promising for the production of highly efficient adsorption membranes with low pressure drops. They possibility to surface functionalize the cellulose domains could also improve their selectivity towards specific analytes.

REFERENCES

[1] N. V. Hullavarad, S. S. Hullavarad, and P. C. Karulkar, "Cadmium Sulphide (CdS) nanotechnology: Synthesis and applications," *J. Nanosci. Nanotechnol.*, vol. 8, no. 7, pp. 3272–3299, 2008.

[2] T. Y. Poh *et al.*, "Inhaled nanomaterials and the respiratory microbiome: Clinical, immunological and toxicological perspectives," *Part. Fibre Toxicol.*, vol. 15, no. 1, pp. 1–16, 2018.

[3] J. Fang, H. T. Niu, T. Lin, and X. G. Wang, "Applications of electrospun nanofibers," *Chinese Sci. Bull.*, vol. 53, no. 15, pp. 2265–2286, 2008.

[4] W. Il Park, M. Kang, H. S. Kim, and H. J. Jin, "Electrospinning of poly(ethylene oxide) with bacterial cellulose whiskers," *Macromol. Symp.*, vol. 249–250, pp. 289–294, 2007.

[5] W. E. Teo and S. Ramakrishna, "A review on electrospinning design and nanofibre assemblies," *Nanotechnology*, vol. 17, no. 14, 2006.

[6] B. Zaarour, L. Zhu, and X. Jin, "A Review on the Secondary Surface Morphology of Electrospun Nanofibers: Formation Mechanisms, Characterizations, and Applications," *ChemistrySelect*, vol. 5, no. 4, pp. 1335–1348, 2020.

[7] X. Qin, *Coaxial electrospinning of nanofibers*. 2017.

[8] A. A. Almetwally, M. El-Sakhawy, M. H. Elshakankery, and M. H. Kasem, "Technology of nano-fibers: Production techniques and properties - Critical review," *J. Text. Assoc.*, vol. 78, no. 1, pp. 5–14, 2017.

[9] N. Faldu, "Scholarship at UWindsor Scholarship at UWindsor Electronic Theses and Dissertations Theses, Dissertations, and Major Papers Electrospinning of PEO Nanofibers Electrospinning of PEO Nanofibers," 2020.

[10] T. Ondarçuhu and C. Joachim, "Drawing a single nanofibre over hundreds of microns," *Europhys. Lett.*, vol. 42, no. 2, pp. 215–220, 1998.

[11] X. Xing, Y. Wang, and B. Li, "Nanofibers drawing and nanodevices assembly in poly(trimethylene terephthalate)," *Opt. Express*, vol. 16, no. 14, p. 16815, 2008.

[12] "M I C R O P O R O U S M E M B R a N E F O R M a T I O N Via T H E R M a L L Y," vol. 52, pp. 239–261, 1990.

[13] R. Vasita and D. S. Katti, "Nanofibers and their applications in tissue engineering," *Int. J. Nanomedicine*, vol. 1, no. 1, pp. 15–30, 2006.

[14] H. Yang *et al.*, "A simple melt impregnation method to synthesize ordered mesoporous carbon and carbon nanofiber bundles with graphitized structure from pitches," *J. Phys.*

Chem. B, vol. 108, no. 45, pp. 17320–17328, 2004.

[15] C. R. Martin, "Template Synthesis of Electronically Conductive Polymer Nanostructures," *Acc. Chem. Res.*, vol. 28, no. 2, pp. 61–68, 1995.

[16] M. A. Hassan, B. Y. Yeom, A. Wilkie, B. Pourdeyhimi, and S. A. Khan, "Fabrication of nanofiber meltblown membranes and their filtration properties," *J. Memb. Sci.*, vol. 427, pp. 336–344, 2013.

[17] R. T. Weitz, L. Harnau, S. Rauschenbach, M. Burghard, and K. Kern, "Polymer nanofibers via nozzle-free centrifugal spinning," *Nano Lett.*, vol. 8, no. 4, pp. 1187–1191, 2008.

[18] L. Ren, R. Ozisik, and S. P. Kotha, "Rapid and efficient fabrication of multilevel structured silica micro-/nanofibers by centrifugal jet spinning," *J. Colloid Interface Sci.*, vol. 425, pp. 136–142, 2014.

[19] X. Zhang and Y. Lu, "Centrifugal spinning: An alternative approach to fabricate nanofibers at high speed and low cost," *Polym. Rev.*, vol. 54, no. 4, pp. 677–701, 2014.

[20] M. R. Badrossamay, H. A. McIlwee, J. A. Goss, and K. K. Parker, "Nanofiber assembly by rotary jet-spinning," *Nano Lett.*, vol. 10, no. 6, pp. 2257–2261, 2010.

[21] Z. M. Huang, Y. Z. Zhang, M. Kotaki, and S. Ramakrishna, "A review on polymer nanofibers by electrospinning and their applications in nanocomposites," *Compos. Sci. Technol.*, vol. 63, no. 15, pp. 2223–2253, 2003.

[22] G. E. Zaikov, "NAnostructured Fibers Via Electrospinning (Part II)," *Appl. Nanotechnol. Mater. Appl.*, no. 1, pp. 281–324, 2016.

[23] H. Soderlund, L. Kaariainen, and C. H. Von Bonsdorff, "Properties of Semliki Forest virus nucleocapsid," *Med. Biol.*, vol. 53, no. 5, pp. 412–417, 1975.

[24] J. R. Melcher and G. I. Taylor, "Electrohydrodynamics: A Review of the Role of Interfacial Shear Stresses," *Annu. Rev. Fluid Mech.*, vol. 1, no. 1, pp. 111–146, 1969.

[25] J. Fernández de la Mora, "The fluid dynamics of Taylor Cones," *Annu. Rev. Fluid Mech.*, vol. 39, pp. 217–243, 2007.

[26] A. L. Yarin, S. Koombhongse, and D. H. Reneker, "Bending instability in electrospinning of nanofibers," *J. Appl. Phys.*, vol. 89, no. 5, pp. 3018–3026, 2001.

[27] J. M. Deitzel, J. Kleinmeyer, D. Harris, and N. C. Beck Tan, "The effect of processing variables on the morphology of electrospun," *Polymer (Guildf).*, vol. 42, pp. 261–272, 2001.

[28] J. Doshi and D. H. Reneker, "Electrospinning process and applications of electrospun fibers," *Conf. Rec. - IAS Annu. Meet. (IEEE Ind. Appl. Soc.*, vol. 3, pp. 1698–1703, 1993.

[29] D. H. Reneker, A. L. Yarin, H. Fong, and S. Koombhongse, "Bending instability of electrically charged liquid jets of polymer solutions in electrospinning," *J. Appl. Phys.*, vol.

87, no. 9 I, pp. 4531–4547, 2000.

[30] M. M. Hohman, M. Shin, G. Rutledge, and M. P. Brenner, “Electrospinning and electrically forced jets. I. Stability theory,” *Phys. Fluids*, vol. 13, no. 8, pp. 2201–2220, 2001.

[31] R. Sahay, V. Thavasi, and S. Ramakrishna, “Design modifications in electrospinning setup for advanced applications,” *J. Nanomater.*, vol. 2011, pp. 1–17, 2011.

[32] A. K. Haghi and M. Akbari, “Trends in electrospinning of natural nanofibers,” *Phys. Status Solidi Appl. Mater. Sci.*, vol. 204, no. 6, pp. 1830–1834, 2007.

[33] D. S. Katti, K. W. Robinson, F. K. Ko, and C. T. Laurencin, “Bioresorbable nanofiber-based systems for wound healing and drug delivery: Optimization of fabrication parameters,” *J. Biomed. Mater. Res. - Part B Appl. Biomater.*, vol. 70, no. 2, pp. 286–296, 2004.

[34] W. K. Son, J. H. Youk, T. S. Lee, and W. H. Park, “The effects of solution properties and polyelectrolyte on electrospinning of ultrafine poly(ethylene oxide) fibers,” *Polymer (Guildf).*, vol. 45, no. 9, pp. 2959–2966, 2004.

[35] S. Megelski, J. S. Stephens, D. Bruce Chase, and J. F. Rabolt, “Micro- and nanostructured surface morphology on electrospun polymer fibers,” *Macromolecules*, vol. 35, no. 22, pp. 8456–8466, 2002.

[36] R. M. Nezarati, M. B. Eifert, and E. Cosgriff-Hernandez, “Effects of humidity and solution viscosity on electrospun fiber morphology,” *Tissue Eng. - Part C Methods*, vol. 19, no. 10, pp. 810–819, 2013.

[37] S. Ramakrishna, K. Fujihara, W.-E. Teo, T.-C. Lim, and Z. Ma, “Front Matter,” *An Introd. to Electrospinning Nanofibers*, pp. i–xi, 2005.

[38] S. Ramakrishna, K. Fujihara, W. E. Teo, T. Yong, Z. Ma, and R. Ramaseshan, “Electrospun nanofibers: Solving global issues,” *Mater. Today*, vol. 9, no. 3, pp. 40–50, 2006.

[39] Z. Sun, E. Zussman, A. L. Yarin, J. H. Wendorff, and A. Greiner, “Compound Core-Shell Polymer Nanofibers by Co-Electrospinning,” *Adv. Mater.*, vol. 15, no. 22, pp. 1929–1932, 2003.

[40] R. Kessick and G. Tepper, “Microscale polymeric helical structures produced by electrospinning,” *Appl. Phys. Lett.*, vol. 84, no. 23, pp. 4807–4809, 2004.

[41] K. Liu, Y. Zheng, C. Ge, B. Xin, and X. Dong, “Preparation and Formation Mechanism of Electrospun Porous Beaded Fibers,” *AATCC J. Res.*, vol. 9, no. 3, pp. 134–142, May 2022.

[42] N. H. Vargas, “MASTER ’ S THESIS Aligned Cellulose Nanofibers Prepared by Electrospinning,” 2010.

[43] W. Zhang *et al.*, “Structural design and environmental applications of electrospun nanofibers,” *Compos. Part A Appl. Sci. Manuf.*, vol. 137, no. April, p. 106009, 2020.

[44] J. Li *et al.*, “Filtration of fine particles in atmospheric aerosol with electrospinning nanofibers and its size distribution,” *Sci. China Technol. Sci.*, vol. 57, no. 2, pp. 239–243, 2014.

[45] S. Agarwal, J. H. Wendorff, and A. Greiner, “Use of electrospinning technique for biomedical applications,” *Polymer (Guildf).*, vol. 49, no. 26, pp. 5603–5621, 2008.

[46] B. Yan, Y. Zhang, Z. Li, P. Zhou, and Y. Mao, “Electrospun nanofibrous membrane for biomedical application,” *SN Appl. Sci.*, vol. 4, no. 6, p. 172, Jun. 2022.

[47] D. Liang, B. S. Hsiao, and B. Chu, “Functional electrospun nanofibrous scaffolds for biomedical applications,” *Adv. Drug Deliv. Rev.*, vol. 59, no. 14, pp. 1392–1412, 2007.

[48] K. S. Novoselov, V. I. Fal’Ko, L. Colombo, P. R. Gellert, M. G. Schwab, and K. Kim, “A roadmap for graphene,” *Nature*, vol. 490, no. 7419, pp. 192–200, 2012.

[49] P. Avouris and C. Dimitrakopoulos, “Graphene: Synthesis and applications,” *Mater. Today*, vol. 15, no. 3, pp. 86–97, 2012.

[50] A. Kovtun *et al.*, “Benchmarking of graphene-based materials: Real commercial products versus ideal graphene,” *2D Mater.*, vol. 6, no. 2, 2019.

[51] J. H. Lee, P. E. Loya, J. Lou, and E. L. Thomas, “Dynamic mechanical behavior of multilayer graphene via supersonic projectile penetration,” *Science (80-.).*, vol. 346, no. 6213, pp. 1092–1096, 2014.

[52] S. Stankovich *et al.*, “Graphene-based composite materials,” *Nature*, vol. 442, no. 7100, pp. 282–286, 2006.

[53] H. Kim, A. A. Abdala, and C. W. MacOsko, “Graphene/polymer nanocomposites,” *Macromolecules*, vol. 43, no. 16, pp. 6515–6530, 2010.

[54] A. Bianco *et al.*, “All in the graphene family - A recommended nomenclature for two-dimensional carbon materials,” *Carbon N. Y.*, vol. 65, pp. 1–6, 2013.

[55] A. P. Kauling *et al.*, “The Worldwide Graphene Flake Production,” *Adv. Mater.*, vol. 30, no. 44, pp. 1–6, 2018.

[56] V. B. Mohan, K. tak Lau, D. Hui, and D. Bhattacharyya, “Graphene-based materials and their composites: A review on production, applications and product limitations,” *Compos. Part B Eng.*, vol. 142, no. December 2017, pp. 200–220, 2018.

[57] A. Kumar, K. Sharma, and A. R. Dixit, “A review of the mechanical and thermal properties of graphene and its hybrid polymer nanocomposites for structural applications,” *J. Mater. Sci.*, vol. 54, no. 8, pp. 5992–6026, 2019.

[58] X. Ji, Y. Xu, W. Zhang, L. Cui, and J. Liu, “Review of functionalization, structure and properties of graphene/polymer composite fibers,” *Compos. Part A Appl. Sci. Manuf.*, vol. 87, pp. 29–45, 2016.

[59] L. Graphene *et al.*, “Enhanced Mechanical Properties of,” *ACS Nano*, vol. 3, no. 12, pp. 3884–3890, 2009.

[60] R. J. Young, I. A. Kinloch, L. Gong, and K. S. Novoselov, “The mechanics of graphene nanocomposites: A review,” *Compos. Sci. Technol.*, vol. 72, no. 12, pp. 1459–1476, 2012.

[61] S. Bose, T. Kuila, M. E. Uddin, N. H. Kim, A. K. T. Lau, and J. H. Lee, “In-situ synthesis and characterization of electrically conductive polypyrrole/graphene nanocomposites,” *Polymer (Guildf).*, vol. 51, no. 25, pp. 5921–5928, 2010.

[62] C. C. Teng *et al.*, “Thermal conductivity and structure of non-covalent functionalized graphene/epoxy composites,” *Carbon N. Y.*, vol. 49, no. 15, pp. 5107–5116, 2011.

[63] J. Du and H. M. Cheng, “The fabrication, properties, and uses of graphene/polymer composites,” *Macromol. Chem. Phys.*, vol. 213, no. 10–11, pp. 1060–1077, 2012.

[64] A. M. Díez-Pascual and A. Rahdar, “Graphene-Based Polymer Composites for Flexible Electronic Applications,” *Micromachines*, vol. 13, no. 7, pp. 1–18, 2022.

[65] D. Konios *et al.*, “Reduced graphene oxide micromesh electrodes for large area, flexible, organic photovoltaic devices,” *Adv. Funct. Mater.*, vol. 25, no. 15, pp. 2213–2221, 2015.

[66] Z. Yin *et al.*, “Organic photovoltaic devices using highly flexible reduced graphene oxide films as transparent electrodes,” *ACS Nano*, vol. 4, no. 9, pp. 5263–5268, 2010.

[67] H. Park, S. Chang, X. Zhou, J. Kong, T. Palacios, and S. Gradečak, “Flexible graphene electrode-based organic photovoltaics with record-high efficiency,” *Nano Lett.*, vol. 14, no. 9, pp. 5148–5154, 2014.

[68] H. P. Cong, X. C. Ren, P. Wang, and S. H. Yu, “Flexible graphene-polyaniline composite paper for high-performance supercapacitor,” *Energy Environ. Sci.*, vol. 6, no. 4, pp. 1185–1191, 2013.

[69] Y. Kim *et al.*, “Flexible textile-based organic transistors using Graphene/Ag nanoparticle electrode,” *Nanomaterials*, vol. 6, no. 8, 2016.

[70] Y. T. Wu, T. Yan, and Z. J. Pan, “Wearable Carbon-Based Resistive Sensors for Strain Detection: A Review,” *IEEE Sens. J.*, vol. 21, no. 4, pp. 4030–4043, 2021.

[71] M. Hao, W. Zeng, Y. Q. Li, and Z. C. Wang, “Three-dimensional graphene and its composite for gas sensors,” *Rare Met.*, vol. 40, no. 6, pp. 1494–1514, 2021.

[72] N. Sahiner, “Conductive polymer containing graphene aerogel composites as sensor for CO 2,” *Polym. Compos.*, vol. 40, no. S2, pp. E1208–E1218, 2019.

[73] F. Perreault, A. Fonseca De Faria, and M. Elimelech, “Environmental applications of graphene-based nanomaterials,” *Chem. Soc. Rev.*, vol. 44, no. 16, pp. 5861–5896, 2015.

[74] D. Cohen-Tanugi and J. C. Grossman, “Mechanical strength of nanoporous graphene as a

desalination membrane," *Nano Lett.*, vol. 14, no. 11, pp. 6171–6178, 2014.

[75] K. Javed, M. Oolo, N. Savest, and A. Krumme, "A Review on Graphene-Based Electrospun Conductive Nanofibers, Supercapacitors, Anodes, and Cathodes for Lithium-Ion Batteries," *Crit. Rev. Solid State Mater. Sci.*, vol. 44, no. 5, pp. 427–443, 2019.

[76] F. Navarro-Pardo, A. L. Martinez-Hernandez, and C. Velasco-Santos, "Carbon nanotube and graphene based polyamide electrospun nanocomposites: A Review," *J. Nanomater.*, vol. 2016, 2016.

[77] X. Gao, S. Han, R. Zhang, G. Liu, and J. Wu, "Progress in electrospun composite nanofibers: Composition, performance and applications for tissue engineering," *J. Mater. Chem. B*, vol. 7, no. 45, pp. 7075–7089, 2019.

[78] S. Wu, S. Peng, and C. H. Wang, "Multifunctional polymer nanocomposites reinforced by aligned carbon nanomaterials," *Polymers (Basel).*, vol. 10, no. 5, 2018.

[79] J. K. Y. Lee *et al.*, "Polymer-based composites by electrospinning: Preparation & functionalization with nanocarbons," *Prog. Polym. Sci.*, vol. 86, pp. 40–84, 2018.

[80] X. Lu, C. Wang, and Y. Wei, "One-dimensional composite nanomaterials: Synthesis by electrospinning and their applications," *Small*, vol. 5, no. 21, pp. 2349–2370, 2009.

[81] C. Leyva-Porras, C. Ornelas-Gutiérrez, M. Miki-Yoshida, Y. I. Avila-Vega, J. MacOssay, and J. Bonilla-Cruz, "EELS analysis of Nylon 6 nanofibers reinforced with nitroxide-functionalized graphene oxide," *Carbon N. Y.*, vol. 70, pp. 164–172, 2014.

[82] C. Zhang, L. Wang, T. Zhai, X. Wang, Y. Dan, and L. S. Turng, "The surface grafting of graphene oxide with poly(ethylene glycol) as a reinforcement for poly(lactic acid) nanocomposite scaffolds for potential tissue engineering applications," *J. Mech. Behav. Biomed. Mater.*, vol. 53, pp. 403–413, 2016.

[83] S. Das, A. S. Wajid, S. K. Bhattacharia, M. D. Wilting, I. V. Rivero, and M. J. Green, "Electrospinning of polymer nanofibers loaded with noncovalently functionalized graphene," *J. Appl. Polym. Sci.*, vol. 128, no. 6, pp. 4040–4046, 2013.

[84] D. V. Nikolaev, Z. I. Evseev, S. A. Smagulova, and I. V. Antonova, "Electrical properties of textiles treated with graphene oxide suspension," *Materials (Basel).*, vol. 14, no. 8, pp. 1–11, 2021.

[85] R. Sarvari, S. Sattari, B. Massoumi, S. Agbolaghi, Y. Beygi-Khosrowshahi, and A. Kahaie-Khosrowshahi, "Composite electrospun nanofibers of reduced graphene oxide grafted with poly(3-dodecylthiophene) and poly(3-thiophene ethanol) and blended with polycaprolactone," *J. Biomater. Sci. Polym. Ed.*, vol. 28, no. 15, pp. 1740–1761, 2017.

[86] M. Yanılmaz and A. S. Sarac, "A review: Effect of conductive polymers on the

conductivities of electrospun mats," *Text. Res. J.*, vol. 84, no. 12, pp. 1325–1342, 2014.

[87] H. R. Pant *et al.*, "RGO/Nylon-6 composite mat with unique structural features and electrical properties obtained from electrospinning and hydrothermal process," *Fibers Polym.*, vol. 14, no. 6, pp. 970–975, 2013.

[88] Z. Huang, M. Sun, Y. Li, Z. Guo, and H. Li, "Reduced graphene oxide-coated electrospun fibre: effect of orientation, coverage and electrical stimulation on Schwann cells behavior," *J. Mater. Chem. B*, vol. 9, no. 11, pp. 2656–2665, 2021.

[89] Y. Ahn *et al.*, "Enhanced piezoelectric properties of electrospun poly(vinylidene fluoride)/multiwalled carbon nanotube composites due to high β-phase formation in poly(vinylidene fluoride)," *J. Phys. Chem. C*, vol. 117, no. 22, pp. 11791–11799, 2013.

[90] C. M. Wu, S. A. Yu, and S. L. Lin, "Graphene modified electrospun poly(vinyl alcohol) nanofibrous membranes for glucose oxidase immobilization," *Express Polym. Lett.*, vol. 8, no. 8, pp. 565–573, 2014.

[91] R. Balint, N. J. Cassidy, and S. H. Cartmell, "Conductive polymers: Towards a smart biomaterial for tissue engineering," *Acta Biomater.*, vol. 10, no. 6, pp. 2341–2353, 2014.

[92] J. Miao, M. Miyauchi, T. J. Simmons, J. S. Dordick, and R. J. Linhardt, "Electrospinning of nanomaterials and applications in electronic components and devices," *J. Nanosci. Nanotechnol.*, vol. 10, no. 9, pp. 5507–5519, 2010.

[93] Q. Wei *et al.*, "Porous One-Dimensional Nanomaterials: Design, Fabrication and Applications in Electrochemical Energy Storage," *Adv. Mater.*, vol. 29, no. 20, 2017.

[94] J. G. López-Covarrubias, L. Soto-Muñoz, A. L. Iglesias, and L. J. Villarreal-Gómez, "Electrospun nanofibers applied to dye solar sensitive cells: A review," *Materials (Basel).*, vol. 12, no. 19, pp. 1–18, 2019.

[95] B. Zhang, F. Kang, J. M. Tarascon, and J. K. Kim, "Recent advances in electrospun carbon nanofibers and their application in electrochemical energy storage," *Prog. Mater. Sci.*, vol. 76, pp. 319–380, 2016.

[96] H. Yang, "Recent Advances of Flexible Electrospun Nanofibers-based Electrodes for Electrochemical Supercapacitors: A Minireview," *Int. J. Electrochem. Sci.*, vol. 14, pp. 7811–7831, 2019.

[97] A. M. Al-Dhahebi, S. C. B. Gopinath, and M. S. M. Saheed, "Graphene impregnated electrospun nanofiber sensing materials: a comprehensive overview on bridging laboratory set-up to industry," *Nano Converg.*, vol. 7, no. 1, 2020.

[98] K. Xu, Y. Lu, and K. Takei, "Multifunctional Skin-Inspired Flexible Sensor Systems for Wearable Electronics," *Adv. Mater. Technol.*, vol. 4, no. 3, pp. 1–25, 2019.

[99] J. Kim, J. Lee, D. Son, M. K. Choi, and D. H. Kim, “Deformable devices with integrated functional nanomaterials for wearable electronics,” *Nano Converg.*, vol. 3, no. 1, pp. 1–13, 2016.

[100] F. Torrisi and T. Carey, “Graphene, related two-dimensional crystals and hybrid systems for printed and wearable electronics,” *Nano Today*, vol. 23, pp. 73–96, 2018.

[101] T. Huang, M. Lu, H. Yu, Q. Zhang, H. Wang, and M. Zhu, “Enhanced power output of a triboelectric nanogenerator composed of electrospun nanofiber mats doped with graphene oxide,” *Sci. Rep.*, vol. 5, no. September, pp. 1–8, 2015.

[102] T. Yan, Z. Wang, and Z. J. Pan, “Flexible strain sensors fabricated using carbon-based nanomaterials: A review,” *Curr. Opin. Solid State Mater. Sci.*, vol. 22, no. 6, pp. 213–228, 2018.

[103] W. H. Han *et al.*, “Fabrication of nanofibrous sensors by electrospinning,” *Sci. China Technol. Sci.*, vol. 62, no. 6, pp. 886–894, 2019.

[104] G. K. Sharma and N. R. James, “Progress in Electrospun Polymer Composite Fibers for Microwave Absorption and Electromagnetic Interference Shielding,” *ACS Appl. Electron. Mater.*, vol. 3, no. 11, pp. 4657–4680, 2021.

[105] X. Cai, T. Lei, D. Sun, and L. Lin, “A critical analysis of the α, β and γ phases in poly(vinylidene fluoride) using FTIR,” *RSC Adv.*, vol. 7, no. 25, pp. 15382–15389, 2017.

[106] Z. Zhao, J. Li, X. Yuan, X. Li, Y. Zhang, and J. Sheng, “Preparation and properties of electrospun poly(vinylidene fluoride) membranes,” *J. Appl. Polym. Sci.*, vol. 97, no. 2, pp. 466–474, 2005.

[107] J. Fang, X. Wang, and T. Lin, “Electrical power generator from randomly oriented electrospun poly(vinylidene fluoride) nanofibre membranes,” *J. Mater. Chem.*, vol. 21, no. 30, pp. 11088–11091, 2011.

[108] Y. L. Huang *et al.*, “Self-assembly of graphene onto electrospun polyamide 66 nanofibers as transparent conductive thin films,” *Nanotechnology*, vol. 22, no. 47, 2011.

[109] Z. Wang, C. Zhao, and Z. Pan, “Porous bead-on-string poly(lactic acid) fibrous membranes for air filtration,” *J. Colloid Interface Sci.*, vol. 441, pp. 121–129, 2015.

[110] H. P. S. Abdul Khalil, A. H. Bhat, and A. F. Ireana Yusra, “Green composites from sustainable cellulose nanofibrils: A review,” *Carbohydr. Polym.*, vol. 87, no. 2, pp. 963–979, 2012.

[111] Y. Habibi, L. A. Lucia, and O. J. Rojas, “Cellulose nanocrystals: Chemistry, self-assembly, and applications,” *Chem. Rev.*, vol. 110, no. 6, pp. 3479–3500, 2010.

[112] J. H. Kim *et al.*, “Review of nanocellulose for sustainable future materials,” *Int. J. Precis.*

Eng. Manuf. - Green Technol., vol. 2, no. 2, pp. 197–213, 2015.

[113] J. E. Sanders, Y. Han, T. S. Rushing, and D. J. Gardner, "Electrospinning of cellulose nanocrystal-filled poly (Vinyl alcohol) solutions: Material property assessment," *Nanomaterials*, vol. 9, no. 5, 2019.

[114] Q. Cao *et al.*, "Electrospun bead-in-string fibrous membrane prepared from polysilsesquioxane-immobilising poly(lactic acid) with low filtration resistance for air filtration," *J. Polym. Res.*, vol. 27, no. 1, 2020.

[115] Q. Shi, C. Zhou, Y. Yue, W. Guo, Y. Wu, and Q. Wu, "Mechanical properties and in vitro degradation of electrospun bio-nanocomposite mats from PLA and cellulose nanocrystals," *Carbohydr. Polym.*, vol. 90, no. 1, pp. 301–308, 2012.

[116] S. A. Theron, E. Zussman, and A. L. Yarin, "Experimental investigation of the governing parameters in the electrospinning of polymer solutions," *Polymer (Guildf).*, vol. 45, no. 6, pp. 2017–2030, 2004.

[117] R. Rošic, J. Pelipenko, P. Kocbek, S. Baumgartner, M. Bešter-Rogač, and J. Kristl, "The role of rheology of polymer solutions in predicting nanofiber formation by electrospinning," *Eur. Polym. J.*, vol. 48, no. 8, pp. 1374–1384, 2012.

[118] C. Gasparini *et al.*, "Enhancing triboelectric performances of electrospun poly(vinylidene fluoride) with graphene oxide sheets," *Graphene Technol.*, vol. 5, no. 3–4, pp. 49–57, 2020.

[119] E. Treossi, M. Melucci, A. Liscio, M. Gazzano, P. Samorì, and V. Palermo, "High-contrast visualization of graphene oxide on dye-sensitized glass, quartz, and silicon by fluorescence quenching," *J. Am. Chem. Soc.*, vol. 131, no. 43, pp. 15576–15577, 2009.

[120] Y. Wang *et al.*, "Beads-on-String Structured Nanofibers for Smart and Reversible Oil/Water Separation with Outstanding Antifouling Property," *ACS Appl. Mater. Interfaces*, vol. 8, no. 38, pp. 25612–25620, 2016.

[121] Q. L. Meng *et al.*, "Mixed conduction properties of pristine bulk graphene oxide," *Carbon N. Y.*, vol. 101, pp. 338–344, 2016.

[122] C. Fan, Y. Zhang, S. Liao, M. Zhao, P. Lv, and Q. Wei, "Manufacturing Technics for Fabric/Fiber-Based Triboelectric Nanogenerators: From Yarns to Micro-Nanofibers," *Nanomaterials*, vol. 12, no. 15, 2022.

[123] J. Wang, Y. Zi, S. Li, and X. Chen, "High-voltage applications of the triboelectric nanogenerator—Opportunities brought by the unique energy technology," *MRS Energy Sustain.*, vol. 6, no. 1, pp. 1–23, 2019.

[124] T. Xu *et al.*, "Three-dimensional monolithic porous structures assembled from fragmented electrospun nanofiber mats/membranes: Methods, properties, and applications," *Prog. Mater.*

Sci., vol. 112, no. October 2019, p. 100656, 2020.

[125] M. Nie, B. Li, Y. Lo Hsieh, K. K. Fu, and J. Zhou, "Stretchable One-Dimensional Conductors for Wearable Applications," *ACS Nano*, vol. 16, no. 12, pp. 19810–19839, 2022.

[126] M. Giannelli *et al.*, "Magnetic keratin/hydrotalcites sponges as potential scaffolds for tissue regeneration," *Appl. Clay Sci.*, vol. 207, no. April, p. 106090, 2021.

[127] A. Kovtun *et al.*, "Graphene oxide-polysulfone filters for tap water purification, obtained by fast microwave oven treatment," *Nanoscale*, vol. 11, no. 47, pp. 22780–22787, 2019.

[128] A. Ebadi, J. S. Soltan Mohammadzadeh, and A. Khudiev, "What is the correct form of BET isotherm for modeling liquid phase adsorption?," *Adsorption*, vol. 15, no. 1, pp. 65–73, 2009.

[129] J. C. Santamarina, K. A. Klein, Y. H. Wang, and E. Prencke, "Specific surface: Determination and relevance," *Can. Geotech. J.*, vol. 39, no. 1, pp. 233–241, 2002.

[130] F. Zhu, Y. M. Zheng, B. G. Zhang, and Y. R. Dai, "A critical review on the electrospun nanofibrous membranes for the adsorption of heavy metals in water treatment," *J. Hazard. Mater.*, vol. 401, no. June 2020, p. 123608, 2021.

[131] H. Chen, M. Huang, Y. Liu, L. Meng, and M. Ma, "Functionalized electrospun nanofiber membranes for water treatment: A review," *Sci. Total Environ.*, vol. 739, p. 139944, 2020.

[132] S. Liu, Z. X. Low, Z. Xie, and H. Wang, "TEMPO-Oxidized Cellulose Nanofibers: A Renewable Nanomaterial for Environmental and Energy Applications," *Adv. Mater. Technol.*, vol. 6, no. 7, pp. 1–23, 2021.

[133] D. Wang, "A critical review of cellulose-based nanomaterials for water purification in industrial processes," *Cellulose*, vol. 26, no. 2, pp. 687–701, 2019.